



**Max-Planck-Institut für Metallforschung**  
Stuttgart

---

# **Polyelectrolyte-assisted Preparation and Characterization of Nanostructured ZnO Thin Films**

Shijun Jia

Dissertation  
an der  
**Universität Stuttgart**

---

Bericht Nr. 165  
Mai 2005





# **Polyelectrolyte-assisted Preparation and Characterization of Nanostructured ZnO Thin Films**

**Dissertation**

Von der Fakultät Chemie der Universität Stuttgart

zur Erlangung der Würde eines

**Doktors der Naturwissenschaften (Dr. rer. nat.)**

genehmigte Abhandlung

Vorgelegt von

**Shijun Jia**

Aus Shanxi, China

**Hauptberichter : Prof. Dr. rer. nat. Fritz Aldinger**

**Mitberichter : Prof. Dr. rer. nat. Dr. hc. mult. Günter Petzow**

Tag der mündlichen Prüfung : 17.05.05

**Institut für Nichtmetallische Anorganische Materialien der Universität Stuttgart**

**Max-Planck-Institut für Metallforschung, Stuttgart**

**Pulvermetallurgisches Laboratorium**

**2005**





## **Acknowledgements**

I have been truly fortunate to have the opportunities to work in PML with many nice, talented people. With a deep sense of gratitude, I wish to express my sincere thanks to my supervisor Professor Fritz Aldinger for encouraging me to investigate the topic of this work. During the course of doing this thesis, he provided a good balance of guidance and freedom. I really appreciate that. I would also like to thank Dr. Joachim Bill for his kind guidance, and for countless discussions, from which this thesis benefits so much. The enthusiasm and confidence with which Dr. Rudolf Hoffmann guided the work requires no elaboration. His company and assurance in the course of difficult time would be remembered lifelong.

I would like to thank Professor Günter Petzow for accepting to be the co-examiner and Professor Eduard Arzt for being the chairmen for my thesis defense.

I also want to thank Jean Barholome for her assistance with SAMs synthesis. She was a lady with fun and the time when we spent together in the lab is always nice memory for me. I must also thank Marion Kelsch for her great help and training with TEM. I can't thank her enough for the effort she spent teaching me about the TEM specimen preparation and TEM operation. I am grateful to Dr. Peter Lamparter for assistance with XRD and for many invaluable discussions on this subject. His insight is very much appreciated. I also want to thank Peter Gerstel, he is very nice and helpful. Thanks are also given to Dr. Jiangyong Wang and Dr. Lars Jeurgens for XPS investigation, Sabine Kühnemann for assistance with SEM, Ulrika Täffner for her training with AFM, Dr. Lars Jeurgens for help with ellipsometry.

My sincere thanks are due to Dr. N.Y. Jin-Philipp for her help given to me when I approached her and the valuable discussions that I had with her. Special thanks are due to Dr. Jingzhe Zhao, Dr. Q. Fu and Dr. Z. Zhang, for many discussions on various subjects. I am also grateful to Dr. Dongsheng Tang for interesting discussions on quanta mechanics. I am really glad that I have got know them.

There are many people behind the scenes who made working in PML easier. Our department secretary Sabine Paulsen were always ready to help me, and always with a smile. Carmen Garcia was so nice and helpful. Mr. B. Heinze is so nice that he helped me to develop the high-resolution pictures I needed. My officemates Dr. Jiangqiang Peng, Dr. Seahoon Lee, Ravi Kumar, Chong Wang also made life more fun. Ravi had a lot of chat with me and we talked so much about India, I do hope I can visit India one day. I would also like to thank Dr.

Hong Li, Manxi Zhu. They were fun people and great company. Samir Hamond was very nice and we really enjoyed the time we shared in the French class.

My family has always been behind me and always been a source of support in many forms. I would like to share this moment of happiness with my parents, brothers and sister. They rendered me enormous support during the course of the work. Particularly, I am grateful to my husband Guofeng for the moral support he provided throughout my research work and his patience was tested to the utmost by a long period of separation. Without his loving support and understanding I would never have completed my present work.

Finally, I would like to thank all whose direct and indirect support helped me completing my thesis in time.

Shijun Jia

2005, Stuttgart

## Table of Contents

<b>Acknowledgement</b> .....	1
<b>Abstract</b> .....	1
<b>1. Introduction</b>	
1.1. Basic properties and potential application .....	4
1.2. Status study of ZnO .....	6
1.3. Soft solution deposition .....	7
1.3.1. SAM formation .....	7
1.3.2. Deposition techniques .....	8
1.4. Mechanism of oxide film formation onto SAM .....	12
1.5. Scope of the present work .....	13
<b>2. Experimental</b>	
2.1. Characterization methods .....	15
2.1.1. Scanning electron microscopy .....	15
2.1.2. Atomic force Microscopy .....	15
2.1.3. X-ray photoelectron spectroscopy .....	15
2.1.4. X-ray diffraction .....	16
2.1.5. Ellipsometry .....	16
2.1.6. Optical measurement .....	16
2.1.7. Transmission electron microscopy .....	17
2.1.8. TEM specimen preparation .....	17
2.1.8.1. Cross-sectional preparation .....	17
2.1.8.2. Plan-view preparation .....	19
2.1.9. Zeta potential .....	20
2.2. SAM preparation .....	21
2.3. Film deposition .....	24
2.3.1. Copolymer system .....	24
2.3.2. Polyvinylpyrrolidone system .....	24
<b>3. Influence of anionic graft-copolymers on the formation of ZnO thin films in chemical bath deposition</b>	
3.1. Scope of the studies .....	27
3.2. Depositions on silicon wafers modified with mercapto-terminated SAMs .....	28

3.2.1. Influence of the composition of the reaction solution on the film morphology -----	28
3.2.2. Possible quantification of the surface coverage by AFM -----	32
3.2.3. TEM investigations -----	33
3.2.4. XPS investigations -----	37
3.2.5. Film thickness -----	38
3.3. Deposition of ZnO films on silicon modified with SH-C <sub>3</sub> -SAM -----	39
3.4. ZnO film deposition on glass modified with SH-C <sub>16</sub> -SAM -----	41
3.5. Deposition of ZnO films using modified procedure on silicon treated with SH-C <sub>16</sub> -SAM -----	42
3.6. Deposition of ZnO films on silicon substrates modified with different SAMs -----	44

#### **4. Influence of annealing on the structure and photoluminescence of ZnO films prepared by a chemical bath deposition process**

4.1. Introduction-----	46
4.2. Results and discussion -----	46
4.2.1. SEM investigations of annealed films-----	46
4.2.2. XRD investigations of annealed films-----	48
4.2.3. Film grain growth and film texture -----	50
4.2.4. Transmission electron microscopy investigations -----	53
4.2.5. Photoluminescence investigations -----	61

#### **5. Polyvinylpyrrolidone-controlled synthesis and structural property of nanocrystalline ZnO thin films**

5.1. Introduction-----	63
5.2. Results and discussion -----	64
5.2.1. Synthesis of ZnO nanostructured films -----	64
5.2.1.1. Effect of [PVP]/[Zn] concentration ratio-----	64
5.2.1.2. Effect of deposition temperature -----	67
5.2.1.3. Influence of water -----	69
5.2.2. Detailed investigation of a ZnO Film from an optimized concentrated solution -----	69
5.2.2.1. SEM invesitgations -----	69
5.2.2.2. XRD and XPS investigations -----	70
5.2.2.3. Transmission electron microscopy investigations -----	72

5.2.2.4. Optical transmission spectra of the ZnO film -----	80
5.2.2.5. Photoluminescence investigations -----	80
<b>6. Mechanisms of the formation of nanostructured ZnO thin films on SAM-modified substrates via CBD</b>	
6.1. Status study of the ZnO film growth on silicon wafers modified with various SAMs---	83
6.2. Results and discussion -----	85
6.2.1. ZnO film formation on silicon wafers modified with sulfonate-terminated SAMs--	85
6.2.1.1. ZnO film growth from aqueous solution with the presence of a copolymer-----	85
6.2.1.2. ZnO film growth from non-aqueous solution with the presence of PVP-----	87
6.2.2. ZnO film formation on bare silicon wafers -----	89
6.2.3. ZnO film formation on silicon wafers modified by other SAMs -----	89
6.2.4. ZnO film growth on predeposited ZnO films on SAM-----	93
<b>Zusammenfassung -----</b>	<b>94</b>
<b>References -----</b>	<b>98</b>
<b>Curriculum Vitae -----</b>	<b>105</b>

## Abstract

Zinc oxide (ZnO) is a unique material that exhibits semiconducting and piezoelectric properties. ZnO thin films have been produced by a wide variety of techniques, among which wet chemical synthetic routes are advantageous over others due to their experimental simplicity, economy and suitability for forming large area thin films. However, the deposition of ZnO by these kinds of techniques encounters many difficulties. Such ZnO films often consist of micrometer-sized crystals, thus the careful control of the reaction conditions is indispensable to ensure acceptable adherence, grain morphology and surface roughness. Further problems would arise especially when lateral nanostructured films need to be achieved.

The present work focuses on the synthesis and characterization of nanostructured ZnO thin films onto silicon wafers modified by self-assembled-monolayers (SAMs) via chemical bath deposition (CBD). Two precursor solutions were designed and used for the film deposition, in which two different polymers were introduced respectively to control the growth of the ZnO colloidal particles in solution.

ZnO films were deposited from an aqueous solution containing zinc salt and hexamethylenetetramine (HMTA) in the presence of a graft-copolymer (P (MAA<sub>0.50</sub>-co(MAA-EO<sub>20</sub>)<sub>0.50</sub>)<sub>70</sub>). No deposition was observed on the unmodified silicon wafers and the substrates modified by sulfonate-terminated SAMs. Whereas homogeneous ZnO films were formed on the silicon wafers modified by mercapto-terminated-SAMs. The typical film thickness is in the range of 50-200 nm. A film-formation-diagram was established based on the results obtained by scanning electron microscopy (SEM) and atomic force microscopy (AFM), which describes the influence of the concentration of HMTA and copolymer on the ZnO film formation. According to the film morphology, film formation can be classified into three categories: (a) island-like films, (b) uniform films and (c) canyon-like films. Modification of the deposition process allows the canyon-like featured ZnO films to be tuned into a dense structure. The chemical composition of the films was examined by X-ray photoelectron spectroscopy (XPS). After annealing the Zn 2p<sub>3/2</sub> peak locates at 1022.5 eV, which is the expected value for ZnO, whereas this peak is present at 1023.2 eV in the as-deposited sample, indicating the incorporation of the copolymer in the film. TEM investigations reveal that the as-deposited films are amorphous.

The ZnO films annealed at temperatures of 450°C, 500°C, 600°C and 700°C were examined by X-ray diffraction (XRD) and transmission electron microscopy (TEM). After annealing,

the films are polycrystalline ZnO with wurtzite structure. XRD measurements indicate that with increasing annealing temperature, the average grain size increases accordingly and the crystallinity of the films is improved. Upon heating to 600°C, the ZnO films exhibit preferred orientation with c-axis normal to substrate, whereas the films annealed at 700°C even show a more explicit texture. By annealing at temperatures above 600°C the ZnO film reacts with the substrate to form an interfacial layer of Zn<sub>2</sub>SiO<sub>4</sub>, which grows thicker at elevated annealing temperatures. The ZnO films annealed at 600°C and 700°C show strong UV emission, which is ascribed to exciton emission. The red shift of the emission peak of the film annealed at 700°C compared to that annealed at 600°C is consistent with the grain growth during heating as indicated by TEM and XRD measurements.

Another non-aqueous solution system for ZnO thin film deposition was established, in which 2-propanol was used as a solvent and Zn(CH<sub>3</sub>COO)<sub>2</sub>·2H<sub>2</sub>O as well as NaOH as reactants. Polyvinylpyrrolidone (PVP) was used as an additive. The film growth rate depends strongly on the deposition temperature whereby 55°C was typically selected as deposition temperature. No film deposition was observed on the bare silicon wafers, whereas, homogenous ZnO films were obtained on the silicon wafers modified by sulfonate-terminated SAMs. The addition of PVP is one of the key factors to ensure the successful ZnO film deposition. The influence of PVP on film formation was investigated by varying the [PVP]/[Zn] ratio. XRD investigations reveal that the films are of ZnO wurtzite structure and consist of nanometer-sized crystals. TEM results indicate that the as-deposited films consist of domains of 130 nm in size. Furthermore it was observed that such domain is made up of ZnO nanocrystallites of 5 nm by HRTEM study. The crystallites attach either via a basal (001) or the prismatic (100) facets, so that the polar c-axis of the zincite structure is oriented to the surface in a normal or parallel manner respectively. The film growth proceeds then by oriented attachment of further nanocrystallites from the reaction solution. As a result, domain-structured films form whereby domain of the films has its preferred orientation, which is mainly determined by the arrangement of the ZnO particles on the substrate in the initial stage. The room temperature photoluminescence spectra for the as-deposited ZnO thin films were measured with an excitation wavelength of 325 nm. A strong UV emission peak at ~388 nm and a broad green emission peak centred at ~535 nm were observed.

The growth of the nanostructured films in both reaction systems can be interpreted according to the DLVO (Derjaguin-Landau-Verwey-Overbeek) theory. In the initial stage of the film formation electrostatic interactions between the pristine surface and the first particles to deposit are dominant. Thus a significant electrostatic difference of potential exists between



the charged ZnO/polymer particles and the surface. The subsequent attachment of further ZnO/polymer particles must then proceed mainly by Van der Waals interactions as the electrostatic difference of potential between similar particles is small. As can be seen in Zeta potential measurements the polymer molecules which are coordinated to the ceramic particles affect the electrostatic potential of ZnO. Polymer molecules in the solution might also contribute to the film growth by depletion flocculation.

The present study has demonstrated a novel route to prepare nanostructured ZnO thin films via CBD. Two deposition systems with different polymers as additives were investigated. In the first deposition system, which contains a graft-copolymer, the as-deposited film is amorphous. In contrast, the second deposition system, which contains PVP, yields crystalline ZnO films at low deposition temperature, which can offer a wide use for future applications.

## CHAPTER 1

### Introduction

#### 1.1. Basic properties and potential application

ZnO is an important wide band-gap II-VI compound semiconductor. It has a wurtzite-type structure (space group  $P6_3mc$ ) with lattice parameters  $a = 0.3296$  nm and  $c = 0.52065$  nm. The structure consists of hexagonal Zn and O planes stacked alternatively along the  $c$ -axis (see Fig. 1.1). The effective ionic charges are about 1 to 1.2, which results in a polar  $c$  axis. The oppositely charged ions produce positively charged Zn- (001) and negatively charged O- (00 $\bar{1}$ ) surfaces, resulting in a normal dipole moment and spontaneous polarization along the  $c$ -axis as well as a divergence in surface energy. The other commonly observed facets for ZnO are {010}, which are non-polar surfaces and possess a lower energy than the {001} facets. The basic materials parameters of ZnO are shown in Table 1.1 [2004Nor].

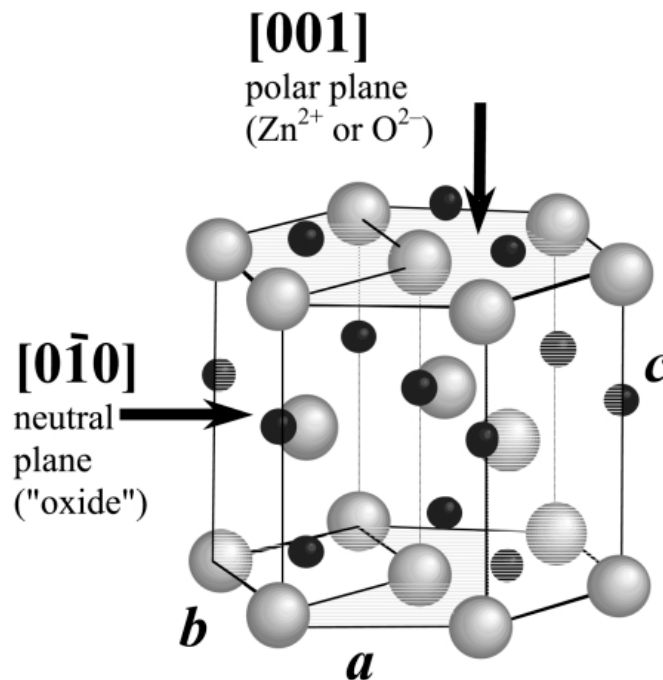


Fig. 1.1 Unit cell of ZnO. Zn<sup>2+</sup> are represented in black, O<sup>2-</sup> anions in grey.

ZnO has three key advantages [2004Wan-1]. Firstly, ZnO is a semiconductor with a direct wide band-gap of 3.37eV, and a large exciton binding energy of 60 meV that is greater than the thermal energy at room temperature (25 meV). It is an important functional oxide that is suitable for short wavelength optoelectronic applications. The advantage of such short

wavelength light emitters lies in the dramatic increase in the data storage capacity of systems such as CDs and DVDs [2001Joh, 2001Kon, 2004Cao]. That is because a device can store more information when the wavelength of the operating laser is shorter. Secondly, because of its noncentral symmetry, ZnO is piezoelectric, which is a key property in building electromechanical-coupled sensors and transducers. Thirdly, ZnO is bio-safe and biocompatible, and can be used for biomedical applications without coating.

Table 1.1 Properties of wurtzite ZnO.

Property	Value
Stable phase at 300 K	wurtzite
Lattice parameters at 300 K:	
$a_0$	0.32495 nm
$c_0$	0.52079 nm
$a_0/c_0$	1.602 (1.633 for ideal hexagonal structure)
Density	5.606 g/cm <sup>3</sup>
Melting point	1975 °C
Thermal conductivity	0.6, 1-1.2
Linear expansion coefficient (/°C)	$a_0$ : $6.5 \times 10^{-6}$ , $c_0$ : $3.0 \times 10^{-6}$
Static dielectric constant	8.656
Refractive index	2.008, 2.029
Energy gap	3.4 eV ( direct)
Intrinsic carrier concentration	$< 10^6$ /cm <sup>3</sup>
Exciton binding energy	60 meV
Electron effective mass	0.24
Electron Hall mobility at 300 K for low n-type conductivity	20 cm <sup>2</sup> /V.s
Hole effective mass	0.59
Hole Hall mobility at 300 K for low p-type conductivity	5.50 cm <sup>2</sup> /V.s

Owing to its unique properties, ZnO has received broad attention for various applications. In each case, the material properties are strongly dependent on the crystal habit, microstructure and impurities. Thus it is important to have full control over the parameters involved in order to realize the desired functionality of a given device technology.

## 1.2. Status study of ZnO

Bulk ZnO is quite expensive and unavailable in large wafers for the time being. In the last few decades, the fabrication of ZnO in the form of powders and films is attracting more and more interest. Most of the ZnO powder used in technical processes is prepared by oxidation of zinc in a vapor-phase process (“French process” or “American process”) [1992Pea]. Nanocrystalline ZnO may be prepared by hydrolysis of organometallic compounds [1991Spa]. Another widely used method for the preparation of ZnO is the precipitation from an aqueous solution of zinc salts at temperatures below 100°C [1992Fuj, 1992And]. Zinc oxide however shows a high tendency to crystallize in the form of micrometer-sized hexagonal needles from solution [1990And]. Andrès-Vergès et al. investigated the morphology of ZnO particles obtained from bulk precipitation and they found that spherical particles were formed in the first 3-7 min, but after 10 min the product consisted only of micrometer-sized hexagonal needles. This feature actually allows the fabrication of aligned ZnO rods on templates [2002Boy, 2002Gov]. Well-aligned ZnO crystallites with c-axis perpendicular to the substrate surface are desirable for applications where crystallographic anisotropy is a prerequisite, e.g. piezoelectric surface acoustic wave or acousto-optic devices. Furthermore, precise control on the lateral dimensions to make vertically aligned ZnO nanorods available is needed for potential application in optoelectronic devices.

Several studies on ZnO powder preparation [1998Öne, 1997Mar] have shown that water-soluble polymers are powerful tools for controlling particle shapes, sizes, and size distributions. Thus a desired equi-axed zincite shape rather than elongated hexagonal rods could be obtained by introducing different polymers. Taubert [2002Tau-1] investigated further the mechanism of the polymer-controlled ZnO particle formation from aqueous solution.

As for ZnO thin films, a variety of thin film deposition techniques have been explored to prepare ZnO thin films, such as sputtering, chemical vapor deposition, sol-gel synthesis, and molecular beam epitaxy and pulsed laser deposition [1983Cho]. Since the electrical and optical properties in these films depend strongly on their microstructure, the stoichiometry of the phase and the nature of the impurities present, each deposition technique with its associated parameters yields films of different properties. Moreover, the techniques based on the physical methods are usually very expensive and high temperature annealing is always required for the films obtained via sol-gel procedure. In contrast, the techniques for depositing

oxide thin films from aqueous solutions at low temperatures (<100°C) offer several advantages and that will be discussed below.

### **1.3. Soft solution deposition**

Soft solution processing is often referred to as low temperature fabrication methods that use solutions of metal salts to create shaped, sized materials [2000Yos]. The synthesis of ceramic thin films from aqueous solutions at low temperatures is of special interest since it provides a possible alternative to vapor-phase and chemical precursor techniques. This chemical solution growth technique, well known for chalcogenide films, has been used for the deposition of oxide films in last few decades. Lower processing temperatures allow films to be deposited on temperature-sensitive substrates such as polymers or peptide. In addition, non-planar or comparably large substrates can also be coated in the liquid baths, which are used as the deposition medium.

Surface chemistry of the substrate is one of the crucial factors controlling the deposition process, regardless of the methods applied. More recently, surface modifications by catalysts [2003Iza], protein monolayers, Langmuir-Blodgett (LB) monolayers and self-assembled monolayers (SAM) [2001Kuz] have been explored to promote the film formation. Among which the formation of an organic SAM has been intensively studied [1996Ulm, 2000Sch].

In the present study, SAM was used to modify the surface of the substrate and its formation is discussed in detail in the following section.

#### **1.3.1. SAM formation**

Partially inspired by the strong degree of control exerted by the deposition surface in biomineralization, the idea of using an organic layer between the substrate and the ceramic film was developed [1996Liu]. For this purpose the self-assembled monolayers have been used by several groups [2001Nie, 2002Sai-1, 1997Aga, 1997Shi]. A SAM is a highly ordered array of molecules with long hydrocarbon chains that are covalently bonded to the substrate surface [1991Ulm] (Fig. 1.2). In combination with the variation of the reaction solution, the organic modification of the substrate has been proved to be a powerful tool to steer the deposition process and thus to act as a template [2002Bil].

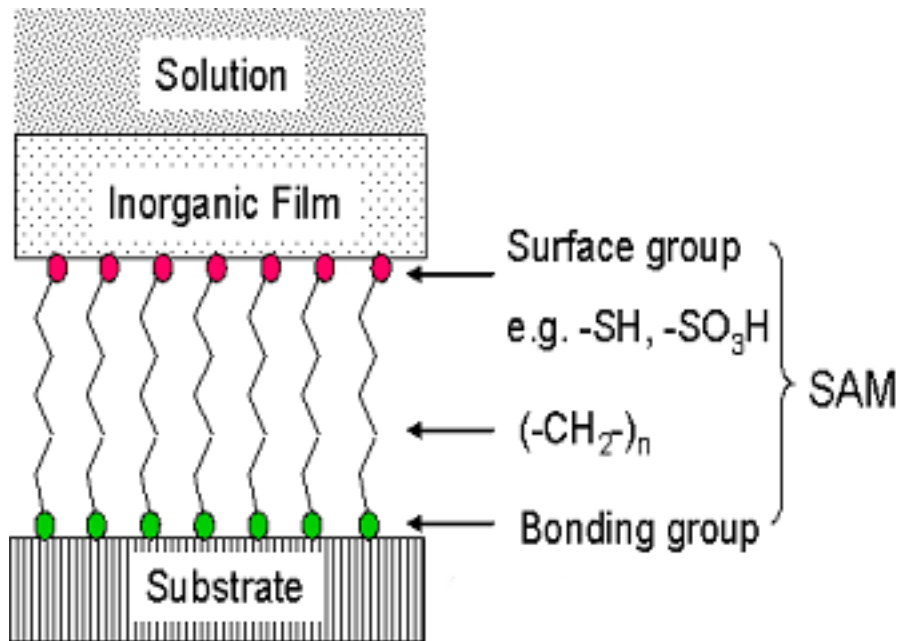


Fig. 1.2 Schematic illustration of oxide film deposition from a liquid solution onto a substrate coated with an organic self-assembled monolayer.

The preparation of siloxane-anchored SAMs on silicon substrates is shown in Fig. 1.3. For the formation of the SAM the substrate is activated by “piranha” solution ( $\text{H}_2\text{SO}_4/\text{H}_2\text{O}_2$ ) leaving behind a layer of hydroxylated amorphous silicon oxide. This layer provides reactive sites for the attachment of trichlorosilyl functional groups ( $-\text{SiCl}_3$ ) of the SAM forming molecules to the substrate. Crosslinking between the trichlorosilyl groups, together with van der Waals interactions between the chains contribute to the formation of the SAM. Terminal functional groups of the SAM molecules can be used for facilitating the deposition of ceramic thin films. Additionally, the terminal functional group can be in-situ exchanged ( $\text{X} \rightarrow \text{Y}$ ) [1991Ulm]. Therefore the surface energy, the sign and magnitude of the surface charge density can be readily adjusted in order to meet the requirements of the subsequent film formation. This characteristic of the SAM makes it attractive for the film formation.

### 1.3.2. Deposition techniques

The main techniques for the non-electrochemical synthesis of thin films from aqueous solutions at low temperatures are:

- a. Chemical bath deposition (CBD)
- b. Successive ion layer adsorption and reaction (SILAR)
- c. Liquid phase deposition (LPD)

d. Electroless deposition (ED)

All of these techniques make use of solutions of simple metal salts, but differ in the reaction pathway to the metal oxide [2001Nie].

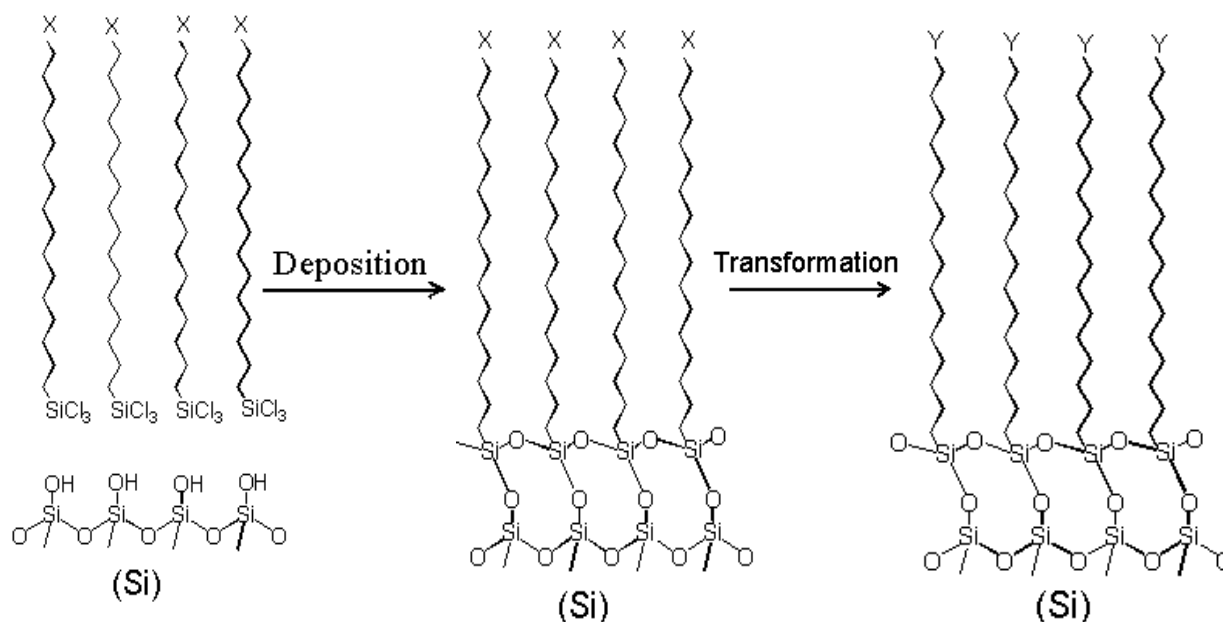


Fig. 1.3 The preparation of siloxane-anchored SAMs on silicon substrates.

a. Chemical bath deposition

Chemical bath deposition (CBD) of metal chalcogenide films is used commercially for the deposition of CdS thin films. Although literatures about this technique are dominated by work on sulfide and selenide thin films, this technique has been used also for the deposition of oxide thin films, with potential for large-area applications in semiconductor devices.

In chemical bath deposition experiments, the film formation mechanisms can be described by two models [1998O'B, 2001Nie], which are illustrated in Fig.1.4. The first is the so-called ion-by-ion process in which ions condense at the reacting surface to form the film. The second is termed as cluster-by-cluster process in which colloidal particles pre-formed in solution by homogeneous hydration reaction will be adsorbed at the surface of the substrate. In this case, polycrystalline films with random crystal orientation may be observed as a result. In practice both processes may occur simultaneously, leading to films in which colloidal particles are imbedded in a matrix phase originating from the ion-by-ion deposition.

The deposition medium for CBD of oxides consists of salts of metal ions ( $M^n$ ). Water serves as the source of oxygen. Careful control over the pH value of the solution and the temperature

is required. Moreover, CBD requires supersaturated solutions, i.e. the product of the concentrations of metal and chalcogenide must exceed the solubility product of the desired solid.

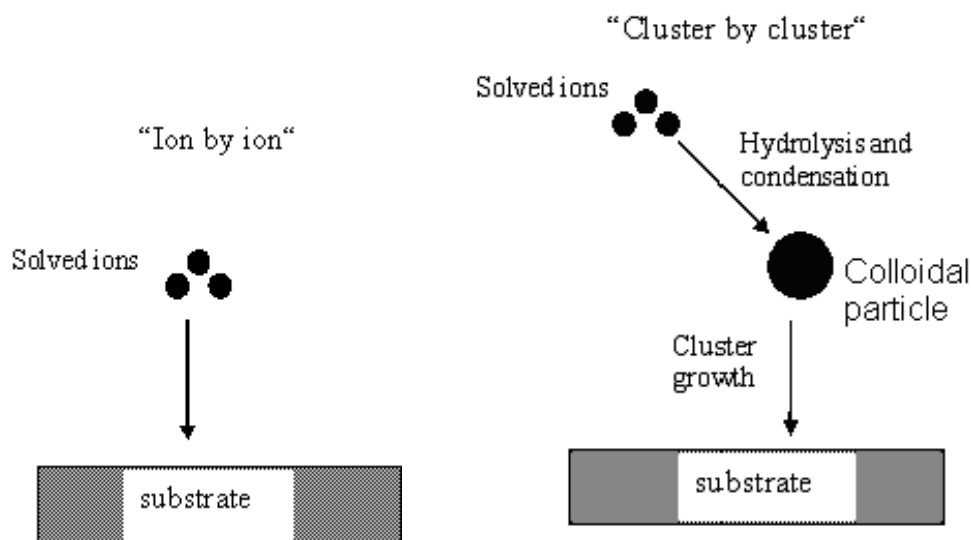


Fig. 1.4 Schematic representation of the heterogeneous and homogeneous formation process for thin films: ion-by-ion, and cluster-by-cluster.

Fundamentally, the formation of the colloidal particles can be divided into three steps [2000Jol]:

- 1) Formation of the zero-charged precursor  $[M(OH)_z(OH_2)_{n-z}]^0$ ,
- 2) Nucleation,
- 3) Growth of oxide nuclei,
- 4) Aging of oxide particles.

Two parameters seem to have a major influence on the deposition of thin films by CBD: 1) the free metal cation concentration; 2) the pH of the solution. ZnO films, e.g. grown from solutions of zinc acetate or zinc chloride at pH values between 6 and 8 consist of micrometer-sized hexagonal crystals [2004Hof]. Depending on the reaction conditions the hexagonal crystals can either grow oriented with c-axis normal to substrate [1996Ito, 2003Fuc, 2002Yam, 2002Boy], or in the form of irregular agglomerates [2003Fuc, 2002Boy]. The presence of such hexagonal shaped crystals is in accordance with investigations on the bulk precipitation of zinc oxide powders under comparable conditions, revealing that zincite has an explicit tendency to crystallize in the form of the elongated hexagonal needles. In contrast, precipitations of powders at pH values between 9 and 12 in the presence of amines as growth modifiers lead to an interesting variety of morphologies [1994Tri, 1990Chi], e.g. zincite films



grown on glass slides employing ethylenediamine or triethanolamine consisted of nodular and acicular particles.

a. Selective ion layer adsorption and reaction (SILAR)

The successive ionic-layer absorption and reaction process was developed for the formation of sulfide thin films [1985Nic]. A comparable technique for the deposition of oxide thin films [1985Ris] appeared independently. The distinguishing characteristic of SILAR is the alternating use of two different aqueous solutions (a metal salt solution, followed by a hydrolyzing or sulfidizing solution). In principle, this is intended to allow ion-by-ion growth of the compound film via sequential addition of individual atomic layers.

Whereas sulfide thin films were usually deposited at room temperature, polycrystalline (hexagonal) ZnO thin films were deposited onto glass, quartz and mica substrates by using hot water as the hydrolyzing agent. Here, the best film quality was obtained from tetra amine zinc(II) complex solutions, probably reflecting the ability of a complexing agent to control the rate of hydrolysis of CBD. The polycrystalline films exhibited a strong texture (c-axis normal to the substrate). Doping was achieved by adding a  $\text{Sn}^{2+}$  salt to the zinc deposition solution.

The crystal structure and the properties of the as-deposited films could be modified by heat treatment. Crystalline defects arising from the transformation of  $\text{Zn}(\text{OH})_2$  to ZnO during heating to 450°C were believed to cause the increased conductivity observed for such films [1996Jim]. The Doping of ZnO thin films by Ni and Cu was reported [1997Jim] as well.

b. Liquid phase deposition (LPD)

The term “liquid phase deposition” refers to the formation of oxide thin films from an aqueous solution of a metal-fluoro complex  $[\text{MF}_n]^{m-n}$  which is slowly hydrolyzed by adding water and boric acid ( $\text{H}_3\text{BO}_3$ ) or aluminum metal (Al). While the addition of water directly forces the precipitation of the oxide,  $\text{H}_3\text{BO}_3$  and Al act as fluoride scavengers, which destabilize the fluoro complex and force the oxide precipitation.

Unlike CBD and SILAR, LPD was developed originally (and is still used exclusively) for the deposition of oxide films. However, it is noteworthy that LPD does not lead to ZnO films directly but to  $\text{Zn}(\text{OH})\text{F}$  deposited on photolysed PTCS-SAMs when solutions of zinc chloride and ammonium fluoride were used. The conversion of  $\text{Zn}(\text{OH})\text{F}$  to ZnO, however, was achieved by annealing at 300°C [2001Sai].

c. Electroless deposition (ED)

ED describes procedures, in which redox reactions are involved [2001Nie]. To initiate and sustain the deposition process catalysis is required.

Recently, ZnO thin films were obtained from solutions of zinc nitrate and dimethylaminoborane [2000Iza, 1997Iza, 2002Ish]. The real mechanism is still unclear, though it is known to occur without visible hydrogen formation and does not succeed from zinc chloride solutions. It was proposed, that the nitrate ion is reduced by the borane and a subsequent reaction between the resulting hydroxide ions and zinc ions lead to the deposition of the oxide [2003Iza, 1997Iza, 2002Ish]. This course of the reaction would be related to the cathodic deposition of ZnO from the electrolysis of aqueous zinc nitrate solutions [1998Nyf]. The deposition of ZnO thin films on photo-patterned SAMs of phenyltrichlorosilane (PTCS) at 55°C was achieved by the above-mentioned ED reaction. For the nucleation of ZnO, palladium nanoparticles had to be deposited on the surface in advance [2003Iza]. Since the palladium catalyst attaches to the phenyl-terminated SAM molecules, the deposition of the ZnO was observed on these sites [2002Sai-1, 2002Sai-2].

#### 1.4. Mechanism of oxide film formation onto SAM

Functionalization of substrate surfaces by SAM enabled the deposition of oxides under conditions where no deposition would otherwise have occurred [1997Aga]. Furthermore, functionalized surfaces offer the possibility of patterned deposition. Hence it has been attempted to inspect the role of the SAM in film deposition. Though the mode of growth (ion-by-ion vs. particle attachment shown in Fig. 1.4) cannot be unambiguously ascertained by an examination of the microstructure, certain guidelines appear valid. The crystallographic randomness of the polycrystalline films argues strongly that homogeneous nucleation occurred, followed by particle attachment growth.

For films that contained crystals smaller than 100 nm, film formation was due to the particle attachment [1997Shi]. It was proposed that forces similar to those that exist between colloidal particles in fluids could lead to film growth. The DLVO (Derjaguin-Landau-Verwey-Overbeek) theory provided a means to estimate the magnitude of these forces.

In the DLVO approach, the total energy ( $V_{\text{tot}}$ ) between the interacting surfaces is given by

$$V_{\text{tot}} = V_e + V_a$$

Where  $V_e$  is the energy associated with electrostatic interactions. It can be either attractive or repulsive, depending on the charge of the interacting surfaces.  $V_a$  is the energy resulting from the London-van der Waals interaction and is always attractive.

(1) Electrostatic interaction

The electrostatic interaction energy between a SAM layer and the oxide particles can be expressed as [1997Shi]:

$$V_e = \frac{\epsilon_o \epsilon_r R}{4} \left[ (\psi_s + \psi_p)^2 \ln(1 + e^{-kx}) + (\psi_s - \psi_p)^2 \ln(1 - e^{-kx}) \right] \quad (1)$$

Where  $\epsilon_o$  is the permittivity of free space and  $\epsilon_r$  is the relative permittivity of the fluid medium.  $R$  is the particle radius,  $\Psi_s$  and  $\Psi_p$  are the surface potentials of the SAM surface and the particle respectively, and  $x$  is the particle surface-to substrate surface distance.  $\kappa^{-1}$  is the thickness of the diffuse electric double layer and can be calculated from

$$\kappa^{-1} = \sqrt{\frac{\epsilon_r \epsilon_o K_B T}{q_e^2 \sum_i N_i^2 \cdot Z_i^2}}, \quad (2)$$

where  $q_e$  is the charge of an electron,  $N_i$  is the number of ions of type  $i$  per cubic meter in the solution and  $Z_i$  is the valence of the ions,  $K_B$  is Boltzmann's constant and  $T$  is absolute temperature.

(2) Van der Waals interaction

The van der Waals potential energy between spherical particles and the SAM surface is given by [1987Hun]:

$$V_a = -\frac{A}{6} \left[ \frac{2R(R+x)}{x(x+2R)} - \ln\left(\frac{x+2R}{x}\right) \right], \quad (3)$$

where  $R$  is the radius of the particle and  $x$  the distance between the SAM surface and the particle surfaces.  $A$  is the Hamaker constant, which depends on the optical and dielectric properties of the particles, substrate surface and the intervening fluid medium.

### 1.5. Scope of the present work

Much of the interest in ZnO centers on the development of the nanodevices. However, ZnO films obtained with the above-mentioned techniques usually consist of micrometer-sized

crystals [1995Sae, 1998Bao]. Such films exhibit high surface roughness, and the adherence of the films is difficult to control. Most interestingly this is an intrinsic problem of many of the above-mentioned techniques and occurs regardless of the chosen chemical process.

Inspired by the polymer-controlled ZnO crystallization, one strategy to make the CBD process more applicable to ZnO thin films is the employment of growth controlling additives. Polymers like those mentioned in section 1.2, are known to inhibit the growth of distinct crystallographic planes of zincite crystals [1998Öne, 2002Tau-1] and are able to stabilize the equi-axed spherical nanometer-sized particles [2000Rie, 2002Ali, 2000Guo, 2001Guo].

In the author's group, the preparation of ZnO thin films from aqueous solution with the presence of a copolymer (P(MAA<sub>0.66</sub>-co(MAA-EO<sub>20</sub>)<sub>0.33</sub>)<sub>70</sub>) onto SAM-treated silicon wafers was pioneered [2003Fuc]. The preliminary work suggested that by adding the polymer to the deposition solution, the CBD method could be applicable for building nanostructured ZnO thin films. Homogenous ZnO films could be obtained from aqueous solution containing the copolymer on silicon wafers modified by mercapto-terminated SAM. The detailed mechanism however, is not yet clear and further investigation on the effect of copolymer and SAM on the film formation is therefore particularly necessary. Furthermore, in contrast to the polymer-controlled ZnO crystallization, the successful polymer-controlled ZnO thin film fabrication is more complicated because more factors are involved in the deposition system. Thus, studies on the deposition of nanostructured ZnO thin films onto the SAM-modified substrates via modified CBD form the subject of the present work.

The present work is arranged as follows: A general review concerning ZnO and the film deposition techniques related to that used in the present work is given in the first chapter. All characterization methods used and experimental procedure are described in the following chapter. The subsequent Chapters 3 and 4 are concerned with ZnO thin films deposited from aqueous solution containing zinc salts with the presence of a graft copolymer. Chapter 4 focuses specifically on annealing effects on the structure and photoluminescence of ZnO films obtained in this way. Chapter 5 deals with ZnO films obtained from a non-aqueous solution system containing polyvinylpyrrolidone. In the final Chapter 6, attempts are made to clarify the mechanisms of ZnO thin films formation onto SAM-modified substrates via CBD.

## **CHAPTER 2**

### **Experimental**

#### **2.1. Characterization methods**

##### **2.1.1. Scanning electron microscopy (SEM)**

SEM studies on the surface morphology of the films were performed with a JSM-6300F scanning microscope using an acceleration voltage of 3 kV. Some samples were also cleaved to facilitate the evaluation of the sample thickness by taking cross sectional scanning electron micrographs of the film. That was not applicable, however, to very thin films (< 50 nm) due to the insufficient resolution of the microscope.

##### **2.1.2. Atomic force microscopy (AFM)**

The surface topography was determined by using a Digital Instruments Nanoscope III in tapping mode utilizing silicon cantilevers. Several scans were taken over a given surface area to ascertain that there was no sample damage induced by the tip and scans were also repeated over several positions to obtain representative images. Height and voltage mode images were recorded at a scan rate of 0.5 Hz.

##### **2.1.3. X-ray photoelectron spectroscopy (XPS)**

The chemical composition of the films was investigated by X-ray photoelectron spectroscopy. XPS were recorded using a Thermo VG Thetaprobe system employing monochromatic incident Al K $\alpha$  radiation ( $h\nu = 1486.68$  eV) or Mg K $\alpha$  radiation (1253.6 eV). For data evaluation, the BE scale of each measured XPS spectrum was corrected for charging effects by setting the corresponding C 1s main peak for adventitious carbon to the recommended value of 284.6 eV. Each sample was analyzed at a detection angle of 53° relative to the surface normal. Survey spectra were first produced before the high-resolution scan for the detailed element scan.

#### 2.1.4. X-ray diffraction (XRD)

The structure of the annealed films was characterized by X-ray diffraction using a Bruker AXS diffractometer, with Bragg-Brentano geometry (equipped with a graphite monochromator in the diffracted beam to select Cu  $K_{\alpha}$  radiation). The XRD patterns from the annealed films were recorded in the range of  $2\theta = 10-60^{\circ}$ . Besides this technique, grazing incidence geometry with incident angles of  $1^{\circ}$  and  $2^{\circ}$  was also used for  $2\theta$  scans. Additionally the structural properties of the films were examined by x-ray diffraction using a Philips X'Pert  $K_{\alpha 1}$  diffractometer (equipped with a primary beam monochromator to select only  $K_{\alpha 1}$  radiation). Pole figure scans were done using the Philips MRD instrument with the intention to determine the texture of the annealed films.

#### 2.1.5. Ellipsometry

Ellipsometry measurements were performed using an ellipsometer (Woollam M2000L). A multi-layer model, which included silicon substrate,  $SiO_2$ , SAM (for as-deposited film) and film layer, was used to fit the experimental data obtained. The film layer was characterized by the optical constants (n: index of refraction, k: extinction coefficient), which could be represented as follows:

$$n(\lambda) = A + \frac{B}{\lambda^2} + \frac{C}{\lambda^4}$$
$$k(\lambda) = \alpha e^{\beta(12400(\frac{1}{\lambda} - \frac{1}{\gamma}))}$$

$\alpha$  : extinction coefficient amplitude,  $\beta$ : exponent factor,  $\gamma$  : band edge. A fit curve that matches well the experimental one can be obtained by defining these three parameters together with A, B, C. Thus the thickness of the film was determined according to the data generated from this model.

#### 2.1.6. Optical measurement

Photoluminescence spectra were measured at room temperature using a spectrometer utilizing a continuous wave He-Cd laser and another instrument with a Xe lamp (FluoroMax-3, Jobin Yvon-Horiba). In the latter case appropriate filters to avoid second-order contributions were installed in the emission light path.

The optical transmission of the ZnO thin film deposited on glass was measured using the Varian Cary 5E UV-Vis-NIR spectrophotometer. The measurements were made from the far infrared to the periphery of ultraviolet region (starting from 2000 to 400 nm).

### **2.1.7. Transmission electron microscopy (TEM)**

The microstructure of the films was examined using a JEOL 4000 FX TEM microscope (acceleration voltage 400 kV), which has a point resolution of 1.7 nm. Besides bright-field, dark-field micrographs, high-resolution TEM images were recorded.

Spatially resolved EELS analysis was performed with a dedicated scanning transmission electron microscope (STEM, model HB501) with a Gatan 666 parallel EELS spectrometer.

Plan-view and cross-section specimens were prepared for TEM investigation. Detailed specimen preparation is described in the following section.

### **2.1.8. TEM specimen preparation**

Transmission electron microscopy (TEM) has become an effective and important technique in the characterization of all kinds of materials and structural defects. Specimens prepared for TEM investigations have to fulfill several physical properties to enable high-quality analyses [2003Str]. The specimen should have a uniform thickness over the area of interest, and should also be transparent for electron beams. For conventional TEM investigations, a thickness in the range of several 100 nm is acceptable. For analytical and high-resolution transmission electron microscopy, however, thickness below 100 nm is more favorable. In addition, the structure visible in the prepared specimen should be representative of that found in the bulk material, in other words the microstructure should be unaltered by the preparation procedure. Therefore specimen preparation is a crucial part for successful TEM study. The specimen can be examined in either cross-section or plan-view.

#### **2.1.8.1. Cross-sectional preparation**

In the following, a procedure for the preparation of cross-sectional TEM specimen of the ZnO thin films including cutting, grinding, dimpling, and ion-milling is described.

##### **1) Cutting**

Slices of ZnO/Si samples with a width of ~2.5 mm were prepared by cleaving the coated substrates. The single crystal silicon (100) wafers cleave easily along the <100> direction. Besides cleavage, wire sawing was used for cutting. In this case, the film side was either protected by a layer of wax, or coated with a aluminum (Al) thin film using sputtering before cutting.

Two sample slices were glued together face-to-face on the coating side with epoxy, cured in the furnace (150°C) under pressure for 1.5 h to obtain a strong bond with minimum glue thickness (< 1 μm). For ZnO films obtained from the deposition system containing polyvinylpyrrolidone (see Chapter 2.3.2.), such high temperature should be avoided, therefore an attempt was made to allow the glued sample be cured at room temperature. In this case, a special epoxy resin was used to glue the sample pieces together and the glued sample was then cured at room temperature under pressure for two days to obtain a strong bond. Subsequently two pieces of pure silicon were glued to both sides of the sample respectively in order to make the cross-section of the whole sandwich reach 3 mm in size. Finally, a thin piece with a thickness of 0.8 mm was cut on a wire saw.

## 2) Mechanical grinding

The piece of 0.8 mm thickness was glued onto a steel support. Using the Gatan model 623 Disc Grinder, one cross-section side of the sample was ground, further polished with ¼ μm polishing paper until a flat and smooth plane was reached (Fig. 2.1). The sample was removed from the steel support and cleaned in acetone. Subsequently the sample was glued onto a plastic support with the unpolished side exposed. Precise grinding with this side was performed until the total sample thickness reached 80~100μm.

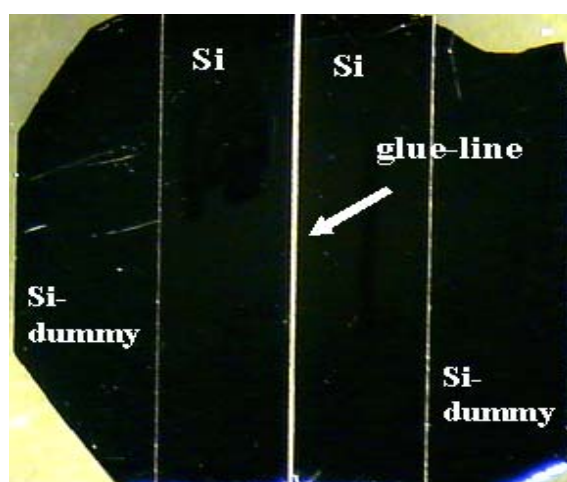


Fig. 2.1 TEM specimen with one-side polished.



### 3) Precision polishing

The plane was further ground and polished on a Gatan model 656 Dimple Grinder (shown in Fig. 2.2) prior to ion milling. Grinding is halted when a preset thickness (e.g 30  $\mu\text{m}$ ) is reached. Further polishing was performed until the small area under the dimpler was transparent to visible light, in which case the thin area thickness is about 10-20 $\mu\text{m}$ .



Fig. 2.2 Gatan model 656 dimpler grinder.

### 4) Specimen quality control

Specimens were examined by performing distance measurements with a thickness sensor prior to ion-milling. Exact final shape, thickness, roughness could be obtained by this contact free method. Fig. 2.3 shows the overview and 3D geometry of one specimen (ZnO film on silicon wafer) after precision dimpling. The specimen exhibits symmetric dimpling centre with final thickness in 10  $\mu\text{m}$ , with total thickness of 85  $\mu\text{m}$  and roughness between 100-200 nm.

### 5) Ion-Milling

The sandwich specimen was glued onto a copper ring to increase the stability so that one can easily handle the specimen. The specimen was mounted gently into a Gatan Duo 691 precision ion-milling machine with the 4 kV Ar<sup>+</sup> ion guns sputtering both sides of the specimen until perforation. The additional low-voltage ion milling (LVIM) polishing was accepted as a final polishing procedure before taking out the specimen, which has been proven to be able to largely decrease the amorphous areas induced by the ion-milling [2003Sch].

### 2.1.8.2. Plan-view sample preparation

For the preparation of a plan-view ZnO/Si sample, only the silicon substrate side was polished, until the total thickness of the film and the substrate reached  $\sim 90 \mu\text{m}$ , followed by dimple grinding and polishing the same side to a thickness of  $< 25 \mu\text{m}$ . the silicon substrate side was ion-milled by 4 kV Ar<sup>+</sup> ion until perforation, followed by the brief low-voltage ion milling as a final step.

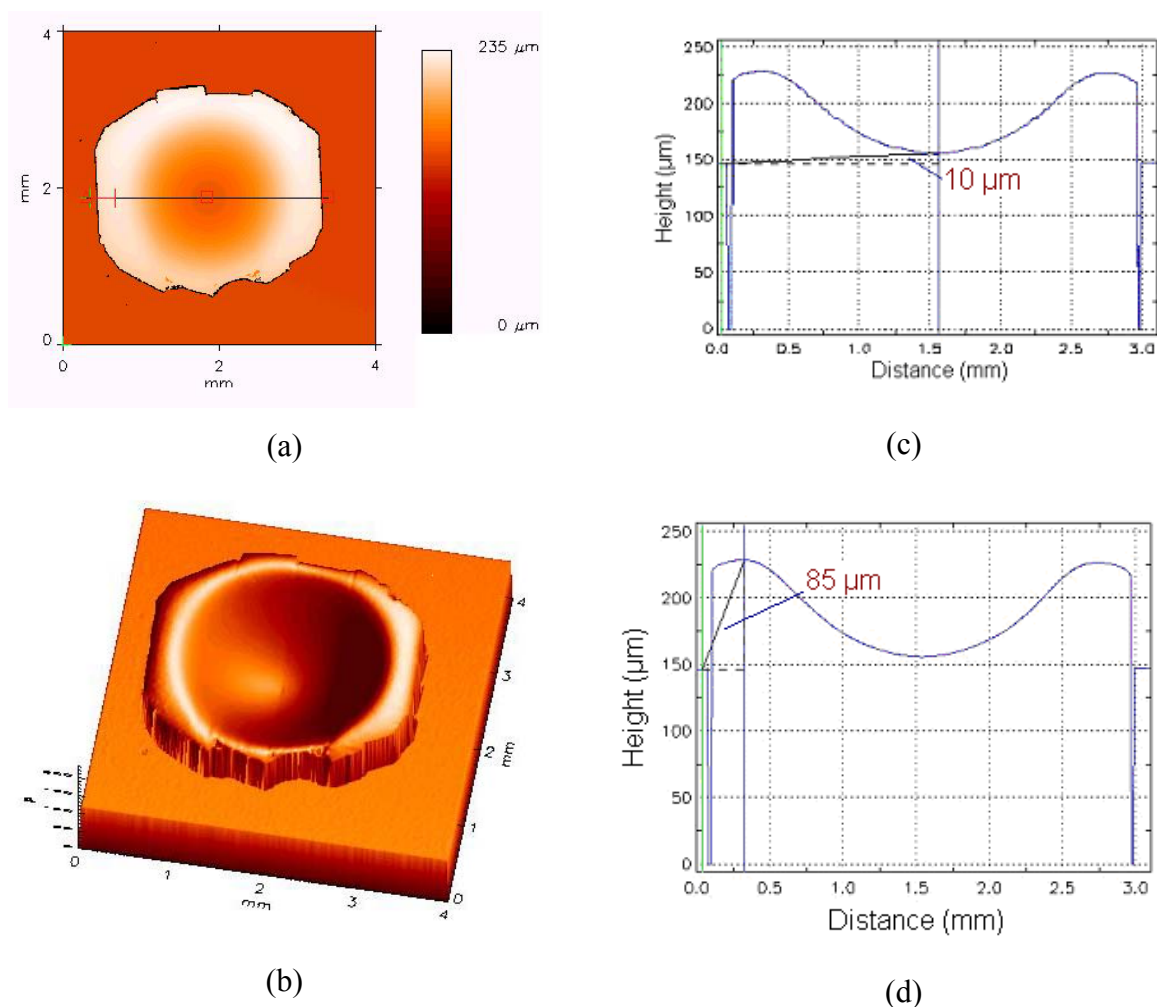


Fig. 2.3 (a-b) Overview and 3D of dimpling side of the specimen. (c) Profile measurement revealing a final thickness of  $10 \mu\text{m}$  after dimpling, (d) Finished sample exhibits a thickness of  $85 \mu\text{m}$ .

### 2.1.9. Zeta potential Measurement

A Zetasizer Malvern 3000 HS<sub>A</sub> was used to measure the electrophoretic mobility. For suspensions of ZnO particles in the presence of the PMAA-PEO graft-copolymer (see Chapter

2.3.1.) measurements were conducted in an aqueous solution of 1 mM aqueous  $\text{KNO}_3$  at  $25^\circ\text{C}$ . The diluted suspension of ZnO (Alfa, BET surface area  $5.788 \text{ m}^2\cdot\text{g}^{-1}$ , particle size distribution from 50 % of the particles ( $d_{50}$ )  $0.780 \mu\text{m}$ ,) was sonicated for deagglomeration. The first measurement was carried out at the intrinsic pH value of the ZnO suspension. The pH was then changed by addition of a 250 mM KOH solution or the dropwise addition of a concentrated aqueous solution of the PMAA-graft-PEO copolymer respectively. To improve the reliability, a series of three separate measurements was collected for each system.

Zeta potential of the ZnO particles with the presence of polyvinylpyrrolidone (PVP) in both aqueous solution and 2-propanol was also measured. The first measurement was carried out at the intrinsic pH value of the ZnO suspension. In case of in aqueous solution, the pH was then changed by addition of a NaOH solution or the dropwise addition of an aqueous solution of the PVP respectively. Whereas in 2-propanol, the deposition solution was taken for measurement and the pH was further changed by addition of a NaOH solution.

## 2.2. SAM deposition

Substrates (silicon wafers, microscope slides) were cleaned, oxidized in piranha solution (70 vol% of  $\text{H}_2\text{SO}_4$ , 30 vol% of 30 wt%  $\text{H}_2\text{O}_2$  aqueous solution) and washed copiously with distilled water afterwards. The SAM was subsequently deposited on these substrates and the surface group of the SAM was converted to the desired one by in-situ transformation (Fig. 2.4).

The freshly hydroxylated substrates were dipped into a 1,1'- bicyclohexyl solution containing 1 vol % of 1-thioacetato-16- (trichlorosilyl)hexadecane at room temperature under argon atmosphere for 5 h and washed thoroughly in chloroform afterwards. Under these conditions a thioacetate-terminated SAM formed spontaneously (Fig. 2.4a).

To convert the thioacetate ( $-\text{SCOCH}_3$ ) into the desired mercapto ( $-\text{SH}$ ) functionality, the substrates were immersed in a 1 M solution of pyrrolidine in acetonitrile at room temperature under argon atmosphere for 4 h [1999Yel] (Fig. 2.4a). Finally, the substrates were soaked in acetonitrile, then washed in ethanol thoroughly, and dried with a stream of dry argon gas.

For conversion of the thioacetate into a sulfonate ( $-\text{SO}_3\text{H}$ ) functionality, the coated substrates were immersed in oxone (potassium hydrogenmonopersulfate, Merck) for a minimum of 4 h at room temperature [1995Col, 2001Nie] (Fig. 2.4a). Finally, the coated substrates were washed in distilled water thoroughly, and dried with a stream of dry argon gas.

Surface functionalization by molecules with chain lengths of only three carbon atoms were also prepared by dipping fresh hydroxylated silicon wafers into a 4 mM  $\gamma$ -mercaptopropyltrimethoxysilane solution in dry toluene under argon atmosphere (Fig. 2.4b). After 5 h, substrates bearing  $-(\text{CH}_2)_3\text{-SH}$  groups were obtained. In order to control the quality of the SAM, attention was paid to the amount of the surfactant and the type of solvent. A higher concentration of the surfactant or the use of undried or even protic solvents, such as ethanol, led to the deposition of whitish stains on the silicon wafers, which presumably consisted of oligomeric silanes [2003Hof, 2001Hu]. No uniform formation of ZnO films was observed on such stained wafers.

For a bromide (-Br) terminated SAM the freshly hydroxylated substrates were dipped into a 1,1'-bicyclohexyl solution containing 1 vol % of 1-bromo-16-(trichlorosilyl)hexadecane at room temperature under argon atmosphere for 5 h (Fig. 2.4c). Finally, the coated substrates were thoroughly washed in chloroform.

To convert the bromide into the an azide ( $-\text{N}_3$ ) functionality, the substrates bearing  $-\text{C}_{16}\text{-Br}$  were immersed in a 20 ml of dry *N,N*-dimethylformamide (DMF) containing 200 mg  $\text{NaN}_3$  under argon at room temperature overnight (Fig. 2.4c). Finally, the coated substrates were washed in chloroform thoroughly, and dried with a stream of dry argon gas.

The amine ( $-\text{NH}_2$ ) was obtained by transformation from the azide functionality (Fig. 2.4c). The substrates coated with  $\text{N}_3$ -terminated monolayer were dipped into a 20 ml saturated lithium aluminum hydride ( $\text{LiAlH}_4$ ) in ether under argon overnight. Finally the coated substrates were dipped into dry  $\text{Et}_3\text{N}$  for 2 h followed by thorough washing with chloroform, and dried with a stream of dry argon gas.

Contact angle measurements were made to confirm the success of the conversion according to the contact angle of the functional groups listed in Table 2.1 [1990Bal].

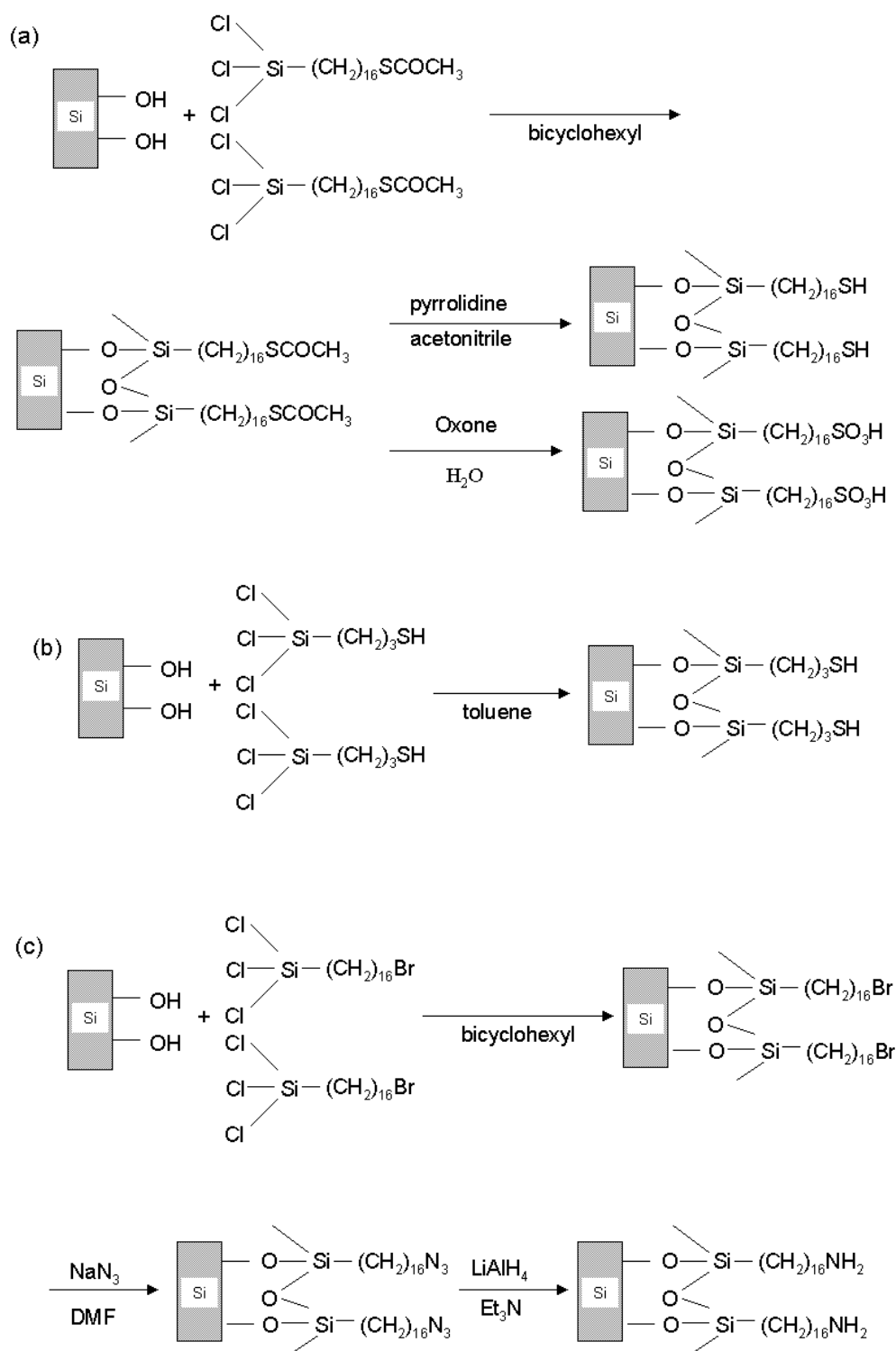


Fig. 2.4 Schematic depiction of the deposition of (a) a thioacetate-functionalized SAM and its transformation to a mercapto- and sulfonate functionalized SAM, (b) a mercapto-functionalized SAM bearing hydrocarbons with chain lengths of three carbon atoms and (c) a bromide-terminated SAM and its transformation to an azide functionalized SAM and further to an amine functionalized SAM.

Table 2.1 Water contact angles of functionalized monolayer surfaces

surface group	advancing water contact angle, deg	receding water contact angle, deg
SCOCH <sub>3</sub>	73±3	65±3
SH	71±3	49±3
SO <sub>3</sub> H	30±2	<10
Br	82±1	77±1
N <sub>3</sub>	77±2	71±2
NH <sub>2</sub>	63±2	42±4

## 2.3. Film deposition

### 2.3.1. Copolymer system

For film deposition reaction solutions consisting of anhydrous ZnCl<sub>2</sub> (0.1 M), hexamethylenetetraamine (HMTA, 1 to 7 mM) and a graft copolymer P(MAA<sub>0.50</sub>-co(MAA-EO<sub>20</sub>)<sub>0.50</sub>)<sub>70</sub> (polymethacrylic acid partially grafted with polyethyleneoxide side chains, 1000-4000 ppm) diluted in deionized water were used. The purpose of the addition of HMTA, which is known to decompose between 60°C and 80°C, was to generate OH<sup>-</sup> ions and correspondingly to result in an increase of the pH value.

To ensure an optically clear solution for the deposition process (i.e. without any turbidity or precipitates) the zinc salt deposition solutions were prepared as follows [2002Hof]. The desired quantity of ZnCl<sub>2</sub> and the ammonium salt of the copolymer were dissolved in 50 ml of water. Then a second solution of the desired amount of HMTA in 50 ml of water was prepared and added to the first solution.

The substrates modified by SAMs were immersed in 10 ml aliquots of the deposition solution, covered and then placed in an oil bath at 80 °C. The solution was renewed every 1 h or 1.5 h, which allows the film growth to occur at the high rates found in the initial stage of deposition. The film thickness was adjusted by varying the deposition time and the total deposition time has been 7.5 h. Finally, the samples were washed with distilled water, dried in a stream of dry argon.

Although the adherence was not quantified, it should be noted, that the films could be subjected to a standard preparation for TEM cross-section micrographs. Furthermore a simple tape-peel test with commercial adhesive tape could not remove the films.

Post-annealing of the films obtained was performed in a program-controlled furnace (Nabertherm S27) at 450°C, 500°C, 600°C, and 700°C for 4h in air (heating rate 20-40 °C/h, cooling rate 40 °C/h).

### 2.3.2. Polyvinylpyrrolidone system

For the preparation of the precursor solution 0.110 g (0.5 mmol)  $\text{Zn}(\text{CH}_3\text{COO})_2 \cdot 2\text{H}_2\text{O}$  (from Aldrich) was dissolved in 20 ml of 2-propanol containing 0.6 vol % distilled water under vigorous stirring at 50 °C. Before adding  $\text{Zn}(\text{CH}_3\text{COO})_2 \cdot 2\text{H}_2\text{O}$  into 2-propanol it was dissolved in distilled water. The solution was then diluted with 2-propanol to a total volume of 50 ml, followed by chilling to 0 °C. Then PVP (Fig. 2.5) was dissolved in this solution in [PVP]/[Zn] molar ratios of 1.5:5, 2:5, 2.5:5, 2.75:5 and 3:5 respectively at room temperature with the aid of ultrasound. Finally, a solution of 0.04 g NaOH in 10 ml 2-propanol containing 3.3 vol % distilled water (pellets of sodium hydroxide dissolved firstly in water then 2-propanol was added at 50 °C) was prepared and added dropwise under continuous stirring by using a peristaltic pump. After placed into an ultrasonic bath for 10 min, the solution was ready for the deposition. This preparation method yields a precursor solution with [Zn] concentration of 10 mM, which is about five orders of magnitude higher than that reported before in the literature [2000Guo]. Table 2.2 shows the solution appearance prepared with various [PVP]/[Zn] molar ratios. It is noteworthy that when no PVP added, the solution turned milky immediately after NaOH was added into  $\text{Zn}(\text{CH}_3\text{COO})_2 \cdot 2\text{H}_2\text{O}$ .

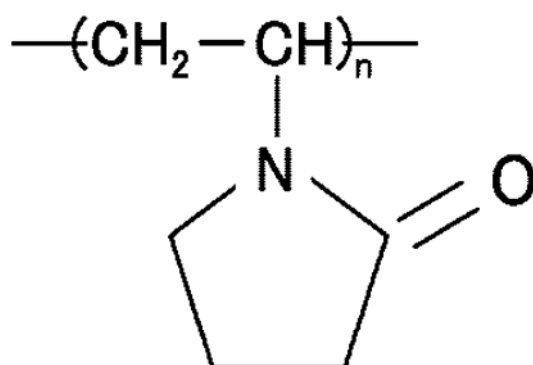


Fig. 2.5 Chemical structure of polyvinylpyrrolidone.

Table 2.2 Appearance of the solutions prepared for film deposition

<i>PVP/[Zn] molar ratio</i>	<i>Solution appearance</i>
<b>without PVP</b>	The solution develops a milky appearance during preparation.
<b>1:5</b>	The solution gets milky shortly after it is ready for deposition.
<b>1.5:5</b>	The solution gets a little turbid during deposition at 55 °C.
<b>2:5</b>	Deposition solution remains clear during deposition.
<b>3:5</b>	Deposition solution remains clear during deposition.

Another concentrated precursor solution was prepared in the similar way. 0.11 g dihydrate zincacetate dissolved in 40 ml of 2-propanol. Then PVP was added with a [PVP]/[Zn] molar ratio of 3:5 at room temperature with the aid of ultrasound. Finally, 0.04 g NaOH dissolved in 8 ml 2-propanol was added dropwise under continuous stirring by using a peristaltic pump. Small amounts of water similar to that in the above described less concentrated solution were also added. This preparation method yields a precursor solution with [Zn] concentration of 12.5 mM.

For the deposition of ZnO films substrates were immersed in 10 ml aliquots of the deposition solution, covered and then placed in an oil bath at 55 °C. The deposition solution was renewed every 1-1.5 h. Finally, the samples were washed with distilled water, dried in a stream of dry argon.



## CHAPTER 3

### Influence of anionic graft-copolymers on the formation of ZnO thin films in chemical bath deposition

#### 3.1. Scope of the studies

The present chapter describes the ZnO film deposition onto the SAM-treated substrates from aqueous solution containing zinc salt and hexamethylenetetraamine (HMTA) with the presence of a polyanionic graft copolymer (polymethacrylic acid partially grafted with polyethyleneoxide side chains). These two components of this copolymer (Fig. 3.1) function as follows [1998Öne]: the PMAA unit interacts with the surface of the particle and acts as an anchor group. The PEO moiety does not bind to the surface and serves as a sterical shield, preventing particles from agglomeration. This concept was used in the present study to stabilize ZnO nanometer-sized particles by the adsorption of the graft copolymer to their surface, and by that preventing them from rapid growth.

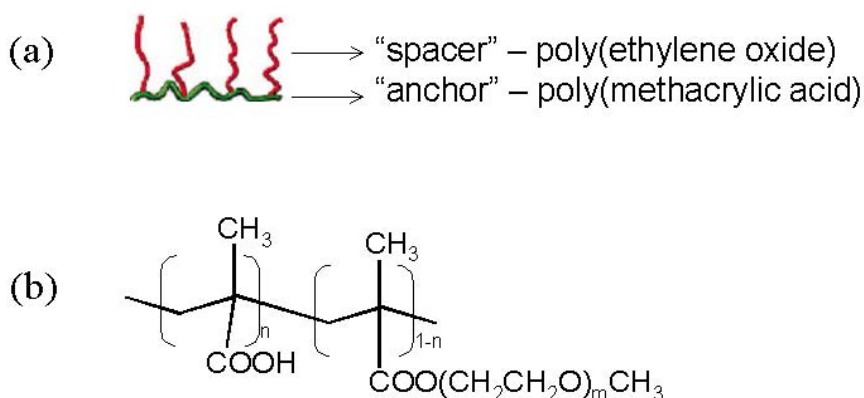


Fig. 3.1 Schematic illustration of the copolymer (a) and its chemical structure (b).

The surface chemistry of the substrate is another decisive factor. In order to investigate this influence, depositions on the following substrates were carried out:

- silicon with mercapto-terminated SAMs (C<sub>16</sub>-SH).
- glass with mercapto-terminated SAMs (C<sub>16</sub>-SH).
- silicon with mercapto-terminated SAMs (C<sub>3</sub>-SH).
- silicon with SAMs bearing various surface groups such as C<sub>16</sub>-SCOCH<sub>3</sub>, C<sub>16</sub>-SO<sub>3</sub>H, C<sub>16</sub>-N<sub>3</sub>, C<sub>16</sub>-NH<sub>2</sub>, C<sub>16</sub>-Br.

The characterization of the substrates concentrated on the morphology (SEM, AFM), however,

further work included the analysis of the microstructure (TEM) and the chemical composition of the films (XPS).

It should be noted that mercapto-terminated SAMs bearing a chain length of 16 carbon atoms (C<sub>16</sub>-SH) were used for film formation in the following. In case a mercapto-terminated SAM with a chain length of three carbon atoms (C<sub>3</sub>-SH) was used, it will be specifically indicated.

## **3.2. Depositions on silicon wafers modified with mercapto-terminated SAMs**

### **3.2.1. Influence of the composition of the reaction solution on the film morphology**

Films were obtained from solutions of zinc chloride, HMTA and graft copolymer. The influence of the concentrations of copolymer and HMTA on the growth rate and the film morphology was investigated.

Detailed studies on the ZnO film formation on silicon wafers modified by mercapto-terminated SAM were conducted (Table 3.1). AFM images of three ZnO films deposited from solutions, which contained the same amounts of zinc salt and copolymer (100 mM ZnCl<sub>2</sub>, 4000 ppm of the copolymer), but differed in the concentration of HMTA (3 mM, 4 mM and 7 mM respectively), are shown in Fig. 3.2. Three distinctive morphologies of the deposited ZnO could be identified in these micrographs. At the HMTA concentration of 3 mM (Fig. 3.2a), no complete film but only sporadic deposits of ZnO (mainly particles or agglomerates with around 20 nm in height) were observed after deposition time of 7.5 h. Whereas homogenous and uniform film with a thickness of 64 nm was obtained, at the intermediate HMTA concentration of 4 mM (Fig. 3.2b), after the same deposition time. With further increasing the concentration of HMTA to 7 mM, the film exhibited canyon-like feature and the film thickness was more than doubled (140 nm) after the same time of deposition (Fig. 3.2c). SEM micrographs (Fig. 3.3) are shown to be consistent with the AFM images. However, the island-like features presented in AFM results couldn't be readily observed due to the low resolution of the SEM for the film developed with the concentration of the HMTA below 3 mM. Complete macroscopic coverage of the wafer with a uniform film was observed (Fig. 3.3a) with HMTA concentration higher than 4 mM. Moreover, canyon-like features were also observed in the film with more than 7 mM HMTA (Fig. 3.3b).

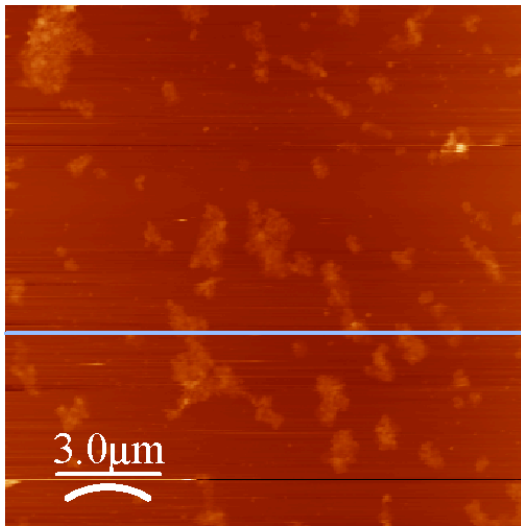
At even higher concentrations of HMTA, bulk precipitation occurred in the solution and the reaction solution rapidly turned turbid. On the substrate only larger particles as a result of sedimentation could be observed. These observations indicate that the degree of

supersaturation of the reaction solution must be carefully controlled in order to achieve an optimal film growth.

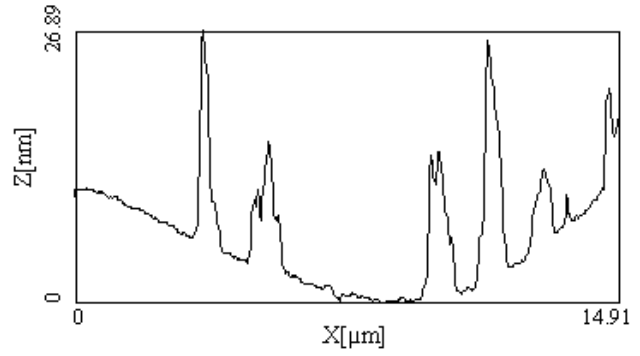
Table 3.1 Experimental parameters used for film deposition on mercapto-terminated SAM (100 mM ZnCl<sub>2</sub>) and the results after deposition time of 7.5 h.

Copolymer (ppm)	HMTA (mM)	Film morphology
1000	2	No film (precipitates)
	3	
2000	1	No complete film
	2	Uniform thin film
	3	Film with canyon-like feature
	3.5	
	4.5	
	5	No film (precipitates)
2500	1.5	No complete film
	2	
3000	2	No complete film
	3	Uniform thin film
	5	Film with canyon-like feature
	7	No film (precipitates)
4000	3	Island-like film
	4	Uniform thin film
	5	Film with canyon-like feature
	6	
	6.5	
	7	

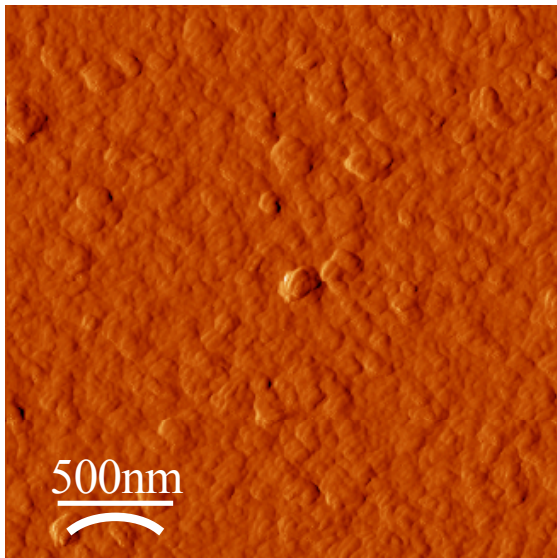
Further experiments showed that the concentration of the copolymer influences the film morphology in a similar way. The addition of the copolymer prevents bulk precipitation in the reaction solution, whereas rather high concentrations inhibit the film growth. At a given HMTA concentration, an optimum value for the copolymer exists, which allows the deposition of homogeneous smooth or also canyon-featured films.



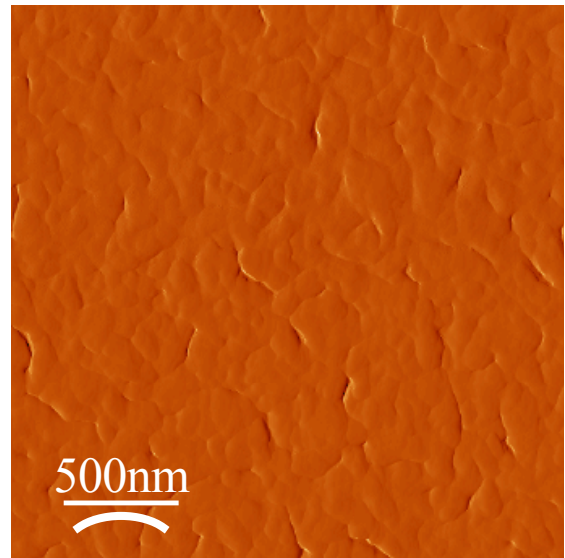
(a)



(b)

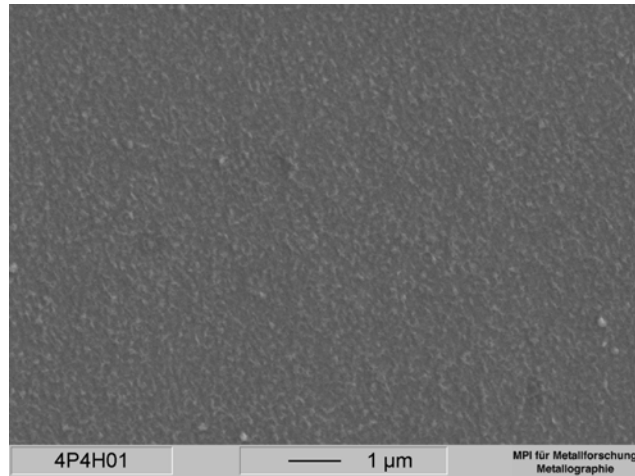


(c)

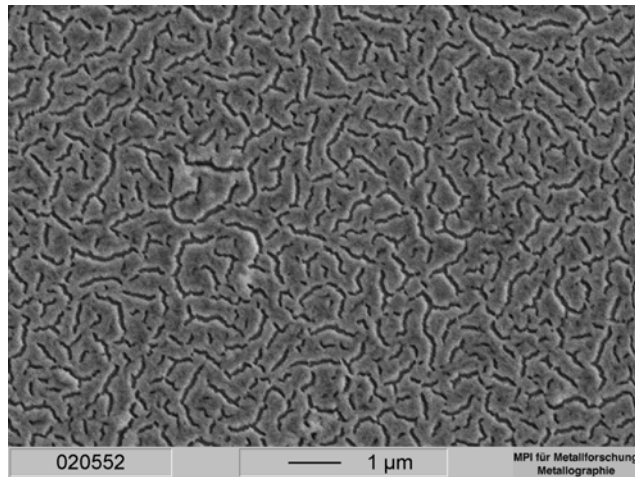


(d)

Fig. 3.2 AFM image of as-deposited film grown at 80 °C for 7.5 h on a SH-modified silicon wafer from a solution containing 100 mM [Zn], 4000 ppm copolymer and (a,b) 3 mM HMTA and accompanying line profile, (c) 4 mM HMTA and (d) 7 mM HMTA.



(a)



(b)

Fig. 3.3 SEM micrographs of as-deposited film grown at 80 °C after 7.5 h on a SH-modified silicon wafer from a solution containing 100 mM [Zn], 4000 ppm copolymer and (a) 4 mM HMTA and (b) 7 mM HMTA.

A film formation diagram was established based on the SEM and AFM results and it is shown in Fig. 3.4. There are three areas in which films are characterized by three distinct film morphologies, which are separated by dashed lines. In the upper left area no complete but only island-like films were formed. In the neighboring area a complete coverage of the substrate by uniform films were observed. In the third area films were formed exhibiting canyon-like features. The solid line shown in the Fig. 3.4 represents the conditions below which the solution develops a milky appearance and no films develop at all.

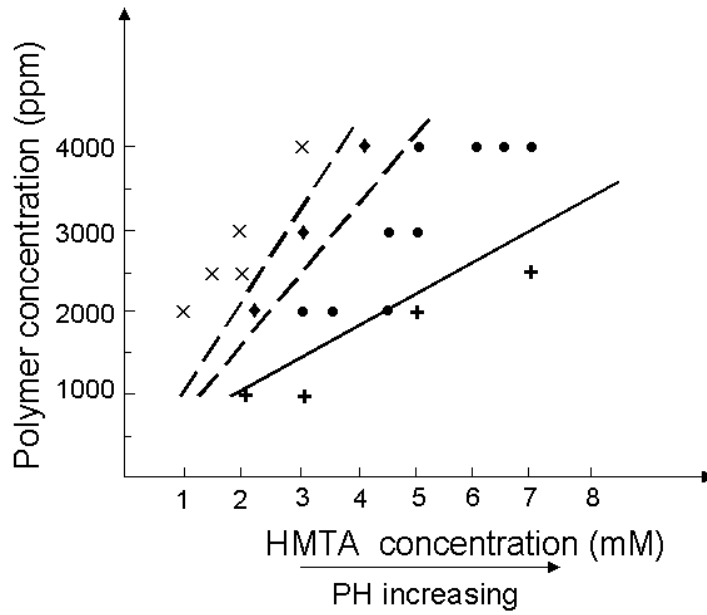
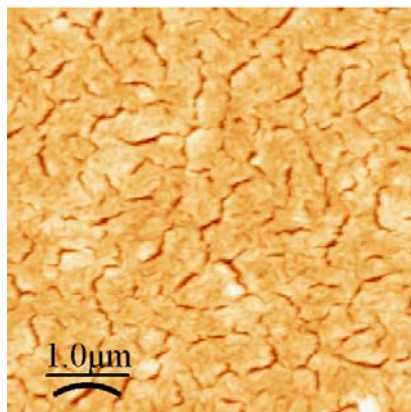


Fig. 3.4 Film formation diagram showing the influence of deposition conditions on the film formation: (x) island-like films, (♦) uniform films (•) films with canyons, and (+) no film formation.

### 3.2.2. Possible quantification of the surface coverage by AFM

Fig. 3.5a shows the AFM image of a ZnO film exhibiting canyon-like features. The canyon-type area, that is, an un-occupied area of the substrate could be quantified. This un-occupied area (which was highlighted as hole area in Fig. 3.5b) is about 5 % of the substrate surface. It can also be seen that the areas of the holes are regularly distributed over the whole substrate surface. The area distributions of the canyon-type areas are shown in Fig. 3.5c.



(a)

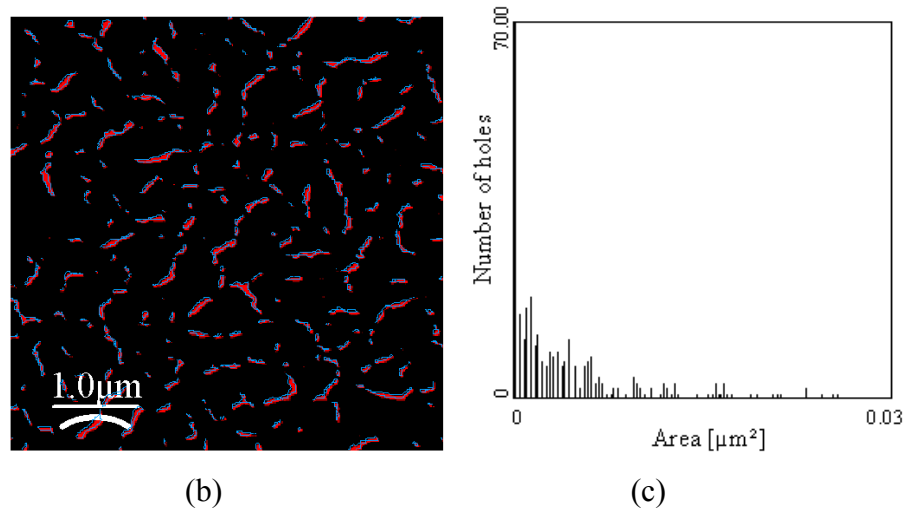


Fig. 3.5 (a) AFM micrographs of as-deposited film grown after 8 h on a SH-modified silicon wafer from a solution containing 100mM [Zn], 4000 ppm copolymer and 7 mM HMTA. (b) Film unoccupied areas (light areas) in Fig. 3.5a. (c) Area distribution of the film unoccupied area.

Films with porous structures can find their applications in different fields. O'Brien et al. covered the synthesis of nanoporous TiO<sub>2</sub> and ZnO films on conducting glass substrates for potential use in dye sensitized cell and related optoelectronic devices [1996O'B]. Moreover, porous films can also be used on dental and orthopedic implants to enhance bone growth on implants [2001Aki]. The present ZnO film synthesis shows another approach to the preparation of such kind of films used in these fields.

### 3.2.3. TEM investigations

TEM micrographs of the ZnO film annealed at 450°C for 4.5 h after initial deposition from a solution containing 100 mM [Zn], 2000 ppm copolymer and 3.5 mM HMTA for 6 h are shown in Fig. 3.6. The film exhibits a thickness of around 60 nm (Fig. 3.6a). The native SiO<sub>2</sub> layer between the silicon substrate and ZnO film has a thickness of 2.5 nm, which is indicated by the arrows. Upon heating pyrolysis of the organic SAM interlayer is expected. Wang et al. [1998Wan] indicated the organic film burned off completely within 2 h at temperatures between 200 °C and 400 °C by studying the thermal decomposition of the silanol-anchored SAMs with and without overlying oxide films. Shin et al. [1999Shi] investigated the pyrolysis of the SAM layer beneath the top TiO<sub>2</sub> thin films as well and similar results were indicated. Interestingly, consistent with the results from other groups [1997Aga], TEM study in the present work reveals no disruption of the adhesion of the inorganic overlayer in spite of the

pyrolysis. The reason for that can be attributed to the extremely small amount of the hydrocarbon combustion products, thus the pyrolysis of the SAM is not expected to deteriorate the adhesion of the films [2001Nie].

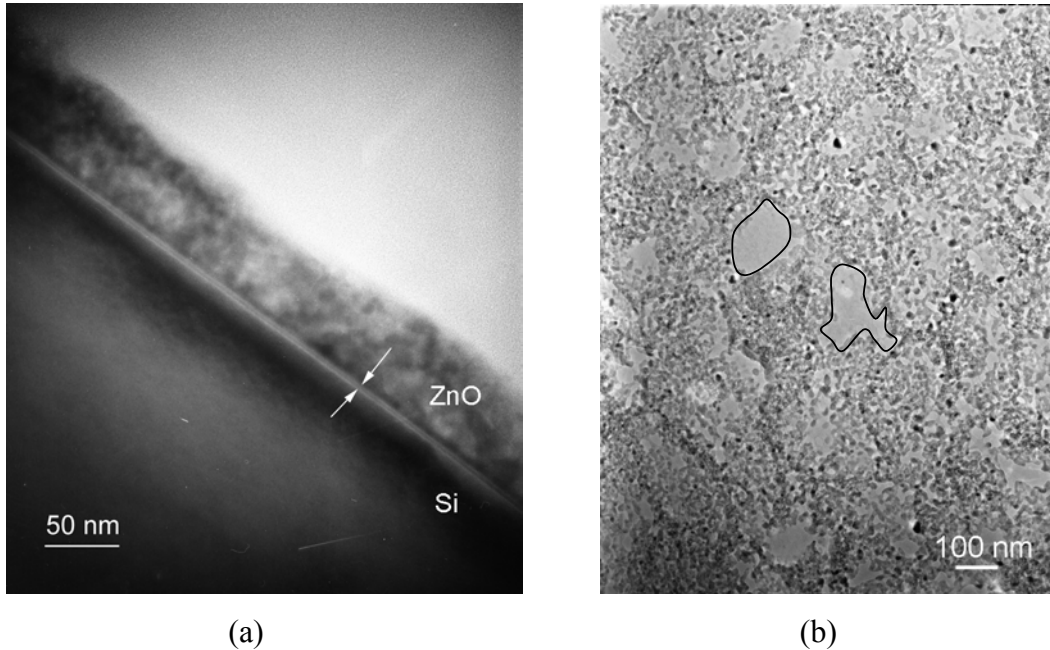


Fig. 3.6 (a) Cross-sectional and (b) plan view TEM micrograph of the ZnO film annealed at 450°C for 4.5 h in air, after initial deposition onto mercapto-terminated SAM-treated silicon wafer from solution of 100 mM, [Zn], 2000 ppm copolymer and 3.5 mM HMTA for 6 h. Open porous area is marked.

A plan-view TEM image of the same sample is shown in Fig. 3.6b. The ZnO film was not completely developed on the whole substrate surface and some uncovered areas can be seen on the surface (the porous area is marked in the Fig. 3.6b).

The plan-view TEM micrographs with higher magnification of the above-mentioned ZnO film are shown in Fig. 3.7. The dark-field (DF) image (Fig. 3.7b) shows that the ZnO film comprises nanocrystallites with an average size of 7 nm. The corresponding diffraction (SAD) pattern shown in Fig. 3.7c also reveals that the film is polycrystalline and has a wurtzite structure.



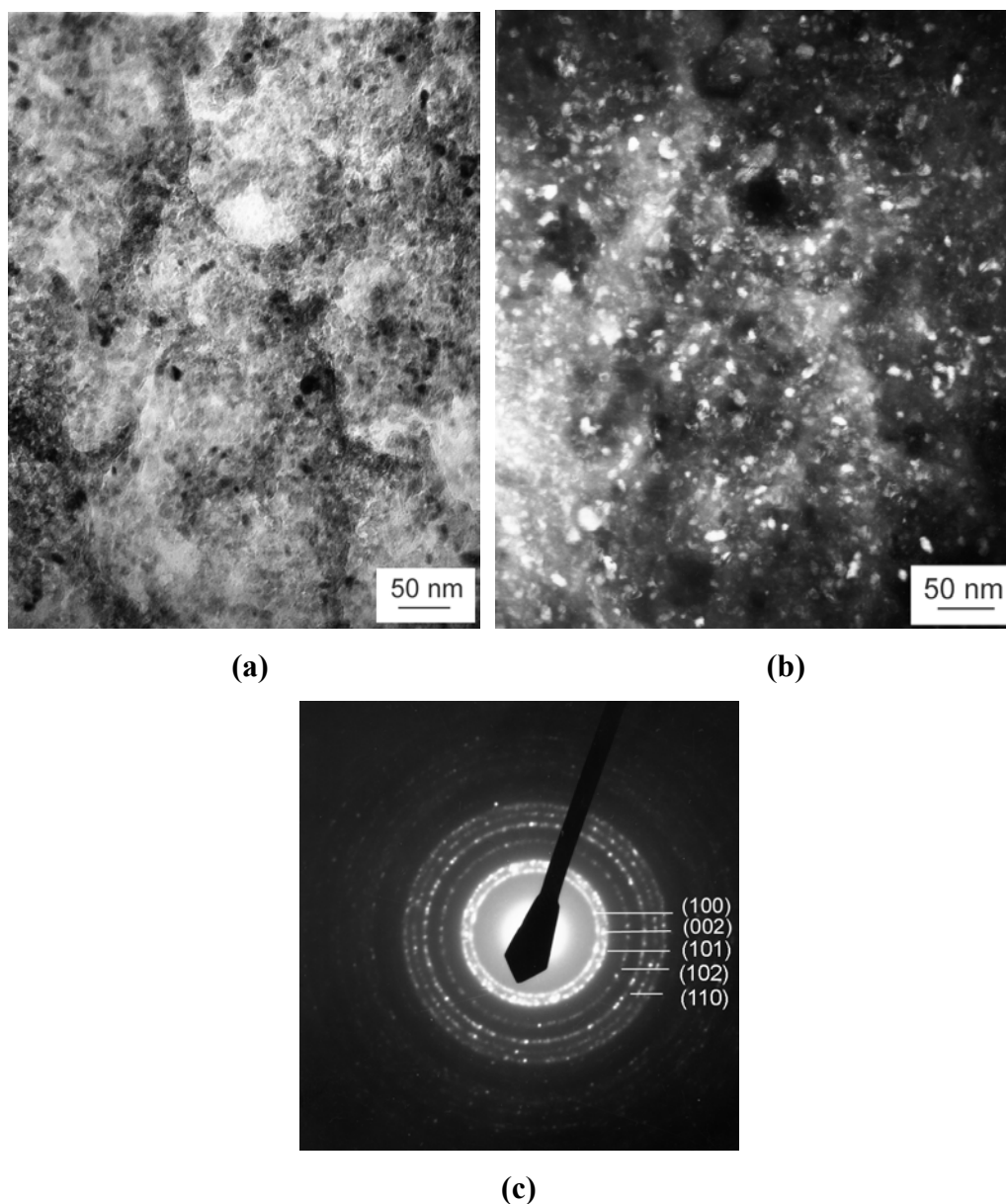


Fig. 3.7 (a) Bright-field and (b) dark-field plan view TEM micrograph of the ZnO film annealed at 450°C for 4.5 h in air, after initial deposition onto mercapto-terminated SAM-treated silicon wafer from solution of 100 mM, [Zn], 2000 ppm copolymer and 3.5 mM HMTA for 6 h and (c) SAD pattern of the film shown above.

The HRTEM investigation (Fig. 3.8) of this annealed film reveals that the average size of the crystallites is about 6 nm, which is consistent with the result obtained from the DF image.

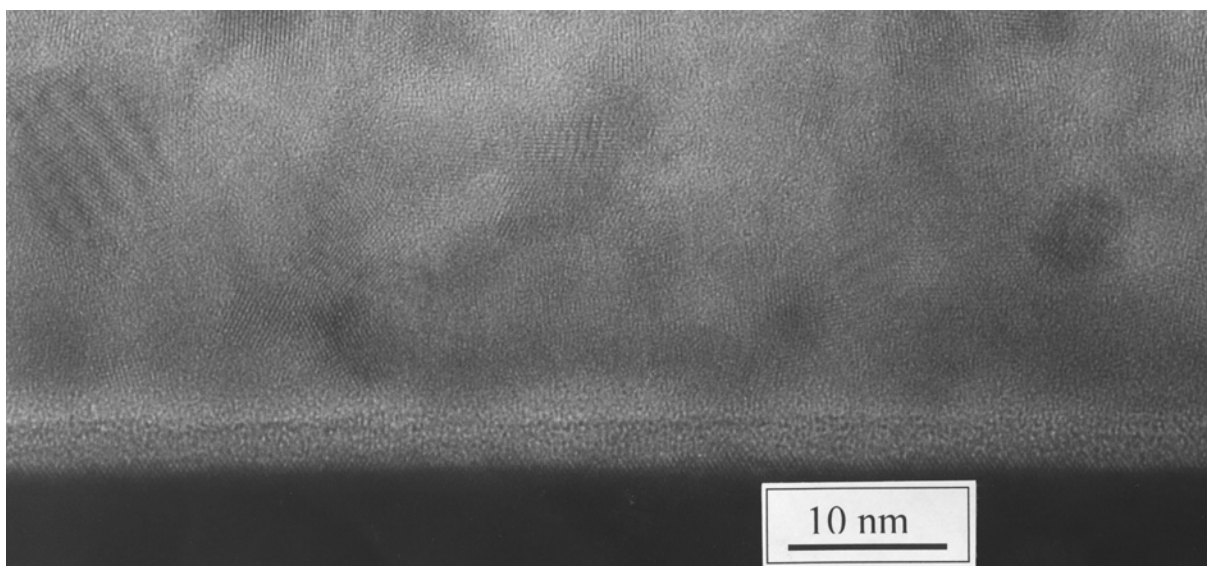


Fig. 3.8 (a) Cross-sectional HRTEM micrograph of the ZnO film annealed at 450 °C for 4 h, after initial deposition from solution of 100 mM, [Zn], 2000 ppm copolymer and 3.5 mM HMTA for 6 h.

The micrometer-sized particles, which are typical in the liquid-based synthesis of ZnO films, were not observed in the present study and this suggested that the nanometer-sized particles occurred at the beginning were stabilized by the polymer used. This is in agreement with the findings by Rieger et al. [2000Rie] who indicated that the nanometer-sized particles were stabilized at sufficient concentration of polymer used. Taubert et al [2002Tau-2] studied the polymer-controlled ZnO precipitation in more detail and found with the addition of the various polymers, the morphologies and size distribution of the precipitated particles changed greatly depending on the chemical nature of the polymer used. Furthermore, it was reported that the adsorption of polymers could stabilize the thermodynamically unstable amorphous nanometer-sized particle precipitated [2002Tau-1]. The fact that the as-deposited ZnO films in this study are in amorphous form is in agreement with their finding. Moreover, in a recent study on the crystallization of CaCO<sub>3</sub> in the presence of a PEO-b-PAsp copolymer [2004Bol], the main function of the polymer was found to slow down considerably the aggregation process of the amorphous particles.

The influence of the present polyelectrolytes on the ZnO thin film formation process is twofold [2002Hof]. In addition to the steric shielding, which is the basis for polymeric scale inhibition, the polyelectrolyte acts as a strong complexant to the zinc ions in solution owing to its numerous carboxylate groups [1998Öne].

### 3.2.4. XPS investigations

Moreover, XPS spectra of the as-deposited film (Fig. 3.9) reveal that with increasing deposition time, Zn 2p peaks are present in films at the identical energy value, suggesting the binding state of zinc atoms is identical at any deposition time. Additionally peaks from the silicon wafer become weaker with increasing deposition time.

Strong binding interactions between the copolymer components and nanometer-sized particles will tend to produce films containing the copolymer. In order to check whether the polymer was incorporated in the ZnO films during deposition, XPS investigations were performed in the present study. The XPS spectra of as-deposited and annealed samples are shown in Fig. 3.10. After calcinations, the Zn 2p<sub>3/2</sub> peak locates at 1022.5 eV, which is the expected value for ZnO, whereas in the as-deposited sample, this peak is present at 1023.2 eV. Considering the fact that the Zn 2p<sub>3/2</sub> peak belonging to zinc acetate locates at 1026.3 eV [1993Mar], which is at an even higher energy due to the involvement of the carboxylate, it can be inferred that the blue shift of the Zn peak in the as-deposited films is due to the presence of the copolymer in the film. This is in agreement with findings of Taubert et al [2002Tau-1] who indicated that the polymer was incorporated into the zincite matrix.

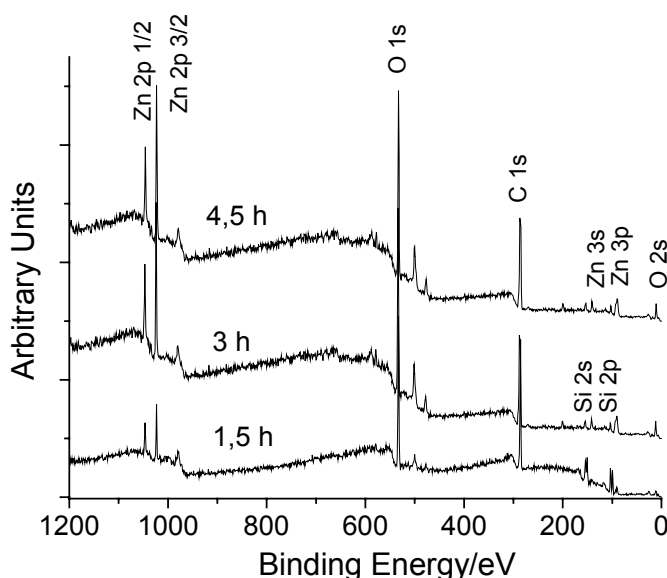
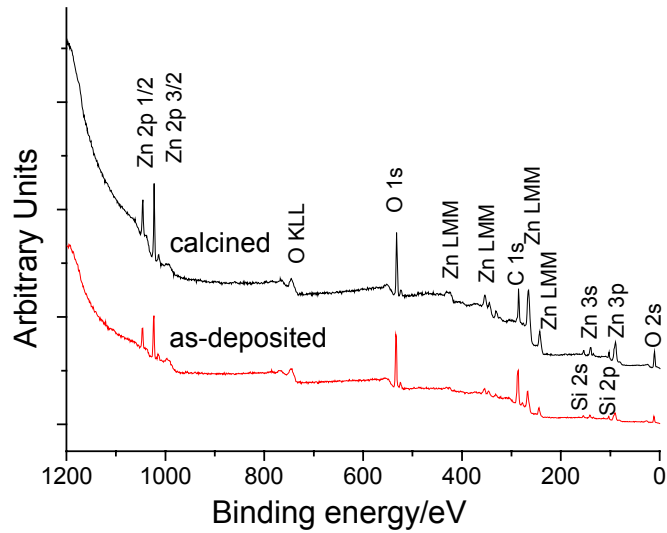
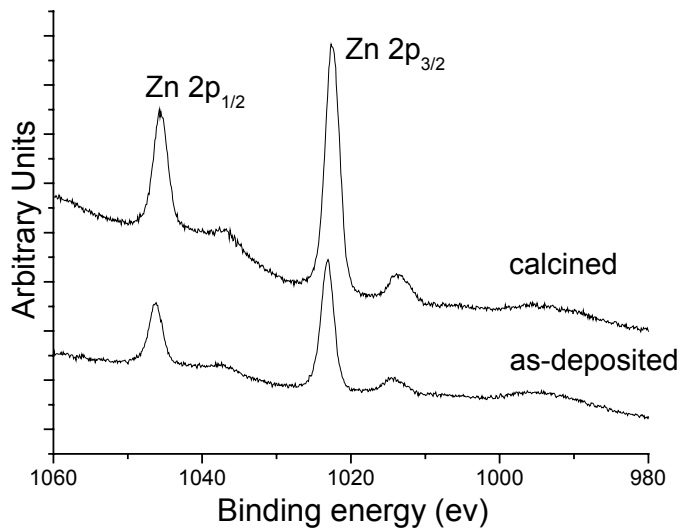


Fig. 3.9 XPS spectra of ZnO films grown from solution containing 100 mM [Zn], 4000 ppm copolymer and 7 mM HMTA for 1.5 h, 3 h and 4.5 h.



(a)



(b)

Fig. 3.10 XPS spectra of ZnO films grown from a solution containing 100 mM [Zn], 4000 ppm copolymer and 7 mM HMTA for 7.5 h: (a) survey of an as-deposited and a annealed sample, (b) Zn 2p<sub>1/2</sub> and 2p<sub>3/2</sub> peaks before and after calcinations at 723 K.

### 3.2.5. Film thickness

The film thickness can be readily controlled by varying the deposition time. Fig. 3.11 shows the film formation kinetics. The film thickness was determined by ellipsometry measurement and it was observed to increase continuously with the deposition time, when a regular exchanging of the deposition solution was performed. After annealing at 450 °C, the thickness of the film decreases by about 50% due to the shrinkage occurred.

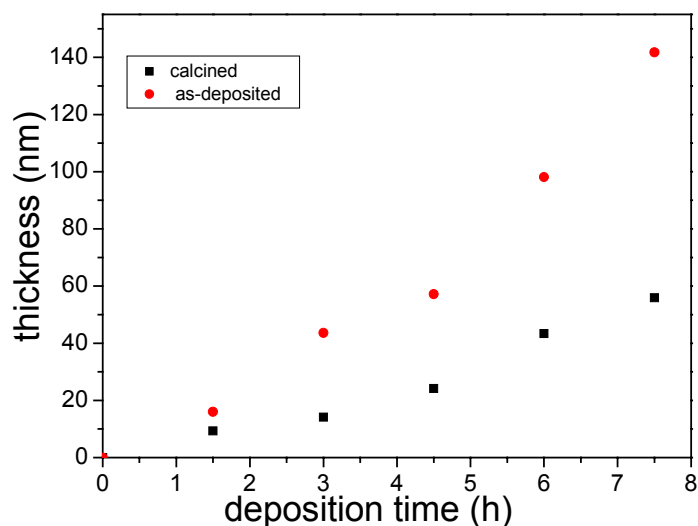


Fig. 3.11 The thickness of as-deposited films and films annealed at 450 °C for 4.5 h with initial deposition on SH-modified silicon wafer from solutions containing 100mM [Zn], 4000 ppm copolymer and 7mM HMTA at 80 °C after 7.5 h.

### 3.3. Deposition of ZnO films on silicon modified with SH-C<sub>3</sub>-SAM

A TEM micrograph of a ZnO film on silicon wafer modified by mercapto-terminated SAMs with hydrocarbon chains consisting of three carbon atoms from a solution, which contained 100 mM [Zn] (80 mM ZnCl<sub>2</sub>, 20 mM Zn(CH<sub>3</sub>COO)<sub>2</sub>·2H<sub>2</sub>O), 4000 ppm of the copolymer and 2.5 mM HMTA is shown in Fig. 3.12a. The SAD pattern of the TEM analysis reveals that the as-deposited film is still amorphous. TEM EELS analyses provide the distribution of Zn, O, and C in the films (Fig. 3.12b-d). The aluminum film (Fig. 3.12e) on the ZnO film was sputtered prior to the TEM specimen preparation with the aim to protect the ZnO film from damage during specimen preparation process. HRTEM investigations of the ZnO film annealed at 450°C for 4 h reveal that crystallization of ZnO occurred. Nanocrystallites of 7 nm in size were formed and imbedded in an amorphous matrix phase (Fig. 3.13).

The results suggest that ZnO film formation also occurs on SAM composed of rather short molecule. However, it should be noted that the use of both fresh surfactant and dry solvent during SAM preparation is prerequisite to a successful film deposition.

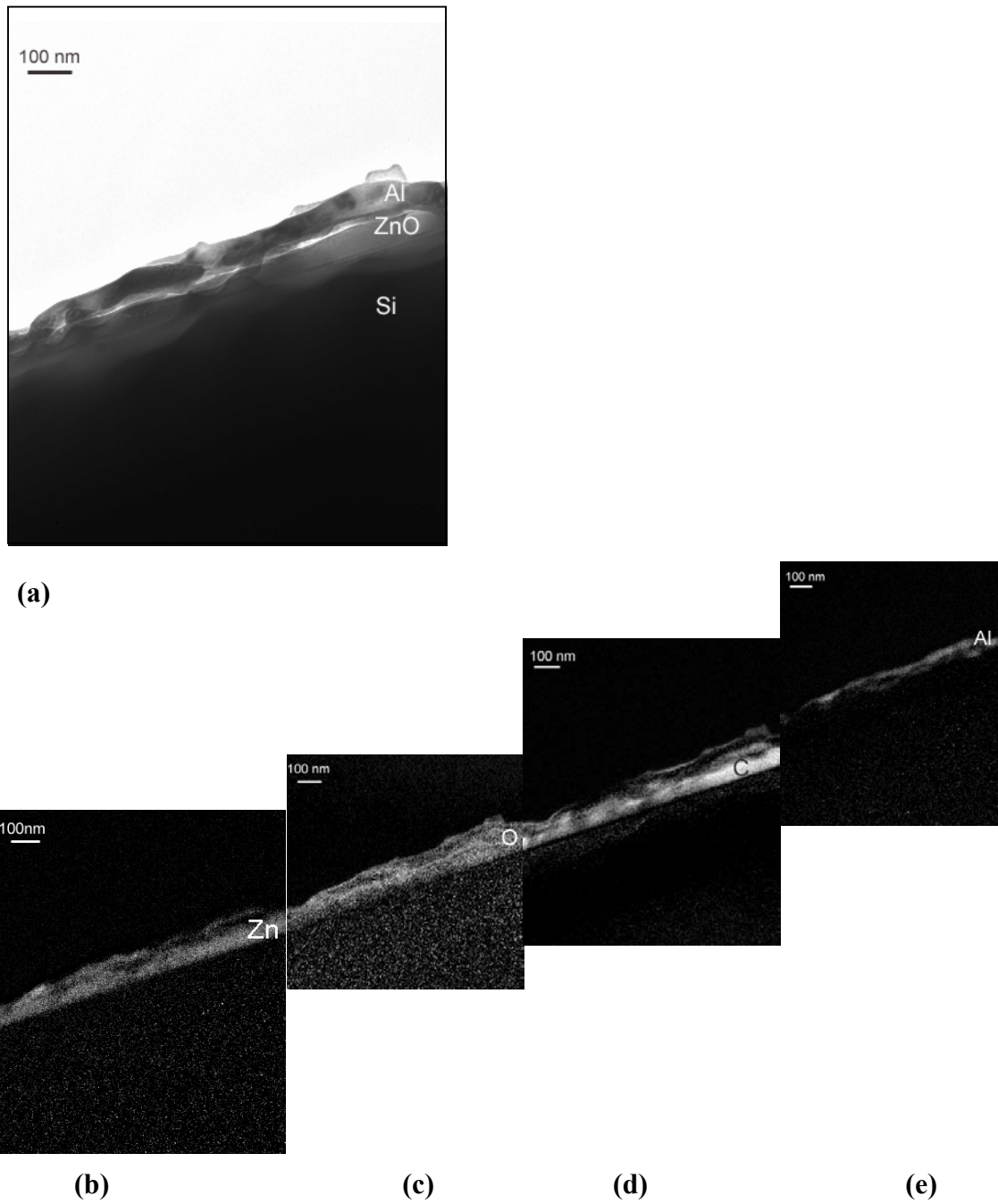


Fig. 3.12 TEM EELS analysis of the as-deposited ZnO films from a solution containing 100 mM [Zn] ( $\text{ZnCl}_2$ ,  $\text{Zn}(\text{CH}_3\text{COO})_2 \cdot 2\text{H}_2\text{O}$ ), 4000 ppm copolymer and 2.5 mM HMTA on silicon wafers modified with mercapto-terminated SAMs with chains consisting of three carbon atoms at 80 °C for 4.5 h. (a) Bright-field image, (b) Zn (c) O, (d) C and (e) Al distribution map.



Fig. 3.13 TEM micrograph of a film annealed at 450 °C for 4 h, after initial deposition on Si wafers modified by mercapto-terminated SAM with hydrocarbon molecules consisting of only three carbon atoms from a solution containing 100 mM [Zn], 4000 ppm copolymer and 7 mM HMTA at 80 °C for 4.5 h.

### 3.4. ZnO film deposition on glass modified with SH-C<sub>16</sub>-SAM

AFM studies, as shown in Fig. 3.14, indicate that the film deposited on the glass has also a canyon-like morphology similar to that formed on silicon wafers. Moreover, the success of the film deposition suggests that substrate surface modification by SAM allows film formation on other substrates different from silicon wafers.

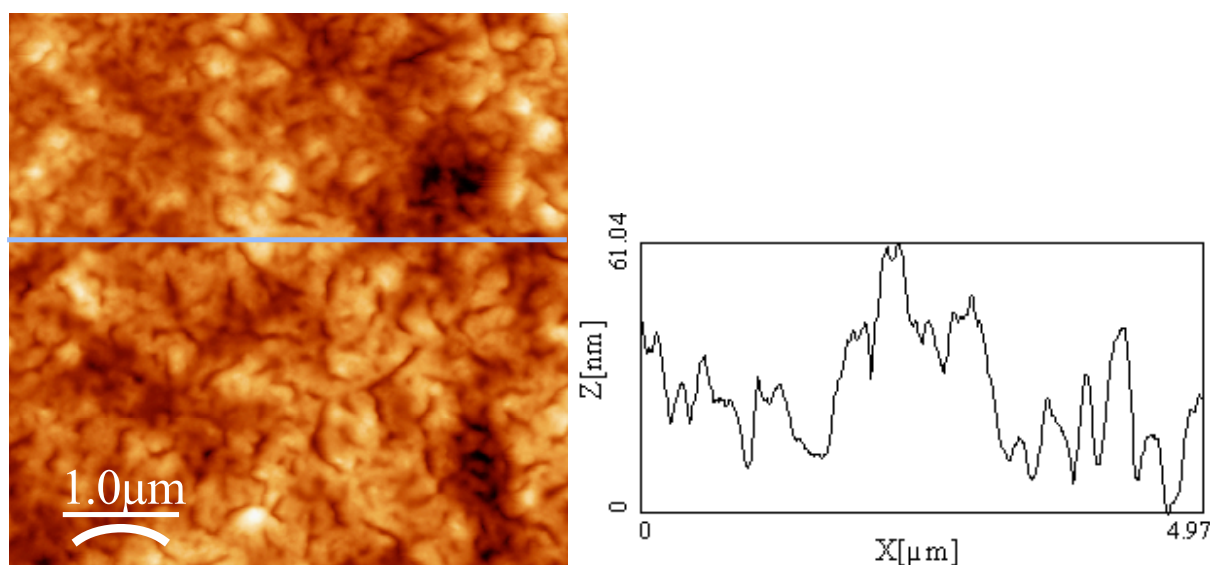


Fig. 3.14 AFM micrographs of an as-deposited film grown on a SH-modified glass substrate from a solution containing 100 mM [Zn], 4000 ppm copolymer and 7 mM HMTA at 80 °C for 7.5 h.

### 3.5. Deposition of ZnO films using modified procedure on silicon treated with SH-C<sub>16</sub>-SAM

The shrinkage within the films upon drying is considered to be the main factor that contributes to the canyon-like features. It is assumed that by decreasing the amount of water adsorbed in the films the shrinkage process might be slowed down. For this purpose film deposition process was modified by heating the sample at 200°C for 0.5 h in air before renewing the deposition solution during deposition (Fig. 3.15), which allowed the dehydration of the ZnO films. SEM results of ZnO films with and without an intermediate heating treatment are shown in Fig. 3.16. Intermediate heating gave rise to dense structured ZnO films that comprise well-packed particles in contrast to the canyon-like structured films obtained from normal procedure. The cross-sectional SEM image shows a compact, homogeneous structure of the film (Fig. 3.16c). Additionally, the cross-section confirms the films thickness derived by ellipsometry measurements (ca. 240 nm).

The successful tuning of the film morphology by the heating treatment supports the assumption that too much water induced in the film leads to the canyon-like feature upon drying. It is assumed that a large amount of water is involved in a network of bridged polymers, which were found by XPS investigation being incorporated in the films (Chapter 3.2.5.).

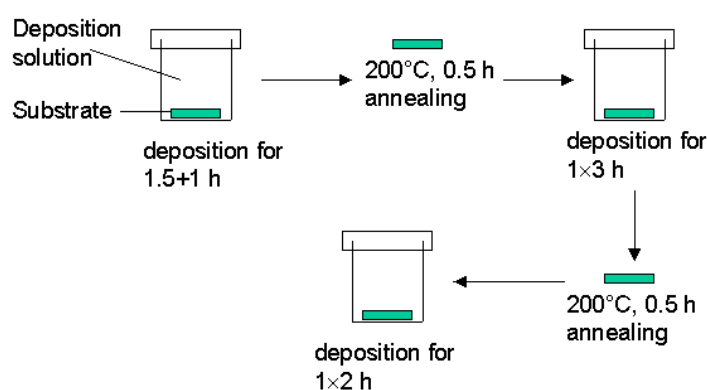
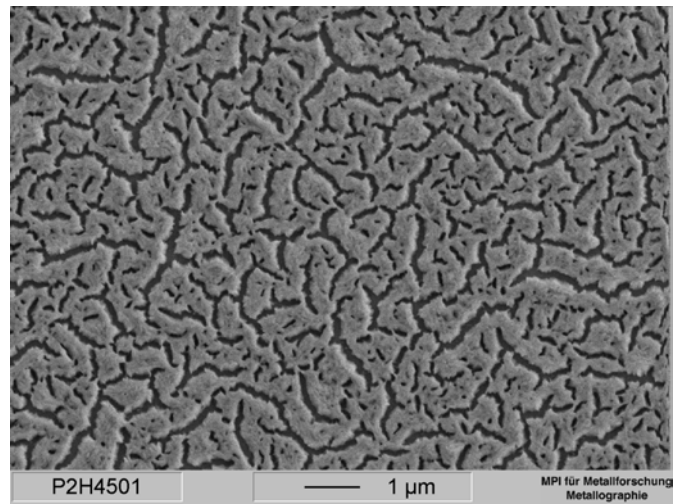
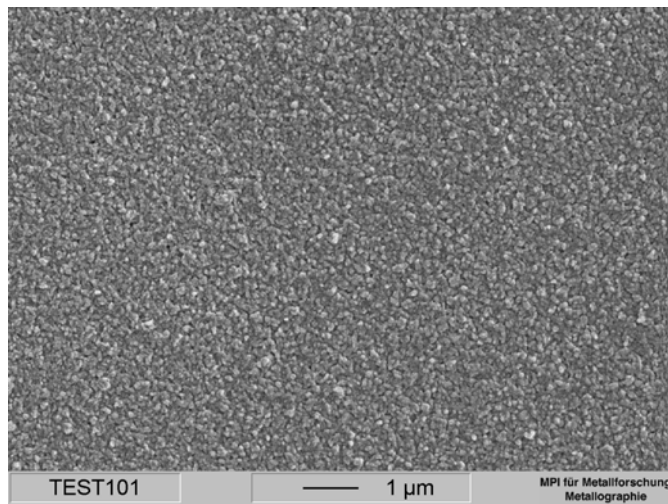


Fig. 3.15 Modified film deposition procedure.

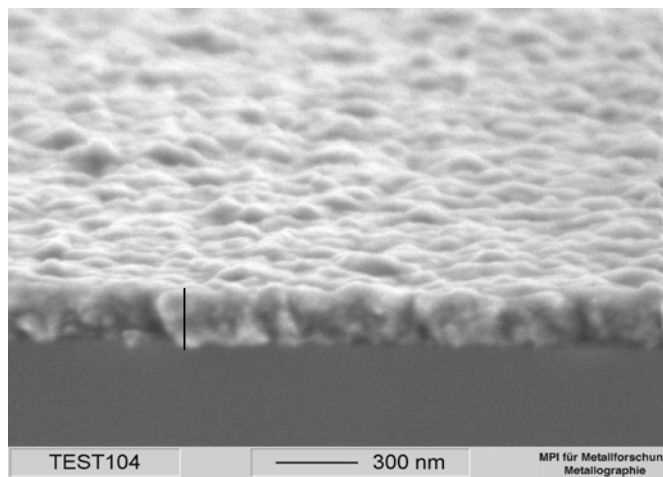




(a)



(b)



(c)

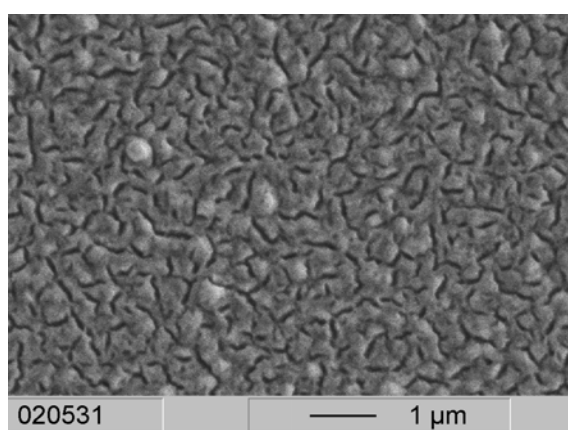
Fig. 3.16 (a) SEM micrographs of as-deposited film grown for 7.5 h on a SH-modified Si-wafer from a solution containing 100 mM [Zn], 2000 ppm copolymer and 4.5 mM HMTA and (b) films obtained with the modified procedure. (c) cross-sectional SEM photograph of the films in (b).

### 3.6. Deposition of ZnO films on silicon substrates modified with different SAMs

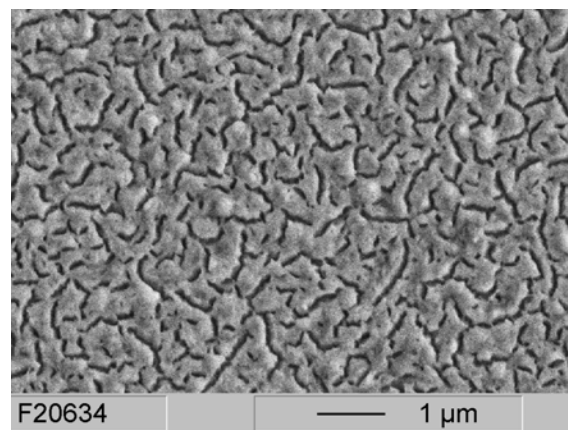
Being consistent with the results of Fuchs [2003Fuc], on bare silicon wafers no film deposition occurs. The same is true on silicon wafers modified by sulfonate-terminated ( $-\text{SO}_3\text{H}$ ) SAM, whereas on SAM functionalized by the mercapto group the film deposition takes place under the same conditions. In order to clarify this discrepancy a variety of differently functionalized SAM coatings were investigated under identical deposition conditions. The surface groups investigated were  $-\text{SCOCH}_3$ ,  $-\text{Br}$ ,  $-\text{N}_3$  and  $-\text{NH}_2$  (Table 3.2). Wafers modified by  $-\text{SCOCH}_3$ ,  $-\text{NH}_2$ , or  $-\text{N}_3$  functionalized SAM provide also depositions with canyon-like features as mercapto-functionalized ones, whereas  $-\text{Br}$ -functionalized SAM result in uniform films comprising rounded particles after the deposition time of 7.5 h (Fig. 3.17). The Influence of various SAM surface groups on the film formation will be further discussed in Chapter 6.

Table 3.2 Results of ZnO film deposition on various SAM surface groups from a solution containing  $\text{ZnCl}_2$  (100 mM), HMTA (7 mM) and copolymer (4000 ppm) at 80 °C after 7.5 h.

Surface groups	Film morphology
$-\text{SCOCH}_3$	Film with canyon-like feature
$-\text{SH}$	
$-\text{Br}$	Film consisting of round particles
$-\text{N}_3$	Film with canyon-like feature
$-\text{NH}_2$	



(a)



(b)

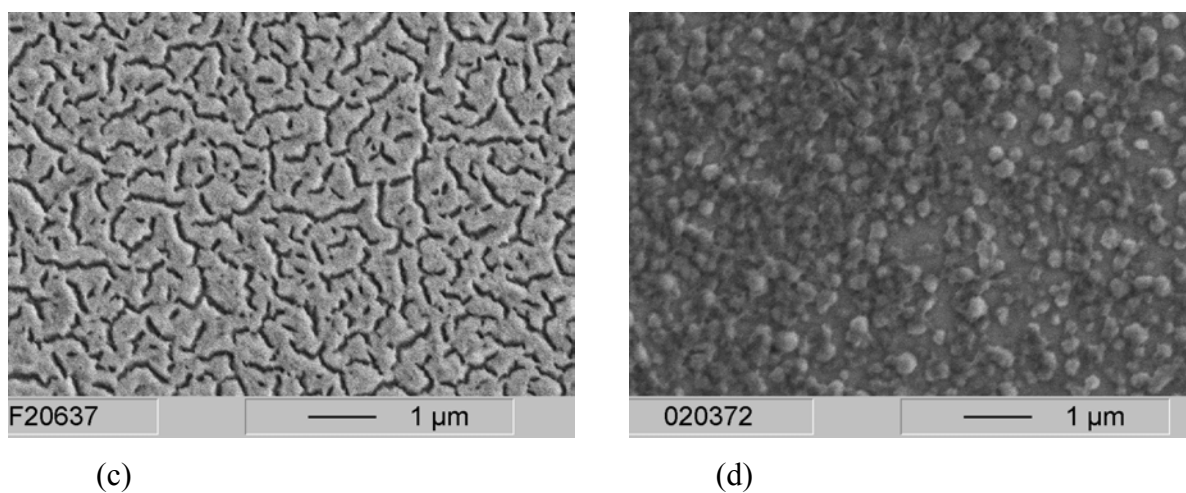


Fig. 3.17 SEM micrographs of as-deposited film grown at 80 °C after 7.5 h on silicon wafers modified with (a)  $-\text{SCOCH}_3$ , (b)  $-\text{NH}_2$ , (c)  $-\text{N}_3$  and (d)  $-\text{Br}$  terminated SAMs from a solution containing 100 mM  $[\text{Zn}]$ , 4000 ppm copolymer and 7 mM HMTA.

## CHAPTER 4

# **Influence of annealing on structure and photoluminescence of ZnO films prepared by a chemical bath deposition process**

### **4.1. Introduction**

The work reported in the previous chapter involved the preparation and characterization of ZnO films from aqueous solution containing polyelectrolyte additives P (MAA<sub>0.5</sub>-co (MAA-EO<sub>20</sub>)<sub>0.5</sub>)<sub>70</sub>. TEM investigations revealed that the as-deposited films were still amorphous and further annealing at 450 °C was required to transform the films into crystalline ZnO (Fig. 3.7, Fig. 3.13). It is known that annealing conditions not only influence the crystal quality of the films, but the crystallite phase and orientation as well [1999Nun]. Therefore, it is important to study intensively the effect of the post-deposition annealing on the film structure.

Many components and devices in electronic and magnetic systems are fabricated from materials that have crystallographic texture. Foster e.g. reported that ZnO films with the [001] axis normal to the surface could be employed for ultrasonic oscillators and transducers [1969Fos]. Owing to the interesting potential of applications, more and more studies have been carried out with the intention to produce oriented ZnO films via different methods [1993Olv, 2003Zna, 1997Ohy, 2002Liu].

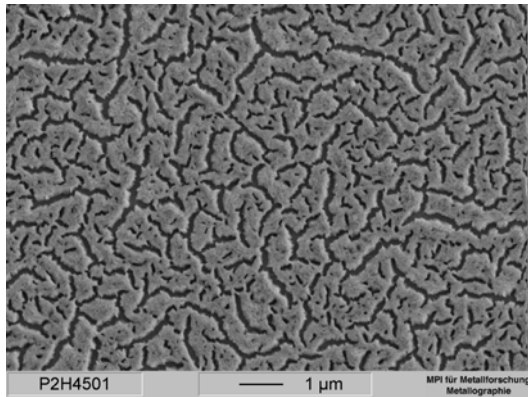
In the present chapter, post-deposition annealing of the ZnO films on SAM-modified silicon wafers was performed in air. The structure of ZnO thin films annealed at various temperatures was investigated by means of XRD and TEM and photoluminescence (PL) measurement. Especially, film texture was examined by XRD pole figure scan.

### **4.2. Results and discussion**

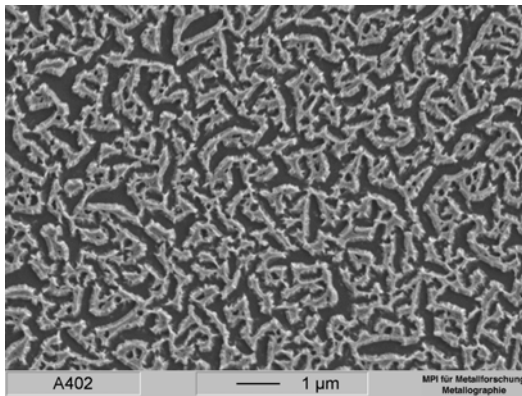
#### **4.2.1. SEM investigations of annealed films**

Films prepared from solutions which contained anhydrous ZnCl<sub>2</sub> (100 mM), HMTA (4.5 mM) and copolymer P(MAA<sub>0.50</sub>-co(MAA-EO<sub>20</sub>)<sub>0.50</sub>)<sub>70</sub> (2000 ppm) were annealed at temperatures of 450°C, 500 °C, 600°C and 700°C in air. The films remained adherent and were investigated by SEM. Although a quantitative evaluation by AFM as described in Chapter 3.2.3 was not carried out, it was apparent, that an increase of the annealing temperature led to significant lateral shrinkage of the film on the silicon surface (Fig. 4.1a). Therefore the canyon-like

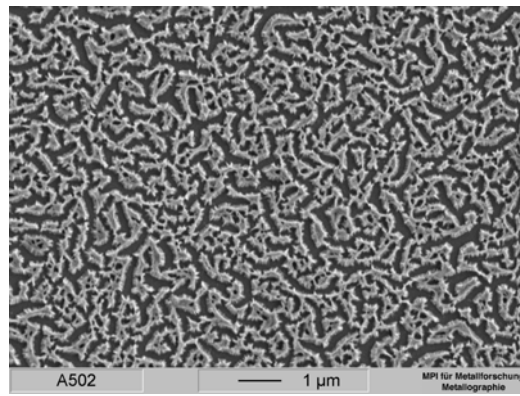
features of the as-deposited film (Fig. 4.1a), which were regularly distributed over the whole surface, obviously became wider upon heating.



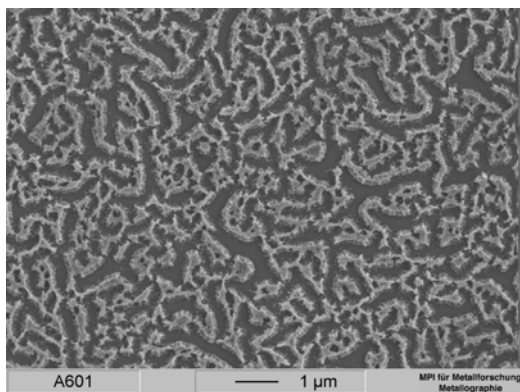
(a)



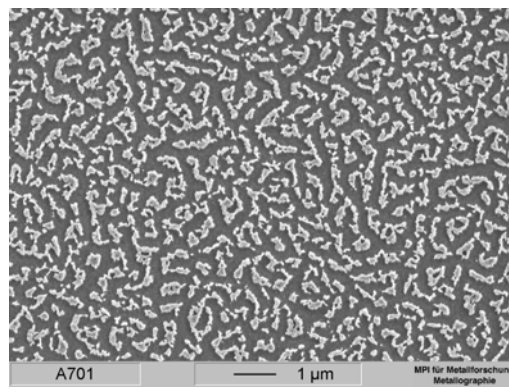
(b)



(c)



(d)



(e)

Fig. 4.1 (a) SEM micrographs of an as-deposited film grown for 7.5 h on a SH-modified Si wafer from a solution containing 100mM [Zn], 2000 ppm copolymer and 4.5mM HMTA and films annealed at (b) 450°C, (c) 500°C, (d) 600°C and (e) 700°C.

#### 4.2.2. XRD investigations of annealed films

Structural characterization of the films annealed at different temperatures was carried out by XRD measurements. For the XRD analysis the data reported in the JCPDS Card (No. 89-1397) (Table 4.1) were used as reference.

Table 4.1 X-ray diffraction results for zincite from JCPDS Card (No. 89-1397).

2θ	Intensity	h	k	l	2θ	Intensity	h	k	l
31.737	569	1	0	0	67.868	220	1	1	2
34.379	415	0	0	2	69.009	109	2	0	1
36.215	999	1	0	1	72.465	16	0	0	4
47.484	212	1	0	2	76.867	34	2	0	2
56.536	308	1	1	0	81.270	16	1	0	4
62.777	265	1	0	3	89.492	67	2	0	3
66.304	41	2	0	0					

The scan taken with the conventional Bragg-Brentano technique of films annealed at 600°C (Fig. 4.2) show three diffraction peaks, which can be attributed to (100), (002) and (101) of zincite. The remaining peaks belong to the (100) silicon substrate. In contrast to the film annealed at 600 °C, that annealed at 700°C exhibits a strong intensity of the (002) peak compared to that of (100) and (101), which suggests a strong texture of the films. A point worthy to note is that with the diffraction technique used only planes diffract which are parallel to the substrate surface.

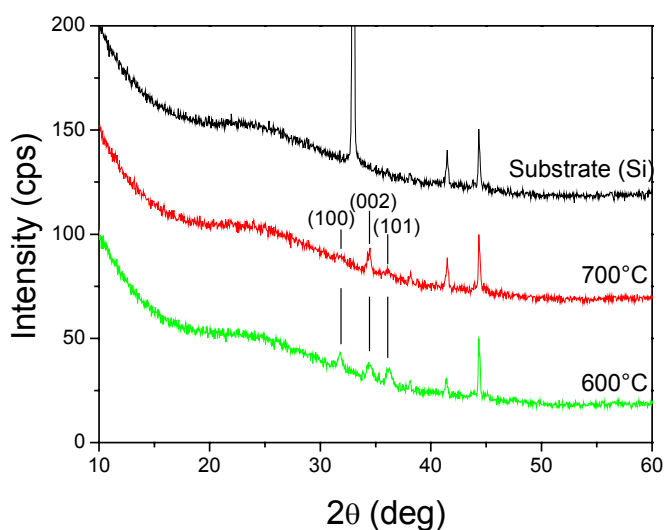


Fig. 4.2 Bragg-Brentano scans of the silicon substrate and films annealed at 600°C, 700°C. (The bars show the peak positions taken from the JCPDS Card No. 89-1397 for ZnO).

Further sets of measurements from these samples were acquired using a grazing incidence configuration with an incident angle  $\alpha$  of  $1^\circ$  (Fig. 4.3.) or  $2^\circ$  (Fig. 4.4.). The employment of this technique leads to an improved peak to background ratio in comparison to the above mentioned Bragg-Brentano configuration. In addition to the (100), (002) and (102) peaks in the film annealed at  $600^\circ\text{C}$ , the ZnO peaks (102) and (103) could be observed. The diffracted intensity around  $2\theta = 55^\circ$  originates from the silicon substrate.

For both films investigated the relative intensities of the individual peaks (100), (002) and (101) are different from the ratio 57:42:100 given by the JCPDS Card No. 89-1397 (Table 4.1). This indicates the presence of a texture in the films. The state of the texture, however, was not the same for both ZnO films. This finding lead to more detailed investigations, which will be discussed in the next section (4.2.3.)

Besides the ZnO peaks two other peaks (marked as \*) could be observed in the film annealed at  $700^\circ\text{C}$ , suggesting that the formation of a new phase might occur during annealing at such high temperature. At the ZnO/silicon interface,  $\text{Zn}_2\text{SiO}_4$  may have occurred upon heating at high temperature [2004Wan-2, 2002Xu, 2001Ohy]. The comparison of these two peaks with the JCPDS Card (No. 85-453) suggests these two peaks can be attributed to  $(\bar{2} 11)$  and  $(\bar{2} 20)$  of the  $\text{Zn}_2\text{SiO}_4$ . This will be further discussed below (Chapter 4.2.4.).

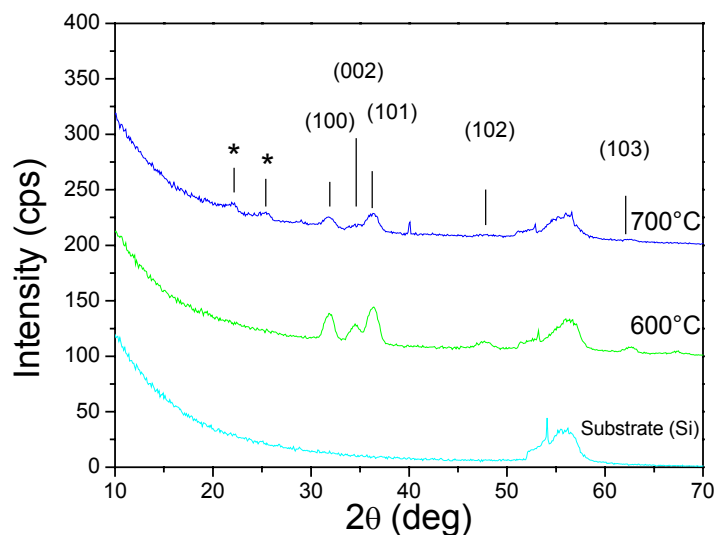


Fig. 4.3 Grazing incidence diffraction patterns of the silicon substrate and films annealed at  $600^\circ\text{C}$  and  $700^\circ\text{C}$ . (The bars show the peak positions taken from the JCPDS Card No. 89-1397 for ZnO).

With increasing the annealing temperature, the intensity of the ZnO peaks becomes stronger. Compared to films annealed at 450 °C and 500 °C, the intensity of the peaks of film annealed above 600 °C is greatly improved, which indicates that annealing at higher temperature improves the crystallinity of the film (Fig. 4.4.)

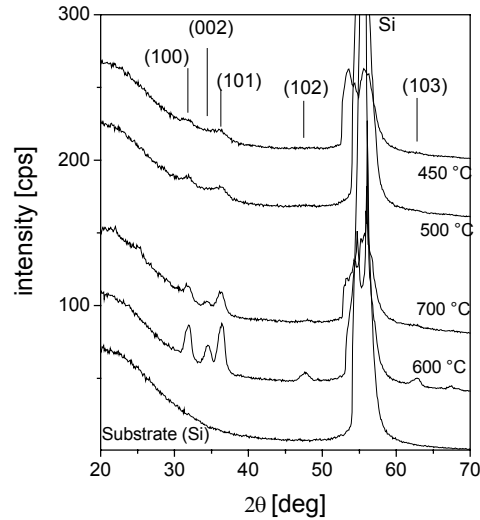


Fig. 4.4 Grazing incidence diffraction patterns of the silicon substrate and films annealed at 450°C, 500°C, 600°C and 700°C (angle of incidence  $\alpha = 2^\circ$ ).

#### 4.2.3. Film grain growth and film texture

For films annealed at 600°C and 700°C, XRD measurements were performed with an instrument probing just with  $K_{\alpha 1}$ , so that the width of the ZnO peak could be determined more accurately. As shown in Fig. 4.5, the (100), (002) and (101) peaks could be observed clearly besides the (002) reflection from the silicon substrate. For the film annealed at 700°C the (002) peak is more pronounced against the two other peaks ((100) and (101)), suggesting the existence of a c-axis texture. For the film annealed at 600°C this effect is less pronounced.

The large broadening of the XRD spectra suggests that the films consist of nanometer-sized particles. The average grain sizes  $D$ , were estimated by using the Scherrer formula:

$$D = 0.9 \lambda / (\beta \cos\theta)$$

Where  $\lambda$  is the wavelength of the x-rays used (Cu  $K_{\alpha 1}$ ),  $\theta$  is the Bragg angle,  $\beta$  is the full width of the diffraction peak at half of the maximum intensity.

Table 4.2 shows the average grain sizes for the ZnO films annealed at 600 °C and 700 °C. The average grain size along c-axis of the film annealed at 600 °C is about 14 nm, whereas it increases to 24 nm when the film was annealed at 700 °C. The a/c ratio of the nanocrystallites



in the film annealed at 600 °C is about 1.4, which suggests that the growth rate of the crystal varies along different directions. For the film annealed at 700 °C, the grain size along a-axis could be hardly estimated due to the weak intensity of the (100) peak.

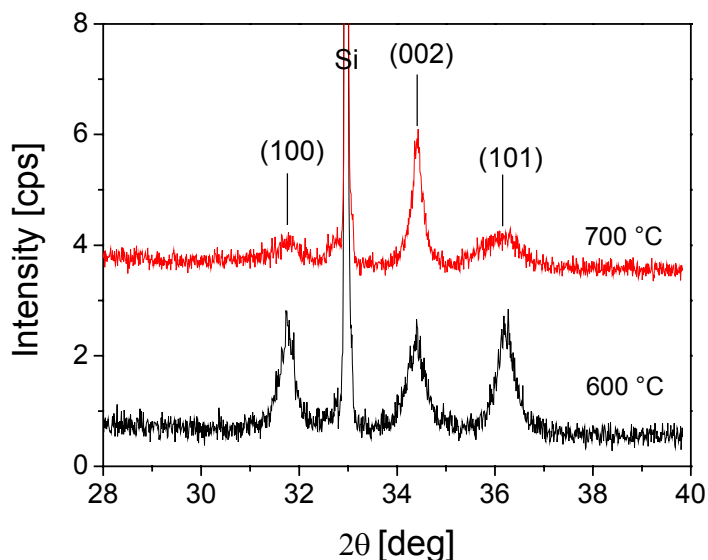


Fig. 4.5 Bragg-Brentano diffraction patterns of films annealed at 600°C and 700°C ( $K_{\alpha 1}$ ).

Table 4.2 Grain size of the ZnO films annealed at 600 °C and 700 °C.

Annealed films	$10\bar{1}0$ (a-direction)	$0002$ (c-direction)	a/c
	D(nm)	D(nm)	
600 °C	19	14	1.4
700 °C	-	24	-

In order to further determine the texture of films annealed at 600°C and 700°C, pole figure scans  $I(\Psi)$  on three (hkl) reflections with the ZnO films annealed at 600°C and 700°C were conducted (Fig. 4.6.). The tilt angle  $\Psi$  indicates the inclination of the normal of the (hkl) planes considered with respect to the sample surface normal.

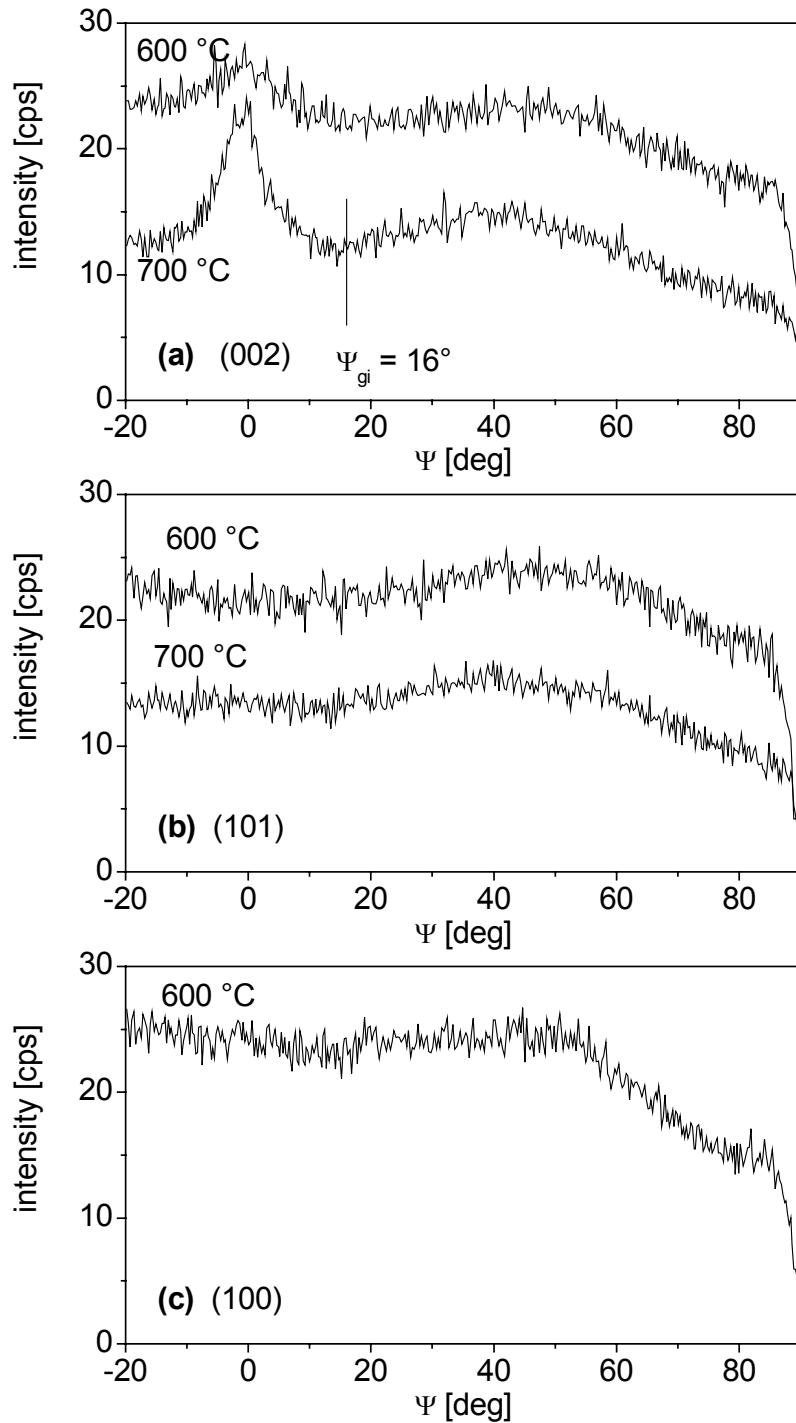


Fig. 4.6 Pole figure scans ( $I(\Psi)$ ) of ZnO films annealed at 600°C and 700°C for the reflections (002) (a), (101) (b) and (100) (c). The tilt angle  $\Psi_{gi} = 16^\circ$  corresponding to the grazing incidence geometry is indicated.

For the (002) reflection (Fig. 4.6a) the occurrence of a peak at  $\Psi = 0$  reveals the presence of a (002) texture, that is, a preference of (002) planes aligned parallel to the film surface. The ratio of the peak areas for the films annealed at 700°C and 600°C is about 2:1, indicating a

stronger texture for the former than for the latter case. The  $\beta$  values of the peak ( $\Delta\Psi = 10^\circ$  for the film annealed at  $700^\circ\text{C}$  and  $\Delta\Psi = 14^\circ$  for that one annealed at  $600^\circ\text{C}$ ) indicates a sharper texture for the former one, i.e., smaller deviations from perfect alignment of the (002) planes parallel to the film surface. The broad distribution of  $I(\Psi)$  in the range  $\Psi = 20^\circ - 90^\circ$  is mainly due to the background.

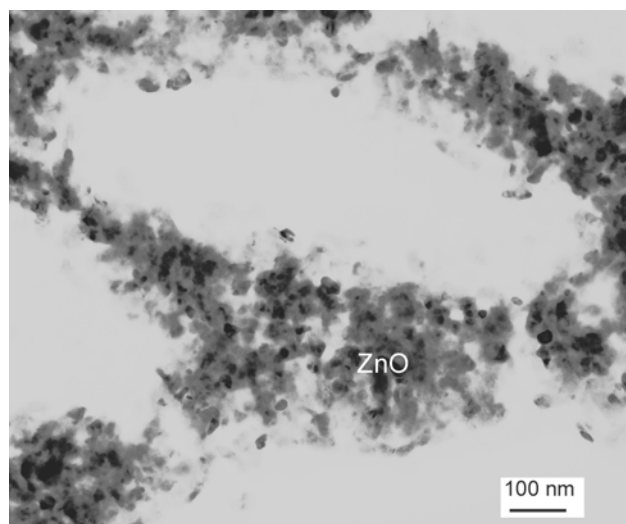
For the (101) peak (Fig. 6b) and the (100) peak (Fig. 4.6c) no indication of texture was observed. The (100) peak of the films annealed at  $700^\circ\text{C}$  is too small in intensity to allow a reliable measurement.

The above observations show clearly that the higher annealing temperature greatly improves the degree of the (002) texture in the films. The present results are comparable to those of films obtained by sol-gel [2003Zna, 1997Ohy] or chemical spray coating [1993Olvy] followed by annealing. Compared to the (100) and (101) texture, a (002) texture has been commonly observed.

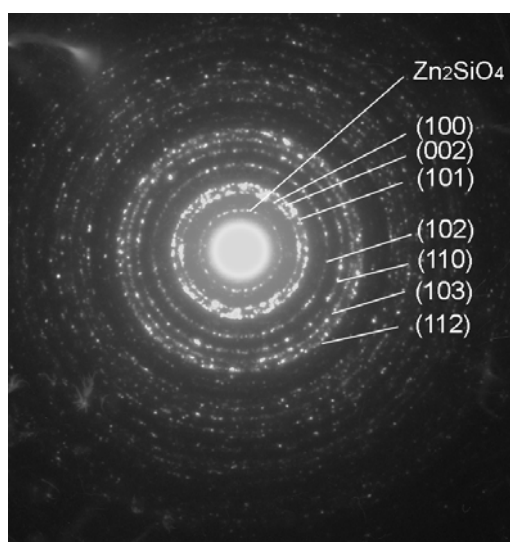
#### **4.2.4. Transmission electron microscopy investigations**

TEM studies were carried out with the films annealed at  $600^\circ\text{C}$  and  $700^\circ\text{C}$ . A plan-view bright-field image of the ZnO film annealed at  $600^\circ\text{C}$  is shown in Fig. 4.7. Island-like deposits of ZnO consisting of nanometer-sized particles can be seen. The corresponding SAD pattern reveals that the film consists of polycrystalline zincite. The ring with the smallest diameter cannot be attributed to ZnO, but to the lattice plane  $(\bar{1}20)$  of  $\text{Zn}_2\text{SiO}_4$ . For the film annealed at  $700^\circ\text{C}$ , the same ring was observed in the plan-view image.

TEM dark-field images of both films annealed at  $600^\circ\text{C}$  and  $700^\circ\text{C}$  are displayed in Fig. 4.8. For the films annealed at  $600^\circ\text{C}$  nanometer-sized particles were observed, the average grain size was found to be between 15 and 20 nm, which is consistent with the results obtained from XRD investigations. As for the ZnO film annealed at  $700^\circ\text{C}$ , crystal growth was observed. However, interestingly, the TEM studies reveal that there are two modes of crystal growth in the films: on the islands, only small crystals (average size 10 nm) were observed, whereas in regions between such islands, bigger crystals could be identified.



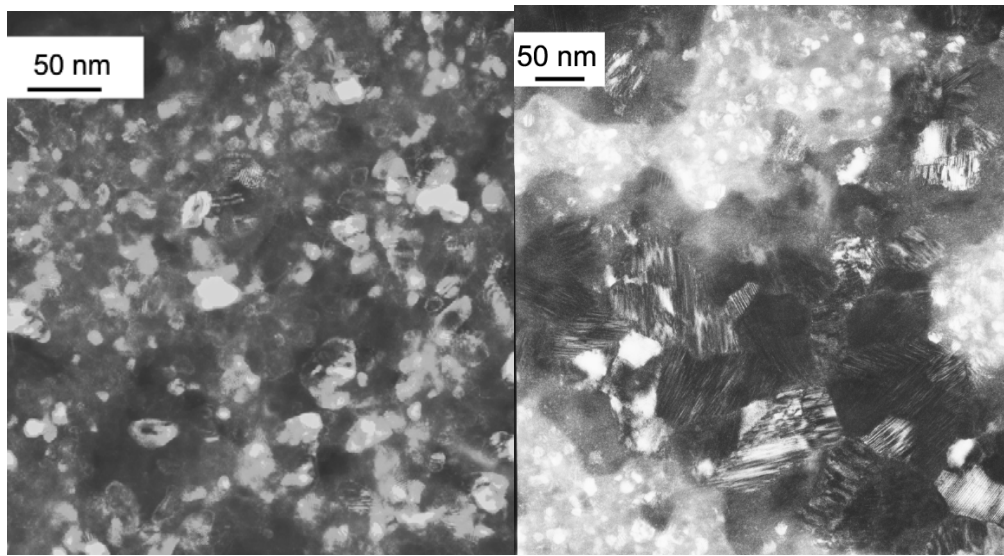
(a)



(b)

Fig. 4.7 (a) Plan-view TEM micrograph for films annealed at 600°C and (b) the corresponding SAD pattern.

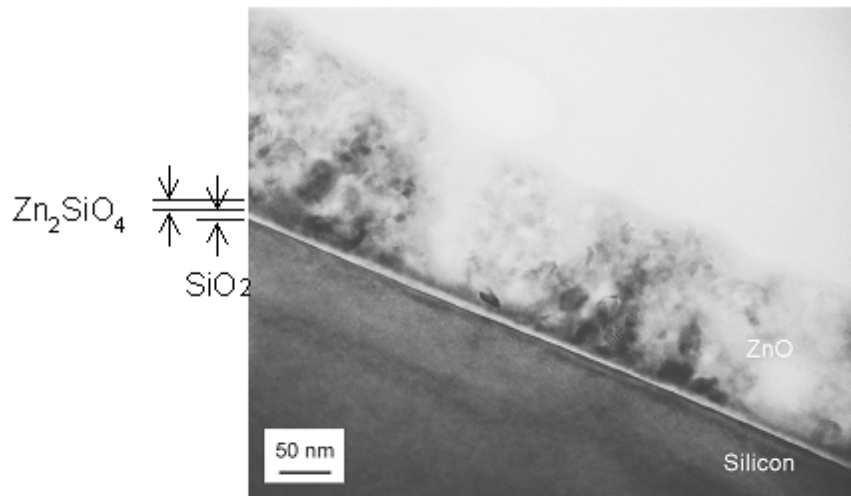
In order to examine the interface area between the silicon substrate and ZnO films, cross-sectional TEM specimen were investigated. Fig. 4.9 shows the TEM micrograph of the ZnO film annealed at 600°C. Next to the silicon substrate, the native oxide layer could be seen which grew to a thickness of around 6 nm during annealing. Additionally, between SiO<sub>2</sub> and ZnO an intermediate layer could be observed, which was determined as Zn<sub>2</sub>SiO<sub>4</sub>. The ZnO film has a thickness of 150 nm. The corresponding SAD pattern shows the film is polycrystalline (Fig. 4.9b).



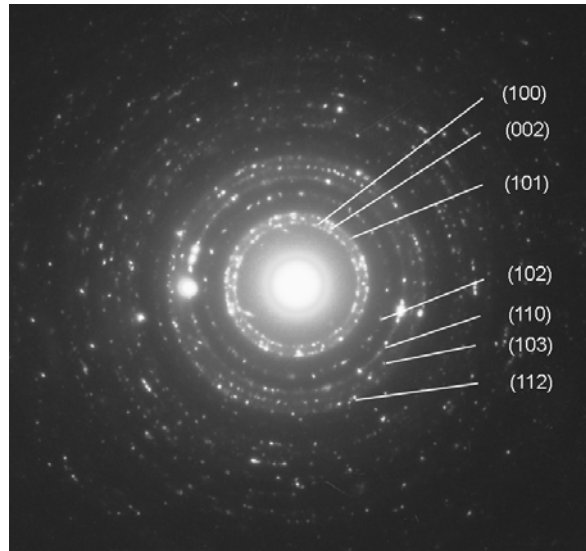
(a)

(b)

Fig. 4.8 (a) Plan-view dark-field TEM micrograph for films annealed at 600°C and (b) 700°C.



(a)

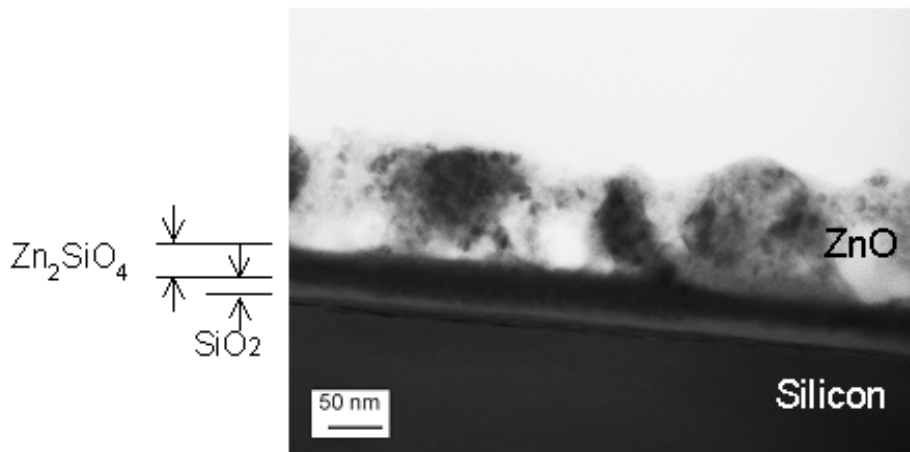


(b)

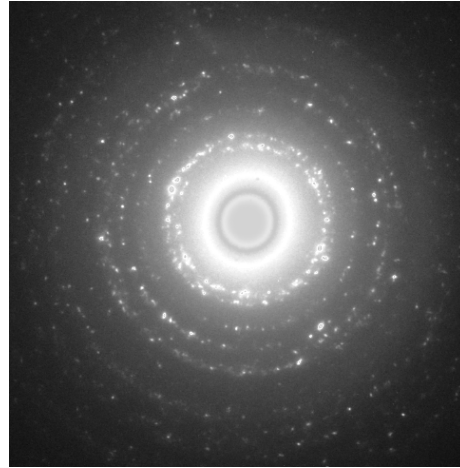
Fig. 4.9 (a) Cross-sectional TEM micrograph for films annealed at 600°C and (b) the corresponding SAD pattern.

Fig. 4.10 shows a cross-sectional TEM micrograph and the corresponding SAD pattern of the ZnO film annealed at 700°C. The intermediate  $Zn_2SiO_4$  layer between the ZnO film and  $SiO_2$  grew to about 30 nm in thickness. Moreover, although the ZnO film presented has an island-like form, this intermediate layer covers the silicon substrate completely (Fig. 4.10c). The island film thickness decreased to ca. 110 nm.

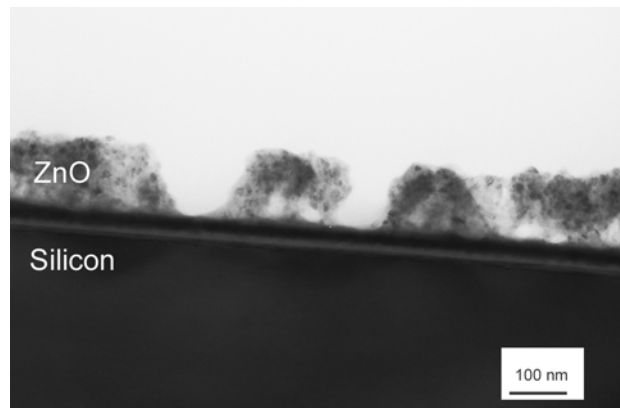
HRTEM investigation was performed to study the multilayer structure. Fig. 4.11a shows a cross-section of the ZnO film annealed at 700°C and the image shows the multilayer including silicon substrate,  $SiO_2$  layer,  $Zn_2SiO_4$  intermediate layer and ZnO film. The HRTEM micrographs of  $Zn_2SiO_4$  and ZnO are displayed in Figures 4.11b and c respectively. Fig. 4.11c reveals that the ZnO film consists of nanocrystallites.



(a)

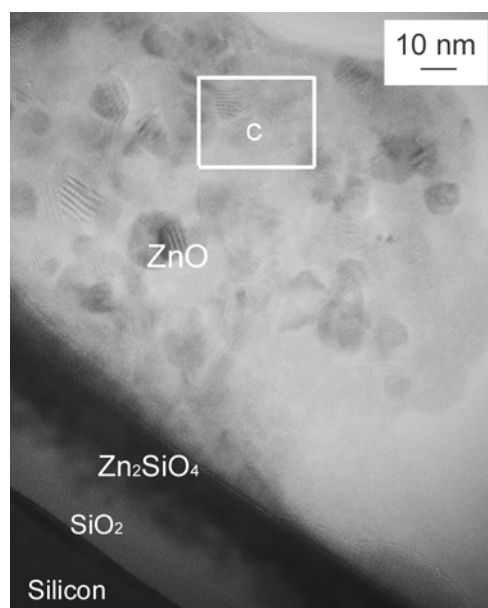


(b)

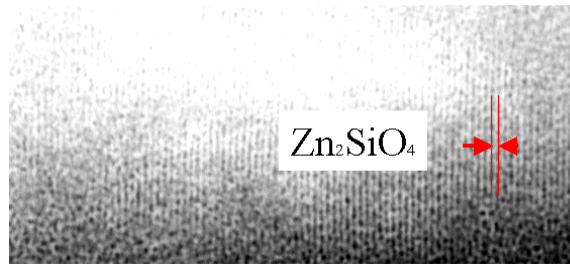


(c)

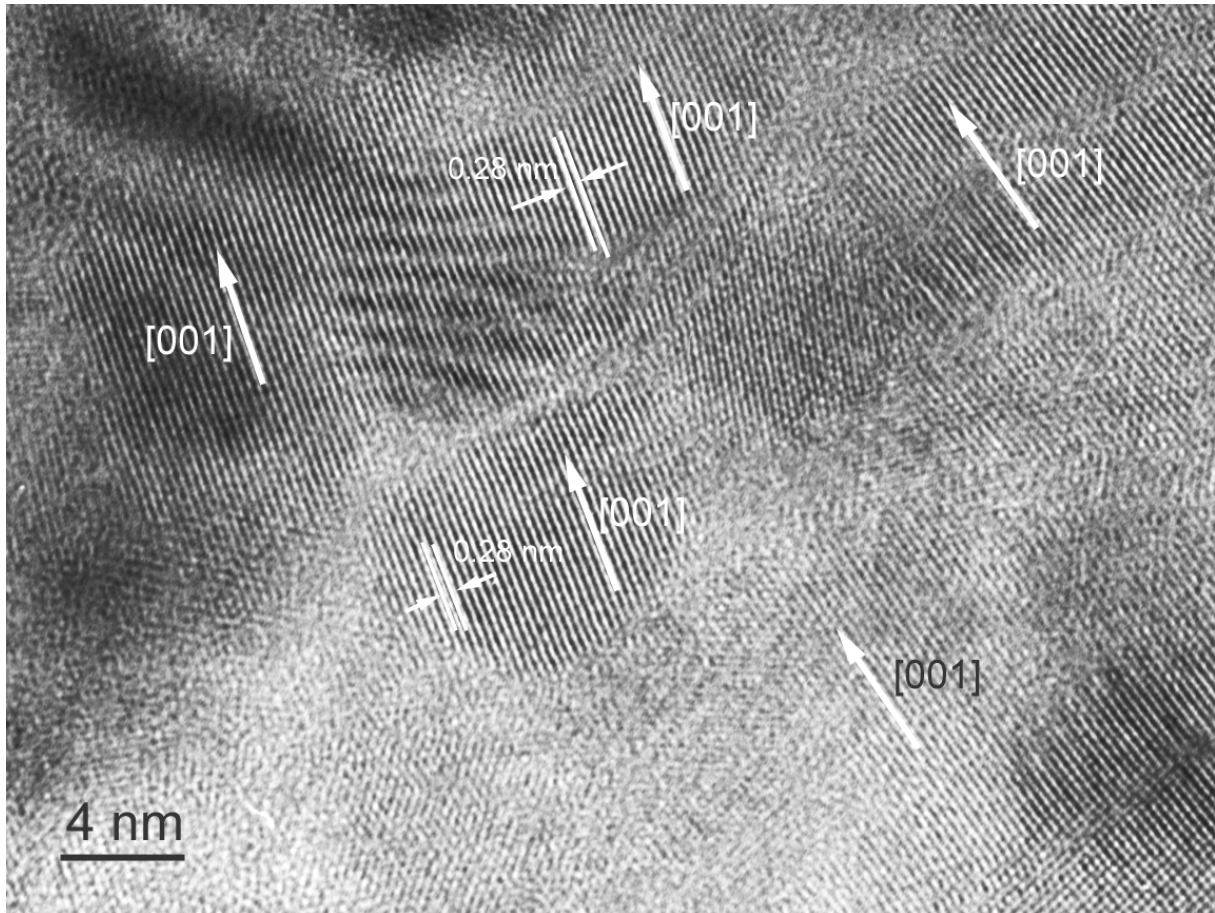
Fig. 4.10 (a) Cross-sectional TEM micrograph for films annealed at 700°C, (b) the corresponding SAD pattern and (c) lower magnification of the cross-section.



(a)



(b)



(c)

Fig. 4. 11 (a) Cross-sectional TEM image of a film annealed at 600°C. (b) HRTEM micrograph of the  $Zn_2SiO_4$  interlayer and (c) HRTEM image of the ZnO film.

The plan-view high-resolution TEM image of an area barely covered with ZnO is shown in Fig. 4.12. The  $Zn_2SiO_4$  structure is clearly resolved.



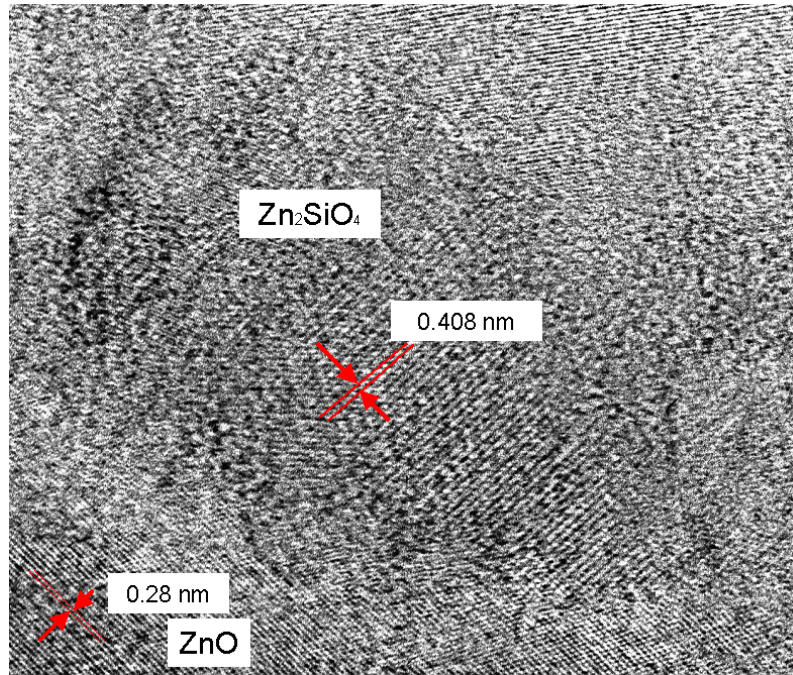
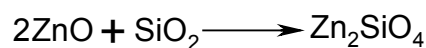


Fig. 4.12 Plan-view HRTEM image of a film annealed at 700°C showing coexistence of ZnO and Zn<sub>2</sub>SiO<sub>4</sub>.

Based on the TEM observations, a phase formation mechanism is proposed as follows (Fig. 4.13). Starting with the Si wafer modified by mercapto-terminated SAM, ZnO films are deposited from the aqueous solution. Upon heating, the mercapto-terminated SAM burns out without disrupting the ZnO films. During further annealing ZnO and SiO<sub>2</sub> react in order to form Zn<sub>2</sub>SiO<sub>4</sub> according to the following reaction:



In addition, zinc silicate may also form on SiO<sub>2</sub> areas uncovered with ZnO by the reaction of vaporized ZnO and SiO<sub>2</sub>.

This is in agreement with recent studies by Xu et al. on the heat treatment of ZnO layer formed on silicon by direct current sputtering [2002Xu, 2003Xu]. Their investigations by depth profile secondary ion mass spectroscopy revealed that a vast inter diffusion between the ZnO film and the silicon substrate, which occurred during annealing at 800°C, led to the formation of Zn<sub>2</sub>SiO<sub>4</sub>. Additionally, the formation of Zn<sub>2</sub>SiO<sub>4</sub> at the ZnO/silicon interface at heating temperatures above 800°C or 900°C has been reported by several other groups [2002Yan, 2002Xu, 2003He, 2001Ohy, 2004Wan-2]. In contrast to their findings, the formation of Zn<sub>2</sub>SiO<sub>4</sub> at considerably lower temperatures in the present study may be due to the nano-size of the particles in the film. Moreover, the present study provides the direct

evidence of the formation of  $\text{Zn}_2\text{SiO}_4$  during annealing by the combined investigations of XRD and TEM.

ZnO films on silicon wafers have been the focus of numerous studies due to their wide applications. Very often post-annealing processes are needed. Therefore, it is important to be aware of the formation of the zinc silicate above 600 °C. Similarly, in the ZnO/ $\text{Al}_2\text{O}_3$  system, the formation of  $\text{ZnAl}_2\text{O}_4$  was observed during annealing due to the reaction between ZnO and  $\text{Al}_2\text{O}_3$  [2002Wes]. Rose and Exarhos [1997Ros] reported also about the formation of  $\text{Zn}_2\text{SiO}_4$  (for ZnO/silica system) and zinc borate (for ZnO/borated glass system) during annealing.

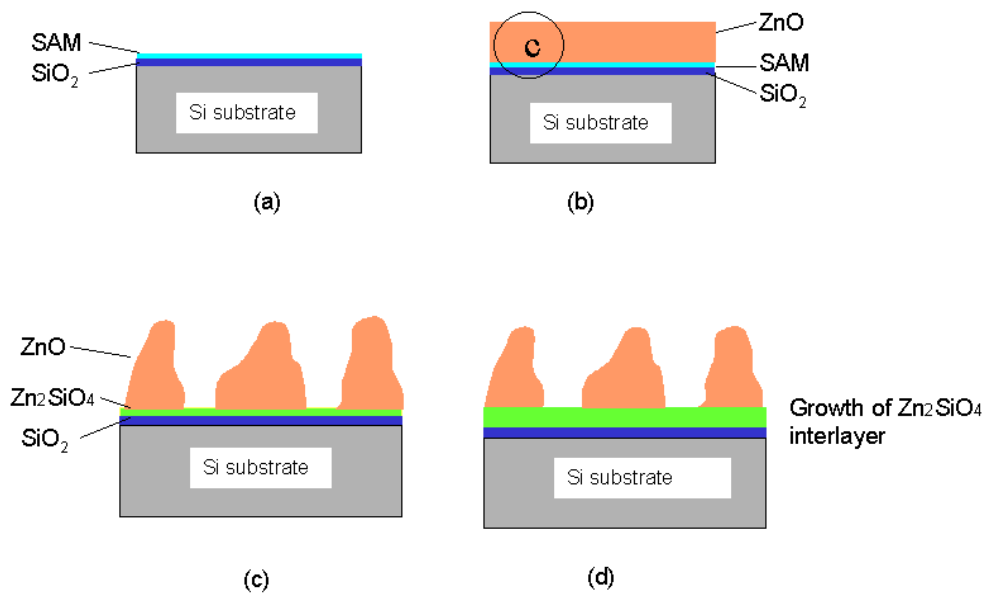


Fig. 4. 13 The schematic illustration of the formation of  $\text{Zn}_2\text{SiO}_4$  during annealing process of the ZnO films. (a) substrate modification by SAM, (b) ZnO film deposition, (c), post-annealing at 600 °C and (d) 700 °C.

It should be noted that neither SAD patterns nor HRTEM investigations provide strong evidence for the presence of the c-axis texture in the films annealed at 600 °C and 700 °C, which can be due to the fact that only small areas (several hundred nanometers) are involved in the TEM investigation. The film texture detected by XRD, however, reflects the distribution tendency of the crystallites in the whole films.

#### 4.2.5. Photoluminescence

No intensive emission was observed for the films annealed at 450°C and 500°C. Upon annealing above 600°C a strong emission centred at 377 nm was observed using an excitation wavelength of 266 nm (Fig. 4.14), whereas the UV emission peak of the film annealed at 700°C shifts to lower wavelength (centred at 380 nm), an increase in the peak intensity was observed as well. The redshift of the UV peak is attributed to the larger grain size and the increase in the peak intensity indicates an improvement of the crystal quality of the ZnO films, which occurred during annealing at higher temperatures. Commonly with ZnO a broad green band emission is also observed [2004Sai], which does not appear in the present study. While the UV emission corresponds to the near band-edge emission, the green band emission has been attributed to the singly ionized oxygen vacancy in ZnO and results from the recombination of a photo-generated hole with an electron occupying the oxygen vacancy [1996Van]. The stronger the intensity of the green luminescence, the more singly ionised oxygen vacancies there are. The absence of the visible luminescence indicates that there is no substantial oxygen vacancy concentration in the annealed ZnO films.

When the excitation is performed at a wavelength of 325 nm, the films annealed at 600°C and 700°C only show very weak UV luminescence. This is attributed to the vibrational absorption of the silica network, which may cause the loss of excitation photon loss before exiting the electron from the valence band to the conduction band of ZnO. A similar energy loss process has been proposed in the earlier work [2003He, 2001Yao].

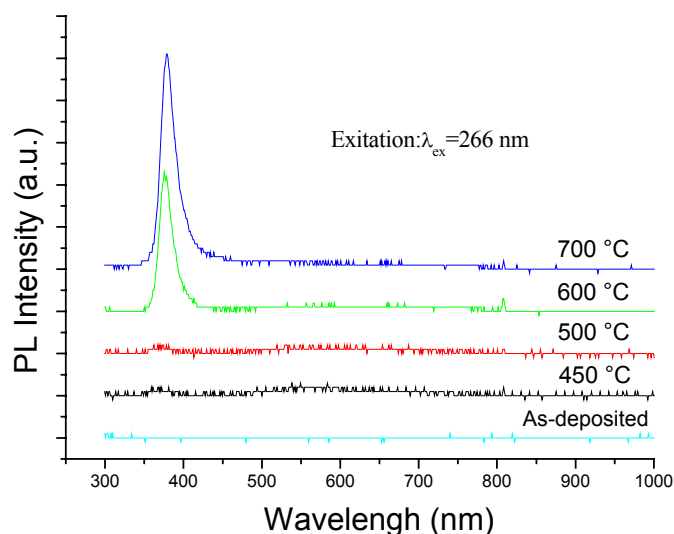


Fig. 4.14 Room temperature PL spectra of ZnO films annealed at various temperature.

The present films reveal no luminescence peak at 525 nm. This is in disagreement with observations that both pure [2002Xu] and magnesium-doped [2003Ji]  $\text{Zn}_2\text{SiO}_4$  bulk crystal show luminescence in this region. This discrepancy may be due to the small amounts of  $\text{Zn}_2\text{SiO}_4$  present in the films investigated here.

## CHAPTER 5

# **Polyvinylpyrrolidone-controlled synthesis and structural properties of nanocrystalline ZnO thin films**

### **5.1. Introduction**

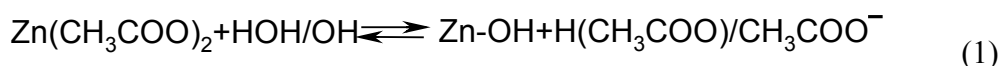
Homogeneous ZnO thin films were successfully deposited from aqueous solution as described in Chapter 3. However, the as-deposited films were still amorphous, post-annealing is necessary to obtain nanocrystalline films, which would not be applicable for the temperature sensitive substrates like polymers. Therefore, a low temperature synthetic procedure that requires no post-deposition annealing step is very desirable.

Usually relatively large particles are formed rapidly in aqueous solutions whereas they grow much slower in non-aqueous solvents, allowing controlled synthesis of nanometer-sized particles. It has been reported that the nanometer-sized ZnO particles can be synthesized via the reaction of  $Zn^{2+}$  and  $OH^-$  in alcohols as the solvent [1985Koc, 1991Spa, 1998Meu]. The stabilization of ZnO nanocrystals was studied by utilizing the same solution system with poly(vinylpyrrolidone) (PVP) as a polymer additive [2000Guo, 2000GuoL-2, 2001Yan]. It was shown that spherical nanometer-sized ZnO particles with quite narrow size distribution could be obtained. Moreover, these ZnO/PVP particles showed enhanced photoluminescence in comparison to ZnO particles without organic modification grown under the same condition. Therefore, it would be interesting to apply this concept for the synthesis of the nanostructured ZnO films. However with the above-mentioned method only small amounts of ZnO material could be produced from the diluted precursor solution due to the limited solubility of zinc salts in the alcoholic solvent, which would not be enough for the fabrication of films.

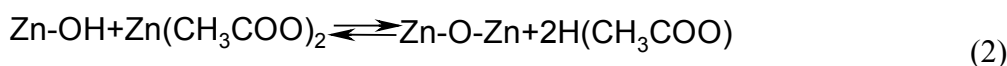
In order to make this system suitable for an efficient film synthesis via CBD, this method was modified in the following way so that the oxide can be produced in high yield. Firstly, water in a controlled amount was used to dissolve the zinc salts and NaOH before the alcoholic solvent was added, thus the zinc concentration in the solution could be greatly increased. Secondly, a modification was made by adding the NaOH-containing solution into the solution of zinc salts at a controlled mixing rate, so that no precipitation occurred in the concentrated bulk solution upon mixing the two solutions.

## 5.2. Results and discussions

Oxides can be formed by hydrolysis (1) and condensation (2) of species dissolved in aqueous or non-aqueous solution according to [1990Bri, 1998Meu]:



and



In the alcoholic solution, ZnO particles, and not the hydroxide product are obtained due to the dehydrating effect caused by this solvent.

### 5.2.1. Synthesis of ZnO nanostructured films

#### 5.2.1.1. Effect of [PVP]/[Zn] concentration ratio

The influence of the homopolymer PVP on the ZnO film deposition on silicon wafers modified with sulfonate-functionalized SAMs was investigated. ZnO films were deposited from solutions containing zinc acetate (10 mM) with various [PVP]/[Zn] molar ratios of 1.5:5, 2:5, 2.75:5 and 3:5. The ZnO films obtained with [PVP]/[Zn] >2:5 show interference colors depending on the actual film thickness after the deposition time of 7.5 h, indicating the surface of the films is smooth. Whereas the ZnO films obtained with [PVP]/[Zn] ≤ 2:5 are lacking luster after the same deposition time, suggesting a high roughness of the film surface compared to other films. Films obtained from solution containing different [PVP]/[Zn] concentration ratios were investigated by scanning electron microscopy. Although no quantitative evaluation was made, the SEM results reveal a general trend, observed for a series of films, namely that the decrease in molar ratio of the [PVP]/[Zn] is roughly proportional to the particles size distribution presented in the films, further to the roughness of the films. SEM results of two typical films are shown in Fig. 5.1, It can be seen that with [PVP]/[Zn] = 2:5, ZnO film exhibits a rough surface. Whereas when [PVP]/[Zn] is slightly increased to 2.5:5, film consisted of particles with narrower size distribution and the large agglomerates is hardly observed that is normally presented in the films with [PVP]/[Zn] = 2:5.

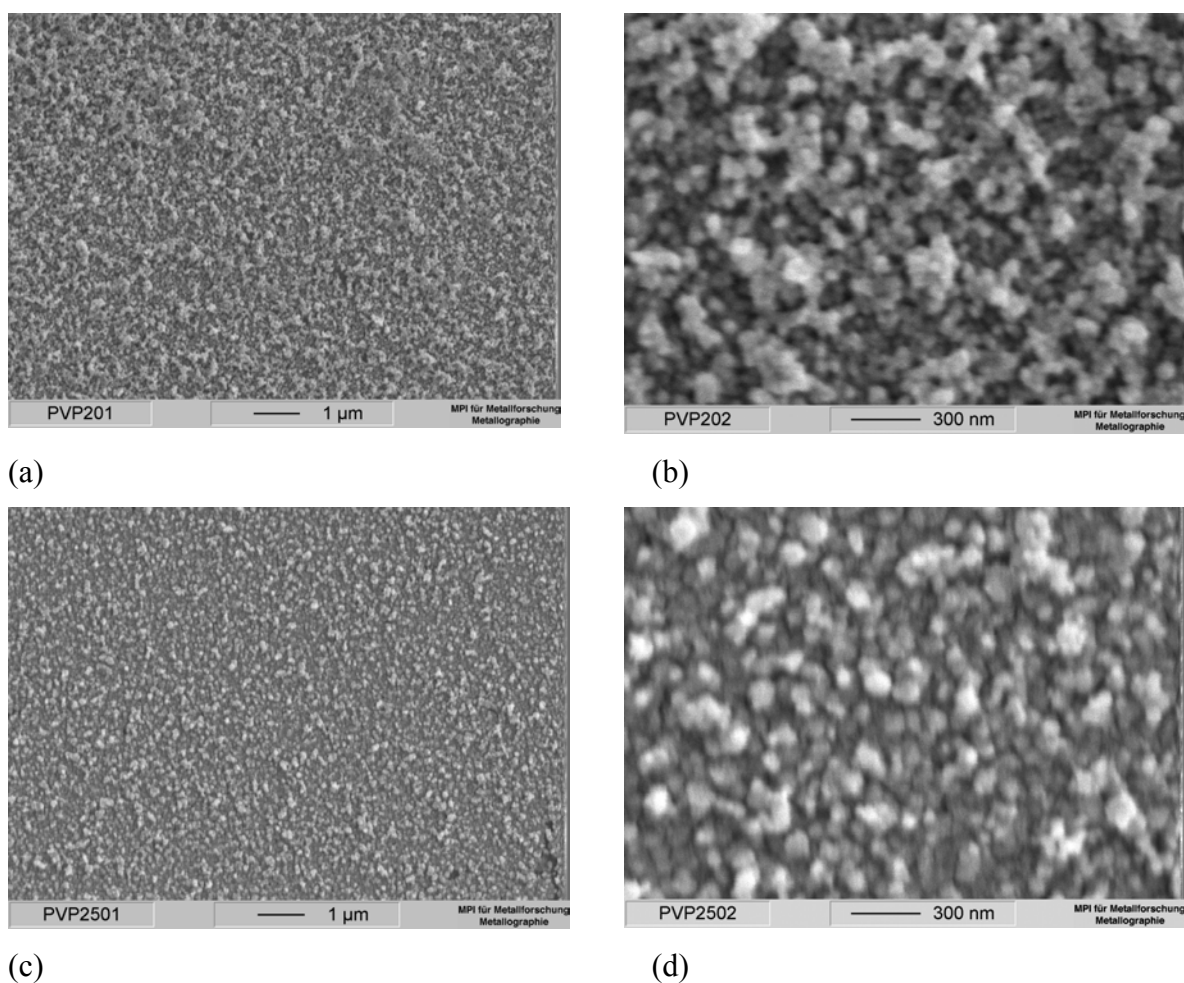
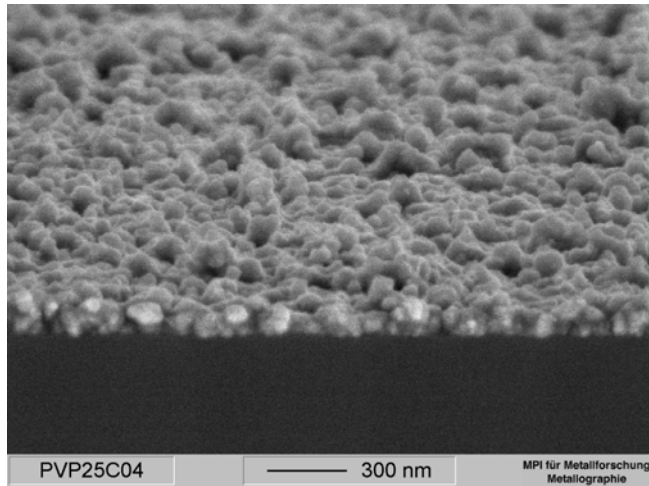
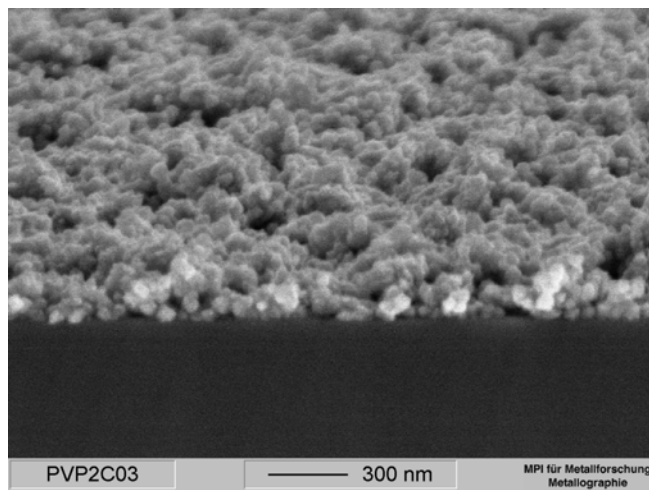


Fig. 5.1 SEM micrographs of ZnO films deposited on SO<sub>3</sub>H-functionalized silicon wafers at 55°C after 7.5 h: (a, b) [PVP]/[Zn] = 2:5. (c, d) [PVP]/[Zn] = 2.5:5.

The cross-sectional SEM images of films obtained with various [PVP]/[Zn] concentration ratios are shown in Fig. 5.2. It can be seen that the thickness of the ZnO film obtained with [PVP]/[Zn] = 2.5:5 is about 120 nm. For the ZnO film obtained with [PVP]/[Zn] = 2:5, no clear cross-section could be observed, which can be considered as a consequence of the formation of the film consisting of large agglomerates.



(a)



(b)

Fig. 5.2 Cross-sectional SEM micrographs of ZnO films deposited on SO<sub>3</sub>H-functionalized silicon wafers for 7.5 hours at 55°C: (a) with [PVP]/[Zn] = 2.5:5 and (b) [PVP]/[Zn] = 2:5.

The X-ray diffraction pattern obtained is shown in Fig. 5.3. The three films consist of zincite, since in each case three typical reflections, i.e. (100), (002) and (101), could be identified. The broadening of the peaks is related to the nanometer grain sizes of the films. The XRD results suggest that nanometer-sized crystallites are formed in the solution, stabilized by PVP and thus contribute to form the films.

It should be noted that no significant films were observed on the bare silicon wafers under the conditions where films occurred on -SO<sub>3</sub>H terminated SAMs.



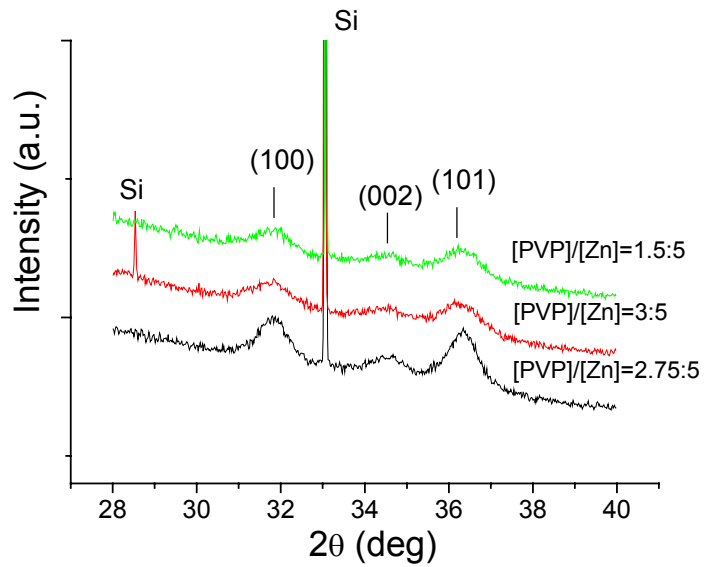
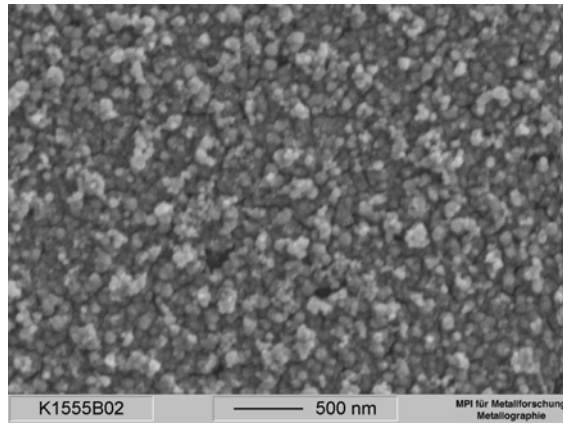


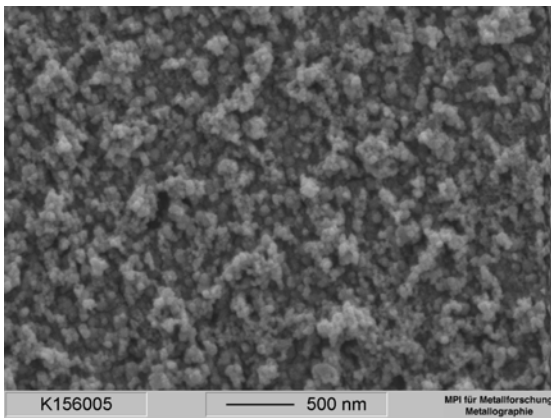
Fig. 5.3 XRD patterns for ZnO films from solution with various [PVP]/[Zn] ratios.

#### 5.2.1.2. Effect of deposition temperature

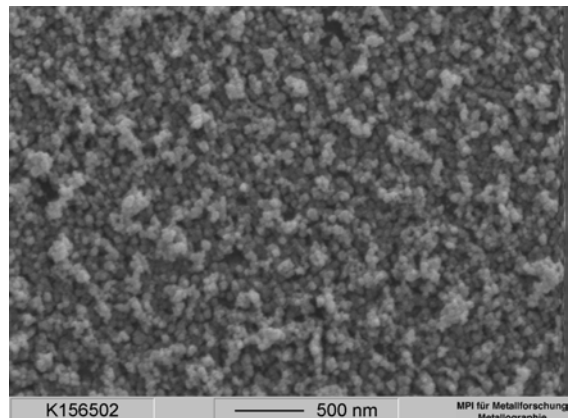
Fig. 5.4 shows SEM images of ZnO films deposited at 55°C, 60°C and 65°C. The film deposited at 55 °C is composed of particles, whereas with increasing reaction temperature, the films consist of larger agglomerates and exhibit an increased roughness. It is noteworthy that ZnO films can be deposited even at room temperature. Fig.5.5 shows the AFM micrograph of a ZnO film obtained at room temperature. The film consists of very uniform nanometer-sized particles and its thickness is around 10 nm after 5 h deposition. Obviously the film formation rate decreases when lowering the deposition temperature and extending deposition time would be necessary to obtain thicker films. Nevertheless the study clearly demonstrates the feasibility of fabricating thin nanostructured ZnO films even on substrates, which are highly temperature-sensitive.



(a)



(b)



(c)

Fig. 5.4 SEM micrographs of ZnO films deposited on SO<sub>3</sub>H-functionalized silicon wafers for 7.5 hours at (a) 55°C, (b) 60°C and (c) 65°C.

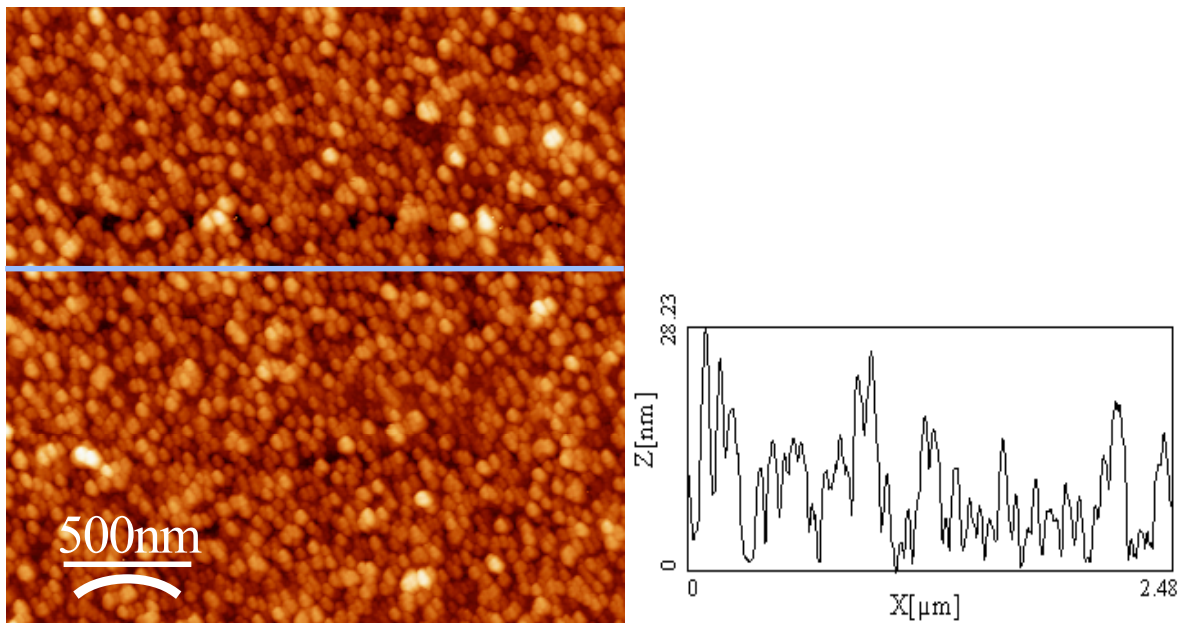


Fig. 5.5 AFM micrographs of a ZnO film deposited on SO<sub>3</sub>H-functionalized silicon wafer for 5 h at room temperature.

### **5.2.1.3. Influence of water**

Zinc salts and NaOH are more soluble in water than in 2-propanol, therefore introducing small amounts of water into a precursor solution is an important step for preparing the precursor solution for further film formation. However, small amounts of water in the solution not only improve the solubility but also change the growth rate of ZnO nanoparticles. According to equation 1, the addition of H<sub>2</sub>O can lead to faster growth of ZnO particles. Therefore, it is important to control the amount of water carefully.

## **5.2.2. Detailed investigation of a ZnO Film from an optimized concentrated solution**

### **5.2.2.1. SEM investigations**

Basically, the film thickness can be readily controlled by changing the deposition time. In addition, the concentration of the solution has a strong impact on the film formation kinetics. Through increasing the zinc ion concentration in the solution, the film growth rate can be increased substantially. It should be noted that in the present case, it is not easy to achieve the solution of higher concentration due to the poor solubility of the reactants. Nevertheless, attempts were made to deposit ZnO film from a highly concentrated solution of zinc acetate (12.5 mM) with the [PVP]/[Zn] molar ratio of 3:5. ZnO film of 125 nm in thickness was obtained after 4.5 h deposition time. The film reveals a rather high surface roughness and is composed of well-packed particles (Fig. 5.6).

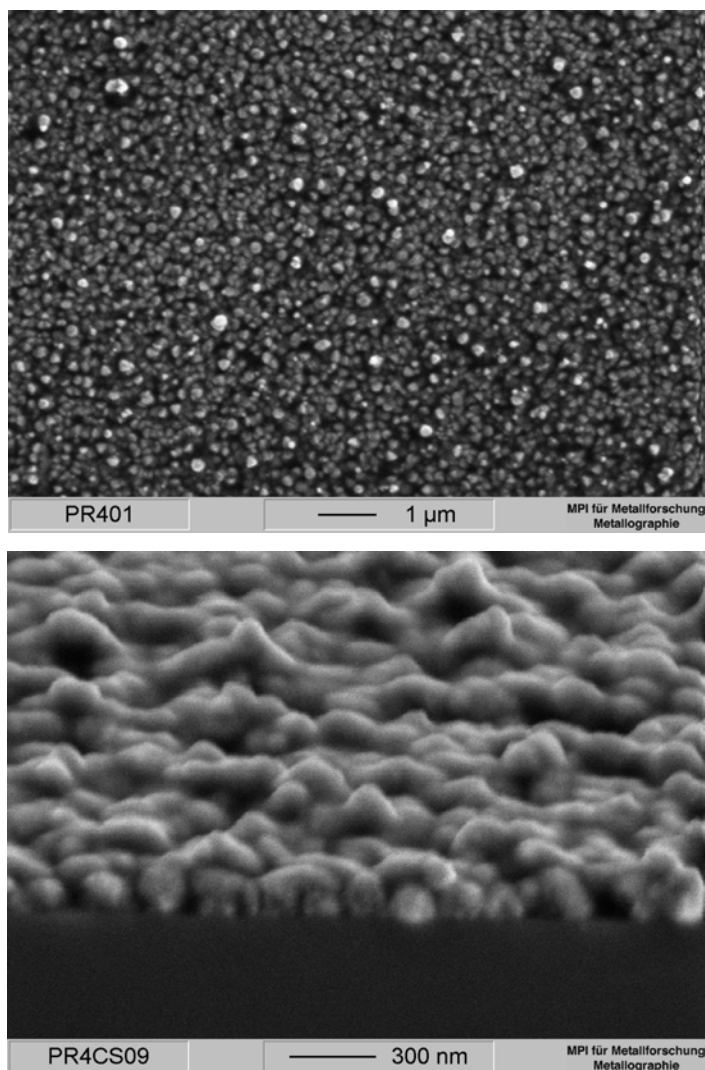


Fig. 5.6 SEM micrographs of a ZnO film deposited on SO<sub>3</sub>H-functionalized silicon wafer from concentrated solution at 55°C for 4.5 hours.

### 5.2.2.2. XRD and XPS investigations

XRD pattern of the ZnO film is shown in Fig. 5.7. The peaks are consistent with that of the zincite phase. The broadening of the reflection peaks indicates that the film consist of nanometer-sized ZnO crystallites. Taking into account the fact of the incorporation of the copolymer in the as-deposited ZnO films obtained from aqueous solution containing a graft copolymer (Chapter 3.2.5.), XPS scans were also performed in the present study with the aim to check the presence of PVP in the film. In survey spectra Zn, O, C and Si were found and Zn 2p peak and O 1s peak were further analyzed. Curve fitting of the Zn 2p peak revealed only one component at 1022.3 eV (Fig. 5.8a), which corresponds to the reference value reported for ZnO [03Hof, 00Dup]. The O 1s peak could be fitted by three contributions (Fig.

5.8b). The high binding energy component (peak 1) can be attributed to the presence of  $\text{SiO}_2$ , which originated from a very small spectral contribution of the  $\text{SiO}_2$  film of the silicon substrate. The medium binding energy component (peak 2) can be attributed to surface hydroxyl group. The presence of OH groups on ZnO nanometer-sized particles was also found in other work [1998Bor, 1985Koc]. It was suggested that the photoluminescence of the particles was related to such OH groups on the surface. The component on the low binding side (peak 3) is attributed to ZnO. The signal of the measured N 1s peak is hardly discernible from the noise of the background intensity, indicating that the nitrogen content in the grown oxide film is very small (i.e. below 1 at.%). The C 1s peak is accurately described with a single component due to adventitious carbon. Conclusively, residuals of PVP in the grown oxide film can be neglected.

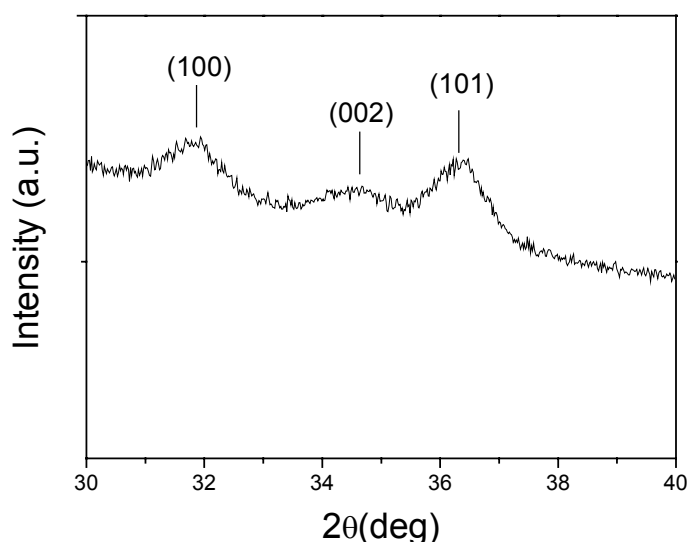


Fig. 5.7 XRD pattern of a ZnO thin film deposited on  $\text{SO}_3\text{H}$ -functionalized silicon wafer for 4.5 h.

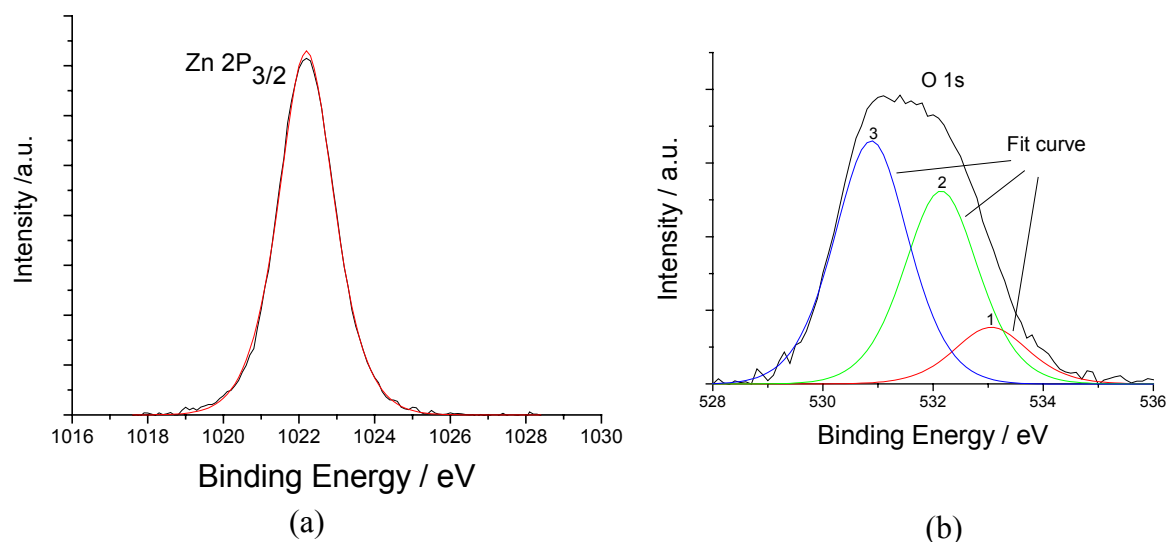


Fig. 5.8 XPS spectra of a ZnO thin film deposited on SO<sub>3</sub>H-functionalized silicon wafers for 4.5 h: (a) Zn 2p<sub>3/2</sub> peak and (b) O 1s peaks.

### 5.2.2.3. Transmission electron microscopy investigations

Fig. 5.9a shows TEM results of the cross-section of a ZnO film. A complete surface coverage of the substrate and a rather uniform thickness of 130 nm can be observed. The thickness obtained from TEM cross-section is in agreement with that from SEM cross-section (125 nm). The slight difference can be due to the thickness fluctuation on the different area of the whole sample. The amorphous layer between the ZnO film and the silicon substrate can also be seen, which consists of the sulfonated SAM and the native oxide SiO<sub>2</sub>. The corresponding SAD diffraction pattern indicates that the ZnO film is polycrystalline (Fig. 5.9b). Compared to the random polycrystalline SAD pattern, which is characterized by a series of continuous rings, the present pattern suggests the presence of texture in that area where the diffraction pattern was taken. More SAD patterns taken from different area of the film show the same tendency, being different from the random polycrystalline pattern. This suggests that the film has local texture.

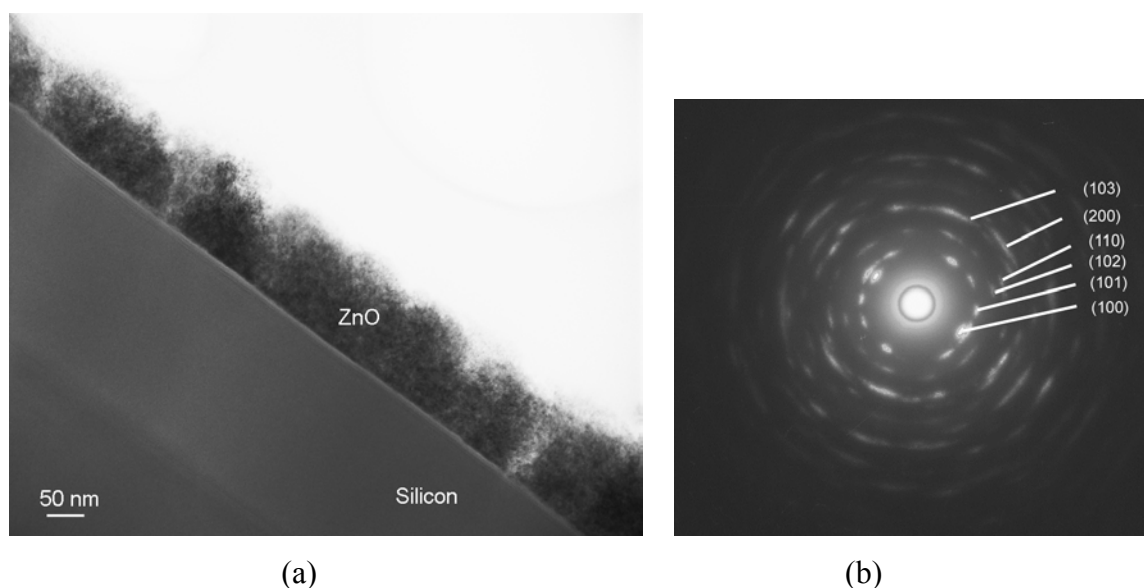


Fig. 5.9 (a) Cross-sectional TEM micrograph of a ZnO film deposited on SO<sub>3</sub>H-functionalized silicon wafer for 4.5 h and (b) the corresponding SAD pattern.

Fig. 5.10a shows the dark field cross-section image of the ZnO film. Domains of about 135 nm in size comprising nanometer-sized ZnO crystallites can be seen (domains are marked in the figure). Attempts were made to gain more detailed structural information by plan-view TEM investigations. Similar to the cross-section image, the DF plan-view TEM micrograph displayed in Fig. 5.11 shows that the ZnO film is composed of domains with average size of 140 nm. A higher magnification DF plan-view image (Fig. 5.11b) reveals the nanometer-sized crystallites, which formed the separate domain, are oriented along a certain preferred direction (see the domain marked in the Fig. 5.11b).

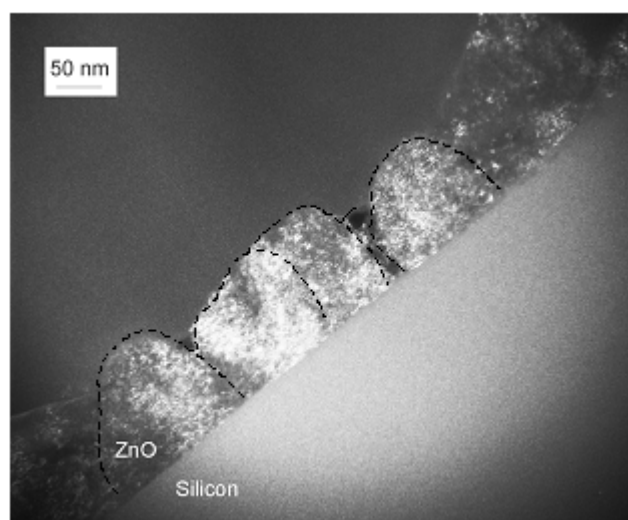
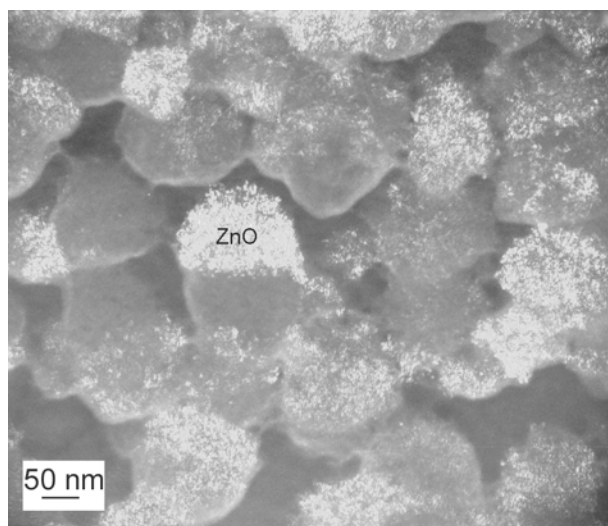
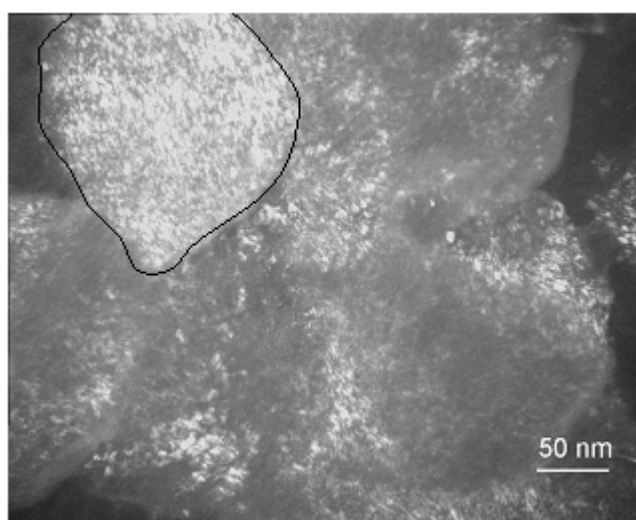


Fig. 5.10 cross-sectional dark-field TEM micrograph of a ZnO film deposited on SO<sub>3</sub>H-functionalized silicon wafer for 4.5 hours.



(a)



(b)

Fig. 5.11(a) Plan-view dark-field TEM micrograph of a ZnO film deposited on  $\text{SO}_3\text{H}$ -functionalized silicon wafer for 4.5 h and (b) higher magnification.

Detailed HRTEM investigation was conducted to clarify the structural property of the nanometer-sized particulate ZnO film. A cross-sectional HRTEM micrograph of the ZnO film areas in the vicinity of the substrate is shown in Fig. 5.12a. It clearly shows the ZnO crystals of the first film layer on the substrate are oriented with their (002) planes almost parallel to the silicon substrate surface. All these nanocrystals have almost the same crystallographic orientation. Nevertheless, small-angle grain boundaries can be observed and this allows the two crystals to be distinguished (Fig. 5.12c). The rotational moiré fringe (Fig. 5.12b) reveals the misfit between two crystals along the a-axis. From the fringe spacing in the moiré pattern, a rotational misfit of  $4^\circ$  between two crystals was obtained from calculation [2002Ful].



Another arrangement of ZnO crystals on the substrate was observed, which is shown in Fig. 5.13. The ZnO crystals of the first layer in the film locate on the substrate with the (100) planes nearly parallel to the substrate surface (Fig. 5.13a). Similar to that case discussed above, small-angle grain boundary was observed between two adjacent nanoparticles.

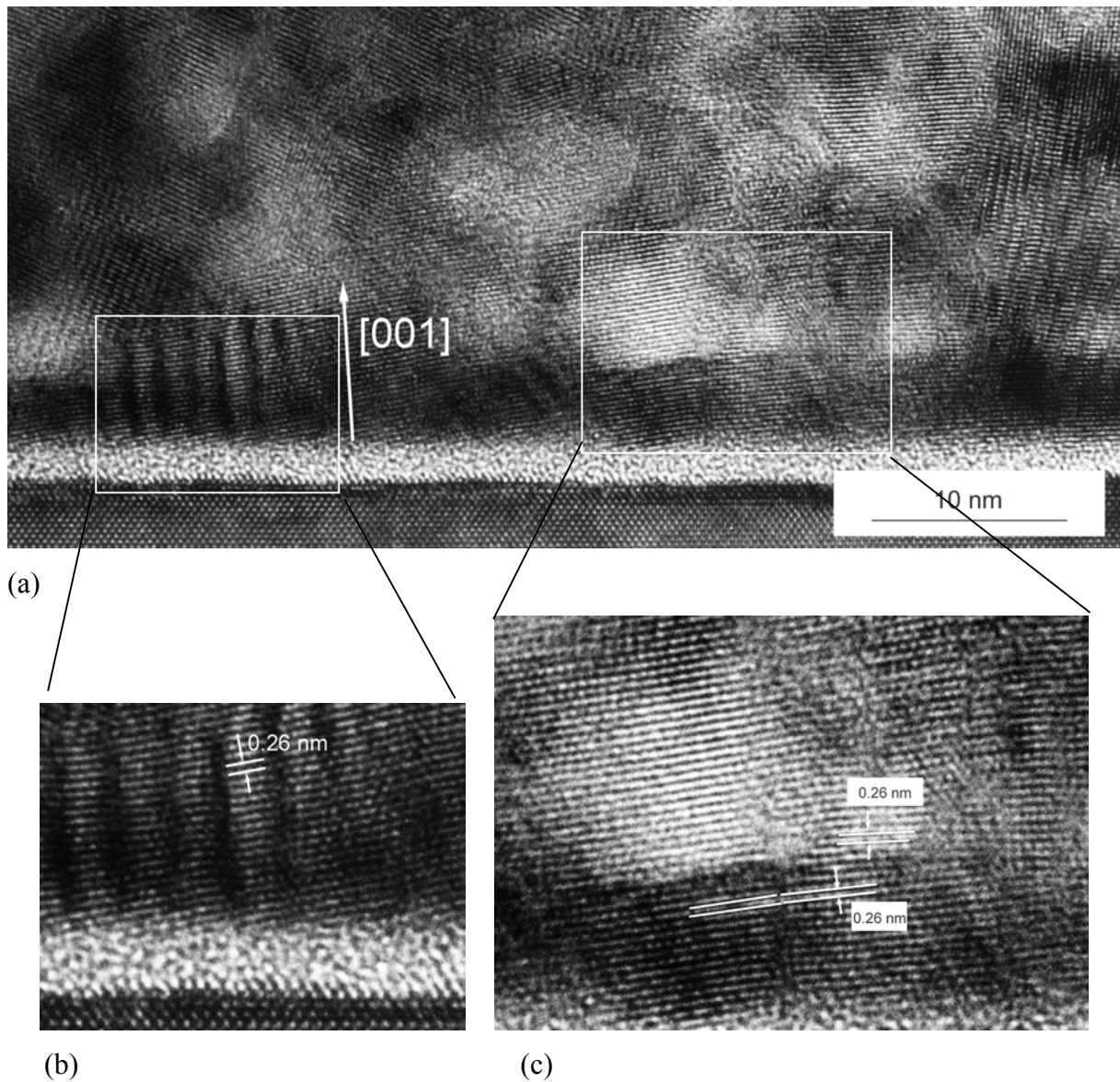


Fig. 5.12 (a) cross-sectional HRTEM image showing ZnO film growth with oriented attachment and (b, c) enlarged area as marked in (a).

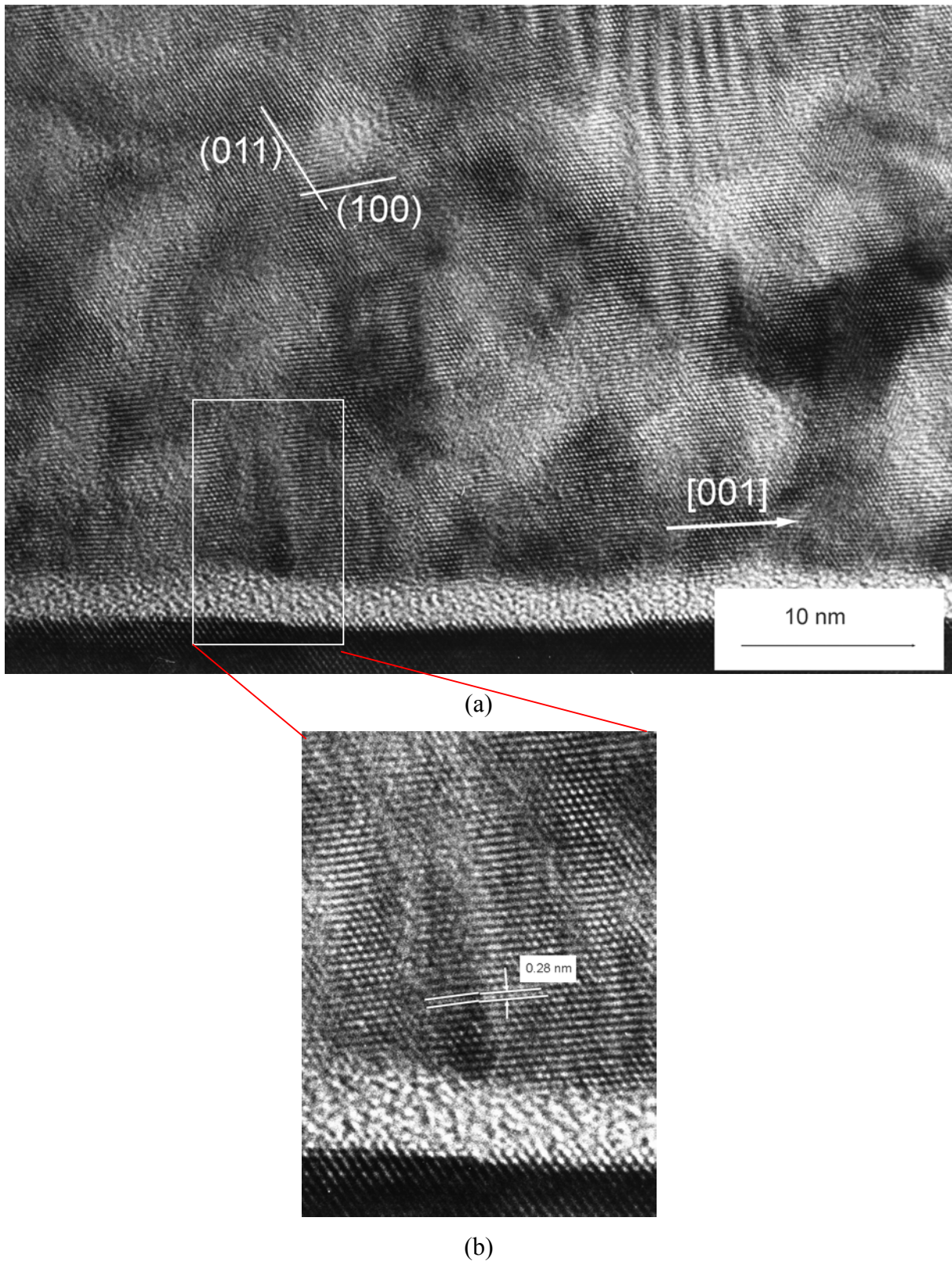


Fig. 5.13 (a) cross-sectional HRTEM image showing ZnO film growth with oriented attachment and (b) enlarged area as marked in (a).

The present results provide the direct evidence of the aggregation-based oriented attachment between crystals, which contribute to form the compact ZnO films. As described in the

introduction, ZnO has a hexagonal structure. The basal plane (002) of ZnO is polar surface, whereas the prismatic planes {100} are non-polar surface. Therefore, the selective oriented attachment, i.e., polar surface to polar surface and non-polar to non-polar surface can occur. It is assumed that during the initial stage of the film formation, individual ZnO particles find their positions on the substrate most probably in two ways discussed above. The first is that the ZnO crystals locate on substrate with the (002) plane parallel to the substrate surface, that is, with c-axis perpendicular to the substrate, as illustrated in Fig. 5.14a. The second is that the (100) plane of the ZnO crystal is parallel to the substrate surface, that is, the c-axis is parallel to the surface (Fig. 5.14b). The way in which these particles are arranged on the substrate determines the alignment of the subsequent surrounding particles based on the oriented attachment.

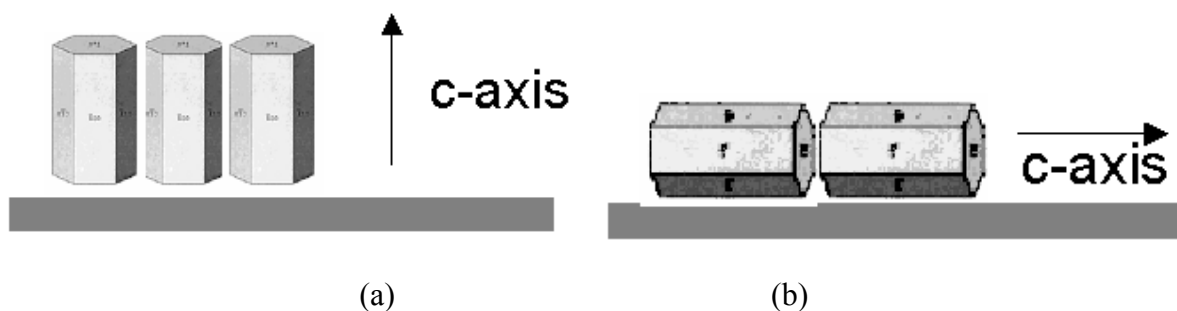


Fig. 5.14 The schematic illustration of the formation of the first ZnO layer on a substrate.

In other words, the oriented aggregation is initiated at multiple sites on the substrate. The orientation adopted within one region is unrelated to that in an adjacent region. At some sites even defect (vacancy, dislocation etc.) can occur. Finally, domains consisting of nanocrystals having preferred orientation occur. Even, in some cases, domains consisting of nanocrystals sharing the common crystallographic orientation can occur (Fig. 5.15). This is in agreement with the concept of oriented particle aggregation developed recently [2000Ban]. It describes the self-assembly of colloidal primary particles into aggregation and the subsequent internal restructuring, which leads to a crystallographically continuous and ordered structure. Evidence of this mechanism with ZnO was also provided by HRTEM investigations of nano-sized rods [2002Pac].

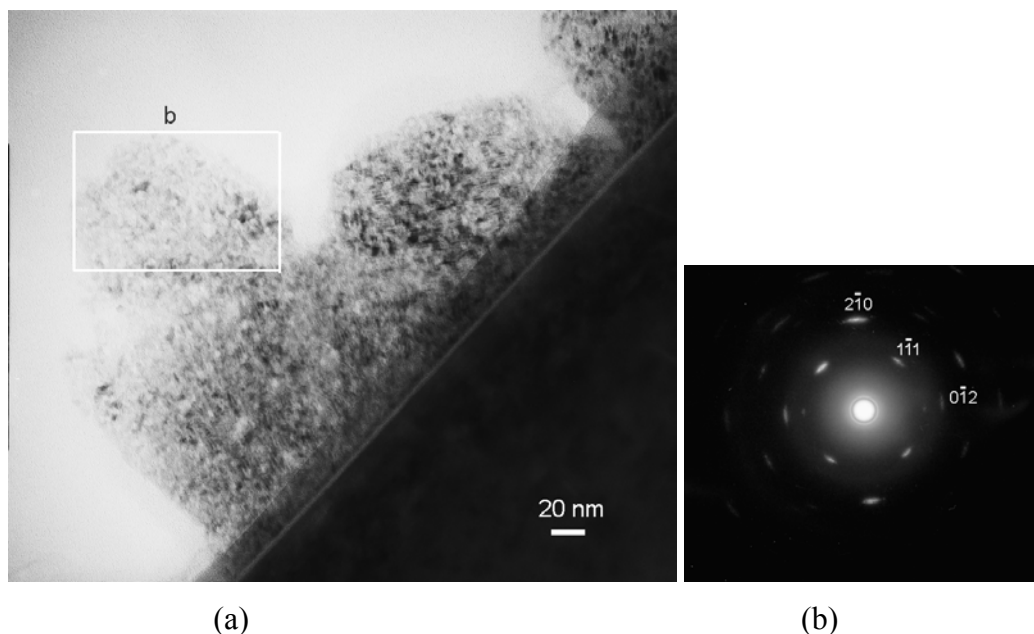


Fig. 5.15 (a) BF Cross-sectional TEM micrograph of a ZnO film and (b) the corresponding SAD pattern.

HRTEM investigation reveals that the ZnO particles of the first one or two layers in the film are small crystallites of 5 nm, whereas in the region further away from the substrate, particles self-assembled themselves in the ordered way and they share a common crystallographic orientation, which makes the determination of the particles size impossible. Additionally XRD investigation in section 5.2.2.2 provided only relatively weak and broad peaks, with which the grain size cannot be estimated. According to the TEM results, the reason for the weak, broad peaks in XRD pattern is three fold: firstly, average grain size is too small. Secondly, film is very thin (130 nm in thickness). Thirdly, the absence of  $K_{\alpha 2}$  inevitably leads to the loss of intensity of the peaks.

Basically, the shape of the inorganic crystals is related to the intrinsic unit cell structure and in fact, it is the outside embodiment of the unit-cell replication and amplification [2004Yu]. Kinetically, the morphology of the crystals is related to the relative growth rates of various crystal faces that bound the crystal. For ZnO, the growth rates of the directions  $\langle 001 \rangle$ ,  $\langle 101 \rangle$ ,  $\langle 100 \rangle$  have the relationship of  $R_{\langle 001 \rangle} > R_{\langle 101 \rangle} > R_{\langle 100 \rangle}$ . The fastest growing faces have the highest surface energies and thus have the tendency to vanish in the final morphology. Along with the above-mentioned oriented attachment mechanism, this principle determines the common shape of the ZnO crystal to be rod or wire-like, which was observed in many studies [1990And, 2003Fuc, 1996O'B]. In the present work, PVP was added with the aim to control the ZnO crystal growth. The presence of the nanometer-sized ZnO crystals in the films confirms that the addition of PVP inhibited the ZnO crystal growth. The nanometer-sized

hexagonal particles were stabilized by the steric interaction of PVP without further growth. It is assumed that the addition of PVP retards particle growth but does not change the ratios of the growth rate between the individual planes. Therefore the building units of the films are the nanometer-sized hexagonal ZnO rods with distinct crystalline facets, not the spherical ZnO nanoparticles described by Guo et al. [2000GuoL-2]. The non-spherical shape of the ZnO particles led to its location on the flat substrate surface with facet-contact. The point-contact occurred in the case of spherical particle would not be favorable. Furthermore the fact that no nitrogen signals was detected in the films by XPS measurement suggested the release or desorption of the PVP into the solution from the surface of the ZnO crystals when the subsequent ZnO particles reached and oriented attachment occurred due to the strong interaction between the two planes of the ZnO crystals. Therefore it is believed that PVP mainly influences the growth of the colloidal particles and has less direct impact on the attachment process.

A scheme of the proposed film formation mechanism is shown in Fig. 5.16. The ZnO particles, which reach the substrate firstly, attach with c axis either parallel or perpendicular to the substrate surface and define the crystallographic orientation of the particles subsequently attached.

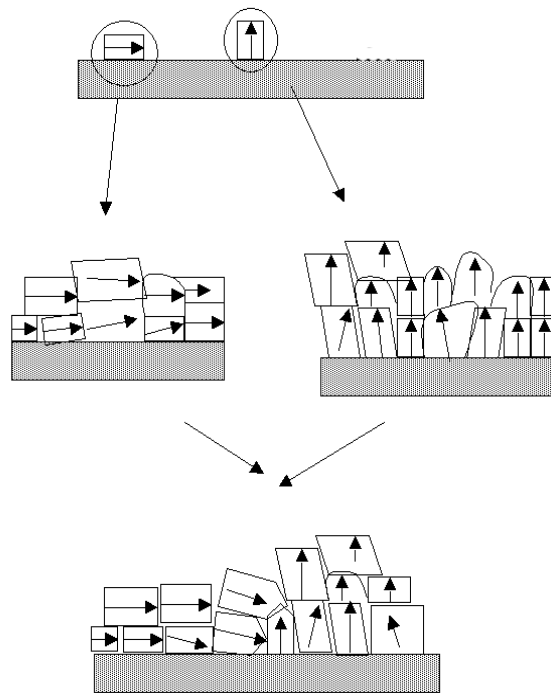


Fig. 5.16 The scheme of the ZnO film growth mechanism proposed.

#### 5.2.2.4 Optical transmission spectra of the ZnO film

Fig. 5.17 a, b show optical transmittance spectra for a ZnO film on glass prepared under identical conditions where films formed on silicon wafers in the range of 430 to 2000 nm. The film was found to be transparent (above 80%) in the visible and infrared region. Comparable results were also obtained with the commercial ZnO crystals [1998Sri] and ZnO films obtained via other routes [1993Olv, 1995Exa]. It is known that ZnO is a UV absorber [1976Bro]. Unfortunately in the present study the transmittance in the UV range could not be measured due to the limitation of the equipment.

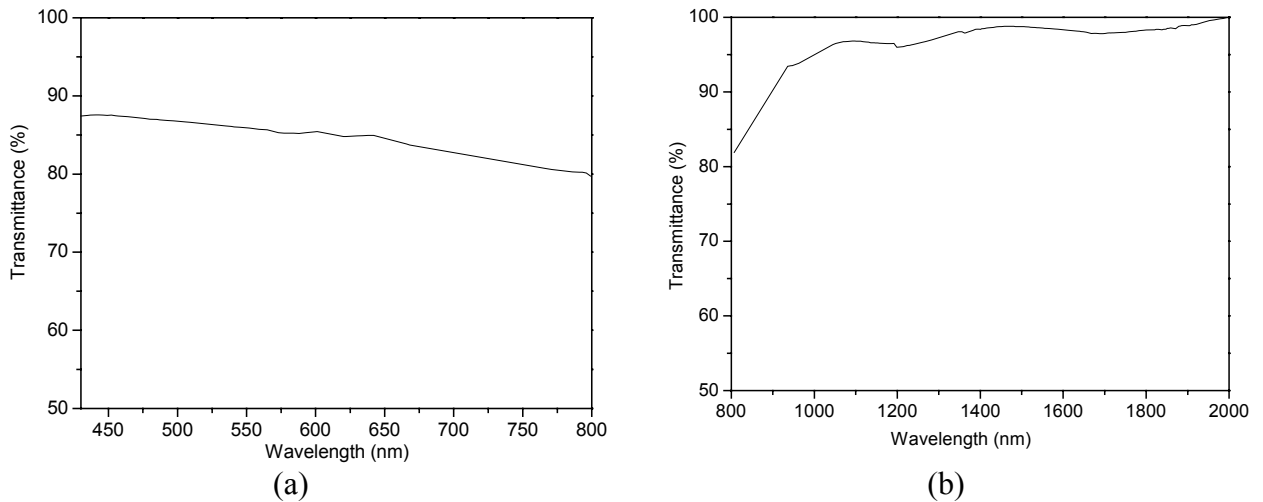


Fig. 5.17 The optical transmittance spectra of a ZnO film (a) in visible light region and (b) infrared region.

#### 5.2.2.5 Photoluminescence investigations

Photoluminescence spectra of the ZnO thin film were measured with a He-Cd laser (325 nm) as an excitation source. A strong near-band-gap edge emission at  $\sim 388$  nm and a broad visible-light emission (centered at  $\sim 538$  nm) can be observed (shown in Fig. 5.18). Whilst the UV emission corresponds to the near band-edge emission, the green emission peak is commonly referred to as a deep-level or trap-state emission. The strong UV luminescence observed demonstrates the good quality of the nanometer-sized particles in the ZnO film. The intensity ratio of the UV luminescence peak to the green luminescence peak is around 1.6.

Guo et al. investigated the influence of PVP on the optical properties of PVP-capped ZnO nanometer-sized particles [2000Guo]. They showed that with the introduction of PVP, the intensity of the UV peak increased dramatically at the expense of the green peak. It is believed therefore that further optimization efforts can also completely eliminate the green emission of the films.

Photoluminescence of the ZnO film obtained was further investigated by exciting with light of different wavelength. The obtained PL spectra are given in Fig. 5.19. When the wavelength of excitation light is 280 nm, a UV emission peak and a 530 nm green emission peak are observed. When the wavelength of excitation light increases up to 308 nm, the above mentioned two PL peaks are much weaker. With excitation wavelength of 350 nm, the film exhibits a much stronger UV emission and a weak green emission. With excitation wavelength of 493 nm, the green emission appears with increased intensity and much smaller peak width. The intensity ratio of the UV luminescence peak to the green one varies with the excitation wavelength. Except in the case of the excitation wavelength of 493 nm, both peaks occurred at any excitation wavelength. This is different from the work done by Zhang et al [2002Zha], they indicated that every PL peak corresponded to a special excitation wavelength for ZnO films. When the films were excited with different wavelength, the corresponding emission peak quenched and new peaks occurred. The inconsistency might be due to the different film fabrication methods used.

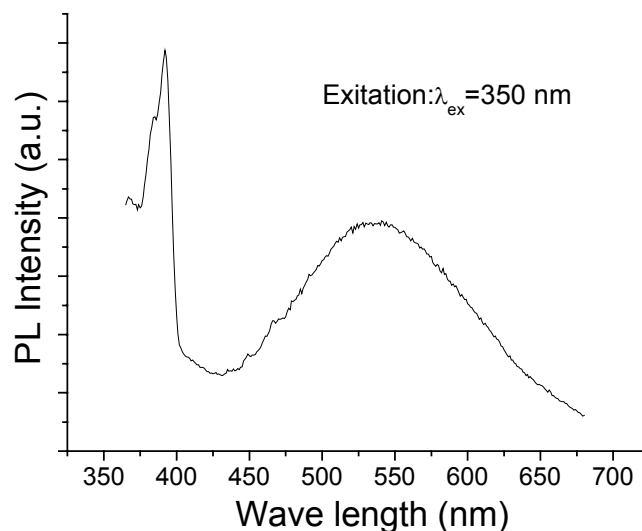


Fig. 5.18 Room temperature photoluminescence of a ZnO film.

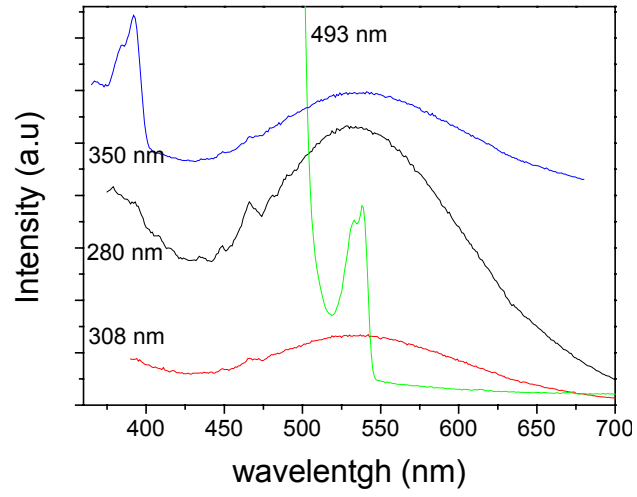


Fig. 5.19 Room temperature PL emission spectra of a ZnO film excited at different wavelengths.



## CHAPTER 6

### Mechanisms of the formation of nanostructured ZnO thin films on SAM-modified substrates via CBD

#### 6.1. Status study of the ZnO film growth on silicon wafers modified with various SAMs

The ZnO film deposition onto SAM-modified substrates via CBD has encountered great difficulties and only very little work has been reported [2004Tur, 1998Deg], besides those covered by the author's group [2002Hof, 2003Hof, 2003Fuc]. The ZnO growth on various SAM surface groups is summarized in Table 6.1. The main difference between the products obtained in the literature [2004Tur] and those in the present study is that the former consisted of micrometer-sized more or less elongated zincite crystals, while the latter consisted of nanometer-sized particles, leading to a homogeneous nanostructured film.

Table 6.1 influences of the SAM-treated silicon substrate surface on ZnO growth via CBD.

Substrate modification	Solution modification by polyelectrolyte		
	Results in literature	Present investigation	
	none	Copolymer (Chapter 3 and 4)	PVP (Chapter 5)
none	Micrometer-sized ZnO crystals (as described in Chapter 1)	No deposition	No deposition
-SO <sub>3</sub> H	[1998Deg] Zn(OH) <sub>2</sub> thin film	No deposition	Homogeneous film
	[2003Fuc] Hexagonal ZnO rods		
-SCOCH <sub>3</sub>	[1998Deg] Zn(OH) <sub>2</sub> thin film	Homogeneous film	N/I
-SH	[2003Fuc] Hexagonal ZnO plates	Homogeneous film	N/I
-Br	N/A	Homogeneous film	N/I
-N <sub>3</sub>	N/A	Homogeneous film	N/I
-NH <sub>2</sub>			
-O-C <sub>6</sub> H <sub>5</sub>	[2004Tur] Hexagonal ZnO rods	N/I	N/I

N/I: not investigated. N/A: not available.

Turgemann et al. [2004Tur] investigated the ZnO crystal growth on silicon wafers modified by SAMs from a solution containing  $\text{Zn}(\text{NO}_3)_2 \cdot 6\text{H}_2\text{O}$  and HMTA at 90 °C. Random oriented ZnO crystals with 0.15  $\mu\text{m}$  in width, 3  $\mu\text{m}$  in length were observed on -O-C<sub>6</sub>H<sub>5</sub> functionalized SAMs. The thickness of the SAM monolayer was observed to have influence on the orientation of the ZnO crystal growth. As for the film covered by De Guire et al. [1998Deg], low temperature (35 °C) was used for film deposition to avoid the formation of the micrometer-sized ZnO crystals. The final product was assumed to be  $\text{Zn}(\text{OH})_2$  rather than ZnO. Fuchs [2003Fuc] studied ZnO film deposition from aqueous solution containing  $\text{ZnCl}_2$  and HMTA. Only micrometer-sized ZnO hexagonal rods or plates were observed. No clear ZnO growth mechanism was proposed for the above-mentioned micrometer-sized ZnO growth. It seems, however, the heterogeneous nucleation played an important role. In contrast, a different film deposition mechanism (details are discussed below) was involved for the nanostructured films obtained in the present study.

As shown in Chapter 3 and Chapter 5, two precursor solution systems were explored for the ZnO thin films deposition onto the SAM-modified substrates. A series of sols were designed and prepared prior to deposition for each system. The sols that exhibited no visible precipitation within 2 h at the deposition temperature were selected as the deposition solution. For the first system, AFM micrograph indicated the presence of nanometer-sized particles of 4 nm in size in the film obtained after 1.5 h deposition time (Fig. 6.1). Whereas for the second one, HRTEM investigation revealed that the films consisted of nanometer-sized particles of around 5 nm (Chapter 5.2.2.3.). Therefore, it is assumed that the particle attachment (homogeneous growth mode) led to the film formation.

One interesting result is that with the copolymer-induced deposition system, no film growth was observed on silicon wafers modified by a  $\text{SO}_3\text{H}$ -SAM. In contrast, a homogeneous film was obtained on a  $\text{SO}_3\text{H}$ -SAM from the PVP-added deposition system. Additionally, in both cases no film growth was observed on bare silicon wafers.

Similarly, De Guire et al. investigated the oxide film formation ( $\text{TiO}_2$ ,  $\text{ZrO}_2$ ) on SAM-treated silicon wafers [1997Shi] and they indicated that particle attachment led to the film formation. A film formation mechanism considering the forces similar to that existed between colloidal particles in fluids was proposed. They evaluated such forces using DLVO theory and indicated that due to the fact that the van der Waals interaction was attractive, the electrostatic interaction would play a critical role in film formation.

In the present study, Zeta potential measurements of the polymer-capped zinc oxide particles in the two deposition systems were conducted, which measured the electrostatic potential at,

or very close to, the beginning of the diffuse double layer. The ZnO film formation on the sulfonated SAM surface and on the bare silicon wafer from these two deposition systems was compared. Additionally, the influence of the SAM surface on the copolymer capped ZnO film deposition was quantitatively discussed based on the electrostatic interaction involved.

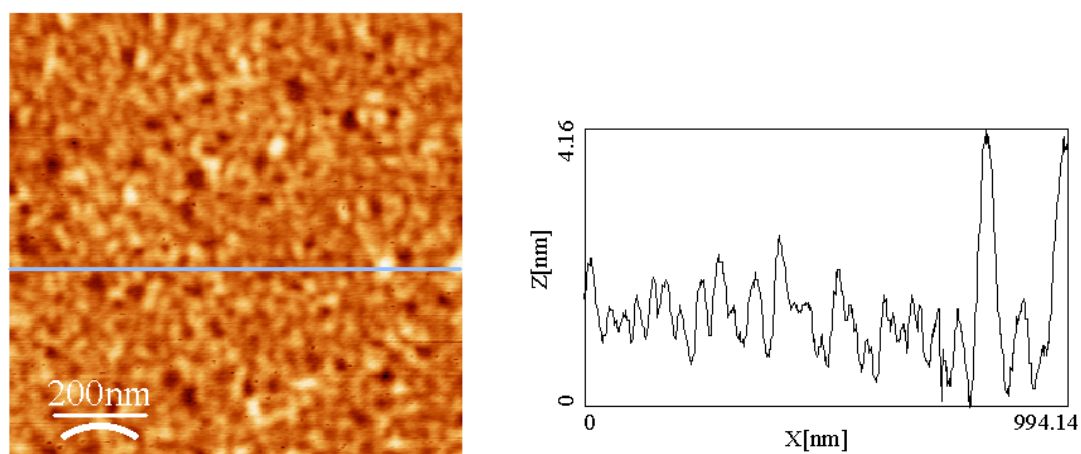


Fig. 6.1 AFM image of as-deposited film grown at 80 °C for 1.5 h on a SH-modified silicon wafer from a solution containing 100 mM [Zn], 4000 ppm copolymer and 7 mM HMTA.

## 6.2. Results and discussion

### 6.2.1. ZnO film formation on silicon wafers modified with sulfonate-terminated SAMs

#### 6.2.1.1. ZnO film growth from aqueous solution with the presence of a copolymer

The sulfonate surface group has a strong tendency to release a proton ( $-\text{SO}_3\text{H} \rightarrow -\text{SO}_3^- + \text{H}^+$ ) even in strongly acidic environments. This results in a uniform, negatively charged surface, which was confirmed by further measurements [2004Shy]. The Zeta potential under the film deposition condition (pH=6.4) was  $-90$  mV (Table 6.2).

When considering the charge of the particles in solution, the effect of polymers adopted has to be taken into account. Zeta potential measurements of ZnO suspensions with and without the copolymer were conducted and the results were shown in Fig. 6.2. The curve of ZnO without the addition of copolymer is in accordance with earlier publications, revealing an isoelectric point (IEP) at a pH of about 9.0 [2000Deg]. The copolymer makes the curve shift to lower pH values [2001Hof] and this shift can be attributed to the presence of the anionic carboxylate component of the copolymer. Based upon these measurements, it can be assumed that in the

film deposition experiments (pH=6.4) the ZnO/copolymer particles are slightly negatively charged (-10 mV).

Table 6.2 Zeta potential of the various SAMs in the deposition solution with the presence of copolymer (pH = 6.4) and the resultant interaction force between SAM and the particles.

Surface group	Zeta potential		Electrostatic force ( $F_e$ )	Van der Waals force ( $F_a$ )	Film formation
	SAM surface $\psi_s$	ZnO/Copolymer Particles $\psi_p$			
-SO <sub>3</sub> H	-90 mV [2004Shy]	-10 mV	repulsive	attractive	No
-OH	-70 mV [2001Hoz]		repulsive		No
-SCOCH <sub>3</sub>	-32 mV [2004Shy]		repulsive		Yes
-SH	-12 mV [2003Mun]		repulsive		Yes
-NH <sub>2</sub>	+38 mV [2004Shy]		attractive		Yes

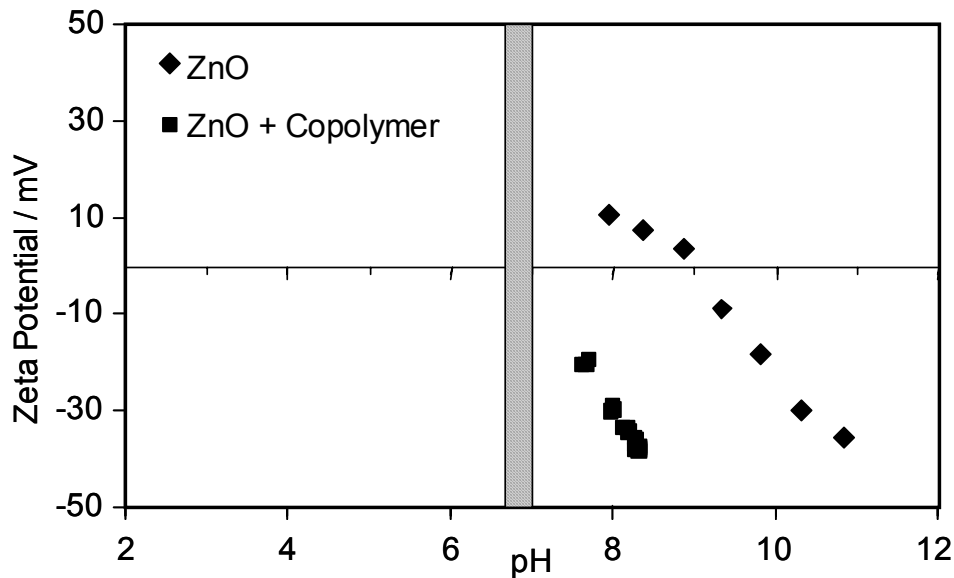
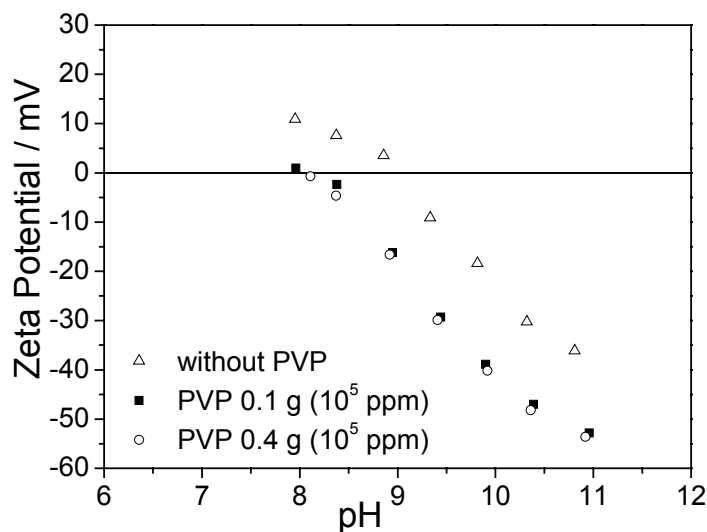


Figure 6.2 Zeta potential of ZnO in water as a function of pH. Operational pH was controlled by addition of KOH (rhombus) or PMAA-graft-PEO copolymer (squares). The pH regime of the film deposition is indicated by the hatched area.

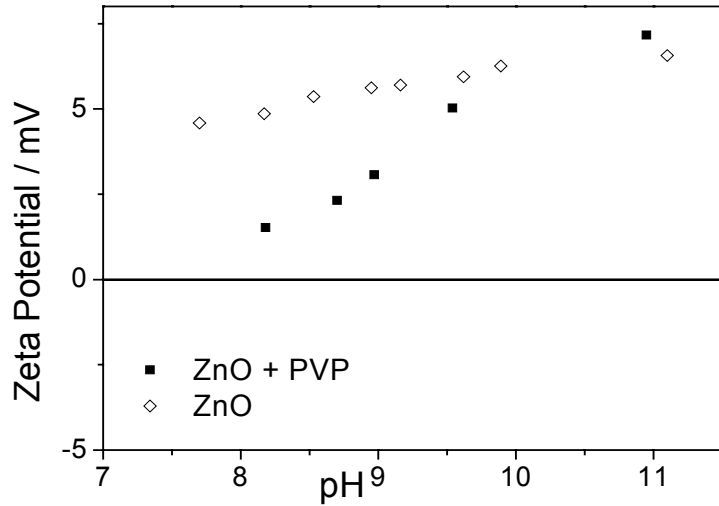
According to the results mentioned above, a model was established by Hoffmann [2001Hof], and it suggested that the negatively charged ZnO/copolymer particles would preferably deposit on positively charged surfaces. The SO<sub>3</sub>H-treated SAM surface, which provides significant negative surface charge density, obviously, will not be suitable for film deposition.

### 6.2.1.2. ZnO film growth from non-aqueous solution with the presence of PVP

Electrokinetic studies on the PVP-capped oxide particles by Pattanaik et al. [2000Pat] revealed that no significant shift of isoelectric point (IEP) occurred compared with the pure oxide particles, such as titanium dioxide, alumina and iron oxide. The influence of PVP on the ZnO surface was determined in aqueous solution (Fig. 6.3a). As shown in Fig. 6.2, the curve of ZnO without the addition of PVP revealed an isoelectric point (IEP) at a pH of about 9.0. PVP shifts slightly the IEP point to around 8.2. This result indicated that PVP, as a nonionic polymer in comparison to the copolymer, had less impact on the IEP shift. Attempts were also made to determine the zeta potential of the ZnO/PVP particle in the reaction solution (Fig. 6.3b). Zeta potential measurements are known to be difficult in non-aqueous solution since much less ions are present to form the electrokinetic charge as was evidenced from the present result. The zeta potential increased with enhancing the pH value. The addition of water in the form of a sodium hydroxide solution for the adjustment of the pH led to an increase of the conductivity of the resulting propanol/water mixture, which is favorable for the proceeding of the measurement. As a result an increase of the zeta potential with the pH value was observed. As indicated in the Chapter 2 (2.1.9), the measurement was started with the reaction solution and the results revealed that both ZnO with and without PVP were surface positively charged. Thus the ZnO/PVP particles, which remain slightly positively charged in the film formation experiments, should be preferably deposited on negatively charged surfaces. The experimental results with the  $-\text{SO}_3\text{H}$  group are in agreement with this assumption. Based on these electrostatic considerations, a film formation model was suggested and shown in Fig. 6.4.



(a)



(b)

Figure 6.3 (a) Zeta potential of ZnO without (rhombs) and with the presence of PVP (squares and ovals) in water as a function of pH. (b) Zeta potential of ZnO without (rhombs) and with the presence of PVP (squares) in 2-propanol as a function of pH.

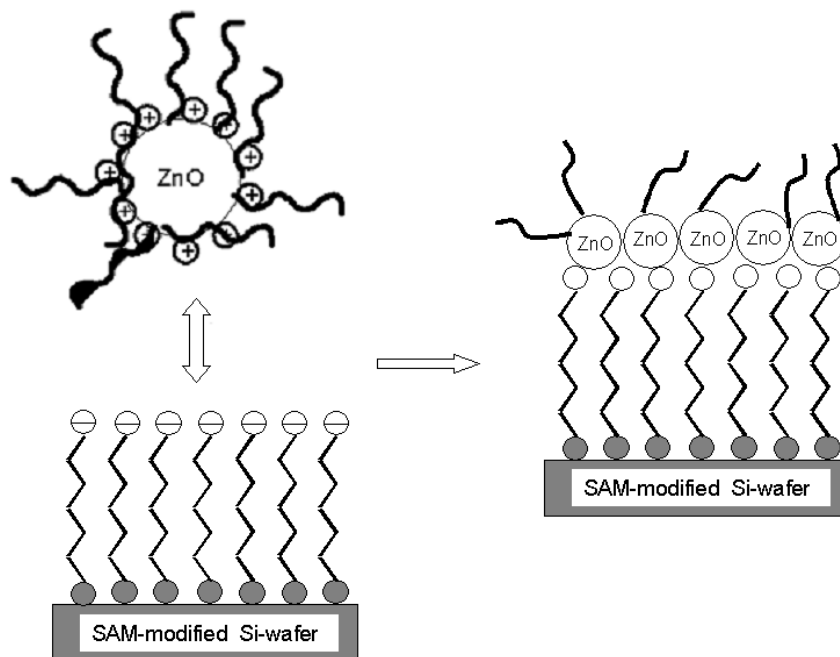


Fig. 6.4 Schematic demonstration of the film formation of PVP-capped ZnO particles onto sulfonate-terminated SAMs.

### **6.2.2. ZnO film formation on bare silicon wafers**

In the case of bare silicon (i.e. oxidized and without SAM), it is known that the isoelectric point of SiO<sub>2</sub> is about two [1965Par, 2001Hoz]. Therefore, the substrate surface is negatively charged (-70 mV) in the aqueous deposition solution with the presence of copolymer. Similar to SAMs bearing sulfonate surface groups, the negatively charged silicon substrate would not be desirable for the deposition of negatively charged ZnO/copolymer particles. In case of the deposition in 2-propanol solution, which is less polar than aqueous solvent, the deprotonation of the substrate surface group was inhibited to a great extent and its dissociation cannot proceed completely. Thus the zeta potential of SiO<sub>2</sub> decreases to -3 mV [1997Shib]. The absence of the ZnO film on the bare silicon wafers, therefore, can be attributed to the weak net attraction.

### **6.2.3. ZnO film formation on silicon wafers modified by other SAMs**

The results discussed above suggest that selecting a suitable deposition solution could allow the successful film fabrication on a given substrate. On the other hand, the substrate surface plays an important role. According to Table 6.1, for the solution with the presence of the copolymer, film formation showed substrate-selectivity. The zeta potential of the various SAMs in the deposition solution and the interaction force involved are shown in Table 6.2. The zeta potential of the various SAMs under deposition condition (pH=6.4) were chosen according to the data available in the literature [2004Shy, 2001Hoz, 2003Mun]. The substrates modified with -SCOCH<sub>3</sub>, -SH surface groups showed much weaker zeta potential than that of -SO<sub>3</sub>H- and -OH-functionalized ones. On the contrary, -NH<sub>2</sub>-terminated SAM-modified silicon wafers exhibited a positively charged surface. One point worthy to be noted is that although -SH groups (pK<sub>a</sub> = 10) [1982Bor] should be somewhat positive under the deposition condition (pH=6.4), the zeta potential charge given in literature [2003Mun, 2004Shy] however is negative. This is plausible because the zeta potential measurement reflected the effect of the whole substrate surface. The negative zeta potential therefore can be attributed to the combined effect of the substrate and SAM surface group, in accordance with the decrease of the surface potential of the bare substrate (-70 mV) to -12 mV of the substrate modified with -SH functionalized SAMs. This substrate effect is observed for the -SCOCH<sub>3</sub> surface groups as well, which is not ionisable and hardly charged. The thioacetate SAM therefore showed a stronger zeta potential of -32 mV than that of thiol SAM.

Obviously, the negatively charged ZnO/copolymer particles would be desirable for the surfaces with positive charges such as NH<sub>2</sub>-terminated SAMs, which is in agreement with the experimental results (Chapter 3.6.). This is also stated by the results obtained from the deposition on surfaces with large negative surface potential, namely in the case of the bare substrates or the -SO<sub>3</sub>H functionalized ones, where no deposition is observed. On the contrary, substrates those bear a less negative surface potential (-SCOCH<sub>3</sub>, -SH-modified ones) according to smaller repulsive forces lead to film deposition. This indicates that in these cases the repulsive forces are small enough to be balanced by attractive van der Waals contributions. Attempts were made to further understand the influence of the SAM surface on the film formation behaviour by discussing the consequences of the static interaction potential quantitatively. Using equations 1 and 2 discussed in the introduction, (1.4), the electrostatic interaction energies ( $V_e$ ) between the ZnO/copolymer particles and various SAM surfaces in the deposition solution ([ZnCl<sub>2</sub>]=100 mM) were calculated. It should be noted that more emphasis was placed on the trends of the calculations and the comparisons that they enable to be drawn between the different SAM surface groups, than on the specific numerical values. To determine the radius (R) of the ZnO/copolymer particle, the presence of the copolymer has to be considered. According to the functions of the copolymer indicated in the Chapter 3 (3.1.), a model was established and shown in Fig. 6.5, which displays that R is the sum of the  $R_{ZnO}$  and the chain length of poly(ethylene oxide).  $R_{ZnO}$  was chosen to be 2.5 nm according to the AFM results (Fig. 6.1), the chain length of the PEO component, which was supposed to act as steric shield, was calculated according to the following formula [1983Nap]:

$$\langle r^2 \rangle^{1/2} \approx 0.06M_w^{1/2}$$

where  $\langle r^2 \rangle^{1/2}$  is the root mean square (rms) end-to-end distance of the PEO-the side chains of the copolymer.  $M_w$  is the molecular weight. Finally, R was chosen as 6 nm.

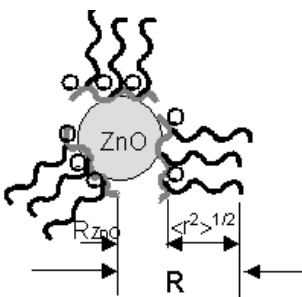


Fig. 6.5 Schematic demonstrations of the ZnO/copolymer particle.



The surface potential of the SAM surface ( $\psi_s$ ) and the ZnO/copolymer particle ( $\psi_p$ ) was chosen based on the zeta potential, which was given in Table 6.2. Additionally, the deposition temperature is 80 °C,  $\epsilon_{r, \text{solution}}$  is 60.

Calculated results are shown in Fig. 6.6. It should be noted that the equation 1 is accurate only for surface separations beyond about the Debye length [2002Isr]. At smaller separations one must resort to numerical solutions of the Poisson-Boltzmann equation to obtain the exact interaction potential for which there are no simple expressions. In addition, several factors such as ion-correlation effects, finite ion-size effects and discreteness of surface charges come into play within such small separation, which are not explicitly treated yet [2002Isr]. Therefore the electrostatic interactions between the ZnO/copolymer particles and different SAM surfaces shown in the Fig. 6.6 started from the separations of the Debye length ( $1/\kappa = 0.53 \text{ nm}$ ). The following trends were observed as a result of the strong variation in zeta potential between the surface groups:

1.  $V_e$  is negative (attractive) for the case of  $-\text{NH}_2$  surface group.
2. For the  $-\text{SO}_3\text{H}$  and  $-\text{OH}$  groups,  $V_e$  has a maximum at small separations ( $< 0.8 \text{ nm}$ ) at which  $V_e$  turns from attractive to repulsive.
3.  $V_e$  remains to be repulsive for the  $-\text{SH}$  and  $-\text{SCOCH}_3$  groups.

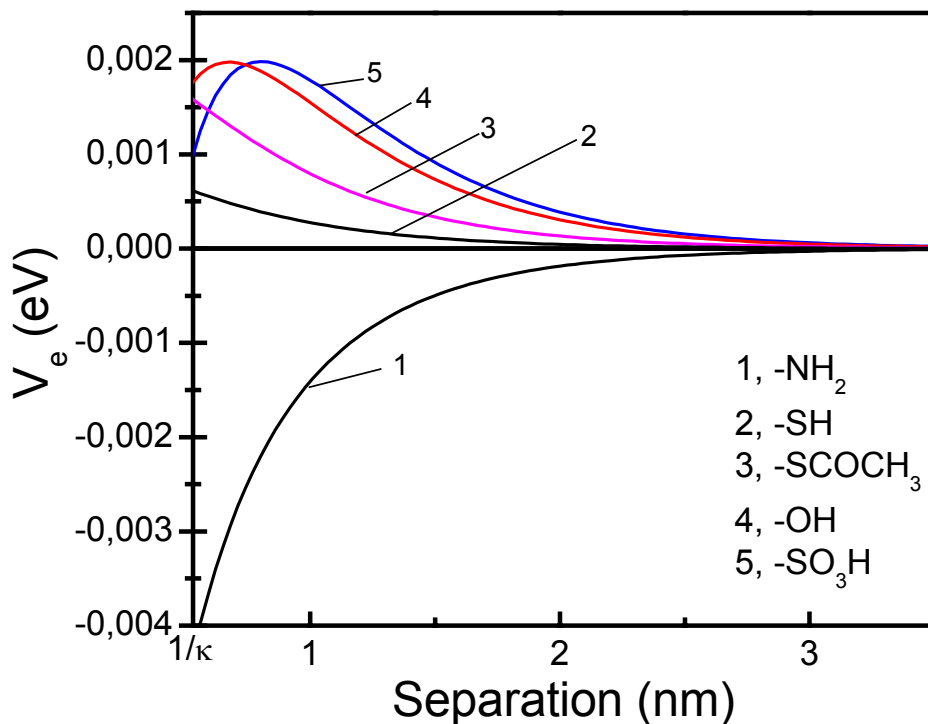


Fig. 6.6 Calculated electrostatic interactions between ZnO/copolymer particles and SAMs with various surface groups. ( $[\text{ZnCl}_2] = 0,1 \text{ M}$ , 80 °C,  $R = 6 \text{ nm}$ ,  $\epsilon_r = 59$ ).

The calculation suggests that the attractive  $V_e$  in the case of  $-\text{NH}_2$  makes a positive contribution to the film formation. This is in agreement with the experimental observations. For the  $-\text{SO}_3\text{H}$ ,  $-\text{OH}$ ,  $-\text{SCOCH}_3$  and  $-\text{SH}$  groups  $V_e$  is however repulsive and differs in magnitude. Table 6.3 shows the  $V_e$  value for these four surface groups at separations of 0,75 and 2 nm. One can see that for the  $-\text{SO}_3\text{H}$  and  $-\text{OH}$  groups,  $V_e$  are more than doubled compared to the  $-\text{SCOCH}_3$  surface group and remain repulsive even at farther separations.  $V_e$  for the  $-\text{SH}$  group is even much weaker. Obviously, for the  $-\text{SO}_3\text{H}$  and  $-\text{OH}$  groups, the strong repulsive  $V_e$  led to the failure of the film deposition. However, the fact that films were formed on the  $-\text{SCOCH}_3$  and  $-\text{SH}$  groups suggests that not only the electrostatic conditions determine the success of the film formation, but van der Waals interaction plays an important role as well. Film formation occurred when  $V_e$  was counterbalanced by the attractive van der Waals interaction. This is in agreement with the DLVO theory.

If the charge on the surface is fixed during an interaction then the interaction free energy is always positive if the signs are like and negative (attractive) if they are unlike. In contrast, if the potential is constant during an interaction and is different on each surface then an attraction can occur at small separations, even when the potentials have the same sign [1987Hun]. For the  $-\text{SO}_3\text{H}$  and  $-\text{OH}$  groups  $V_e$  has a maximum at small surface-to-surface distance of 0.79 nm and 0.67 nm respectively, i.e., the surfaces attract each other at small separations. However, it is impossible for the ZnO/copolymer particles to approach these two SAM surfaces so closely due to the strong repulsive electrostatic force at further separation. Therefore, the attractive  $V_e$  interaction in this region has no practical meaning for the film formation.

Table 6.3 Values of  $V_e$  at separations of 0,75 and 2 nm obtained from the  $V_e$  calculations.

Surface group	$V_e$ (meV)	
	X=0,75 nm	X=2 nm
$-\text{SO}_3\text{H}$	2	0.4
$-\text{OH}$	1.9	0.33
$-\text{SCOCH}_3$	1.1	0.1
$-\text{SH}$	0.43	0.075

It should be noted that no quantitative calculation for the PVP-induced deposition system has been conducted due to the lack of the surface potential data for the SAM surface in the 2-propanol solvent. The same problem exists for the calculation of the van der Waals interaction

in both deposition systems due to the lack of the dielectric permittivity and refractive index of the different SAM. Further experiments are needed to obtain these data.

#### 6.2.4. ZnO film growth on predeposited ZnO films on SAM

In previous sections, the influence of the SAM surface on ZnO film formation was discussed. After the SAM surface is completely covered by the ZnO particles, Van der Waals forces between ZnO particles formed in the solution and the already deposited film become the dominant factor for the continuous film formation [1997Shi, 2001Nie]. A point worthy to be noted is that the nanometer-sized particles formed in the solution will not only be attracted by the growing film, but will also tend to agglomerate in the solution. Fig. 6.7a displays the competition occurring between the film formation (process 1) and particles agglomeration (process 2). Compared to site “a”, on which the minimum contact particle number ( $n$ ) for particle A is 1, site “b” provides  $n \geq 3$ , which can be seen in Fig. 6.7c. Therefore, the reduction of the surface free energy of the total solid system caused by the film formation process is higher than that by particles agglomeration in the solution. As a result, the colloidal particle A in the solution would be preferably incorporated into films rather than be attached to another particle in the solution (Fig.6.7b).

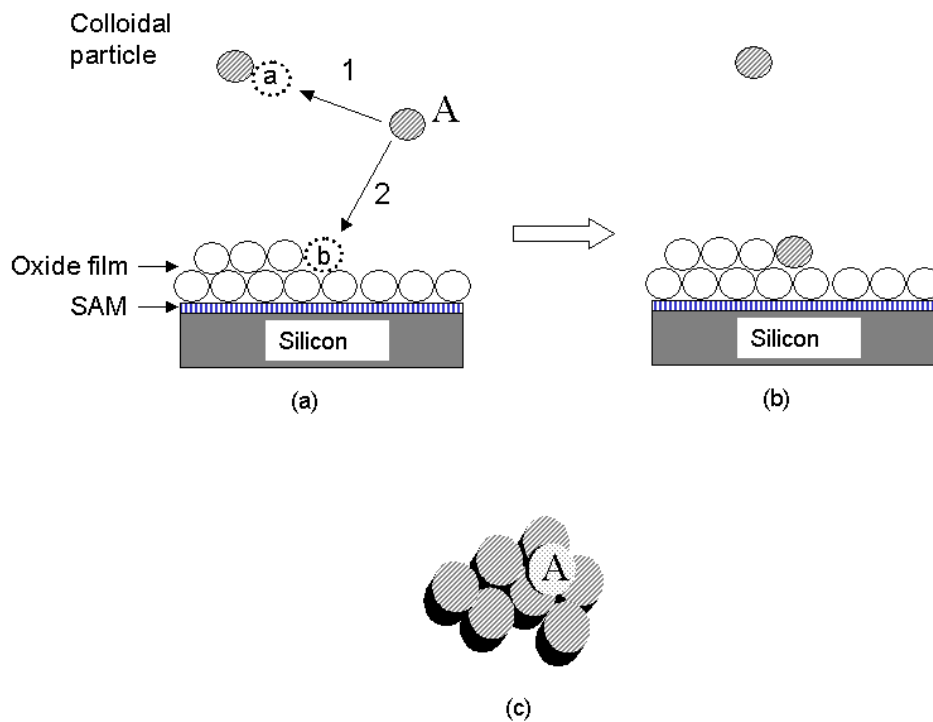


Fig. 6.7 (a, b) Schematic demonstration of the film formation of nanosized ZnO particles onto ZnO-deposited substrate and (c) top view of particle A on the already-deposited film.

## Polymerunterstützte Herstellung und Charakterisierung nanostrukturierter dünner Zinkoxid-Schichten

### Zusammenfassung

Zinkoxid ist ein einzigartiges Material, das halbleitende und piezoelektrische Eigenschaften aufweist. Eine weite Bandbreite von Techniken wurde zur Herstellung von dünnen Zinkoxidschichten untersucht, unter denen nasschemische Verfahren Vorteile aufgrund ihrer einfachen experimentellen Handhabung und ihrer Eignung zur Beschichtung auch größerer Flächen besitzen. Die Abscheidung von Zinkoxid mit diesen Methoden steht jedoch noch verschiedenen Schwierigkeiten gegenüber. Obwohl bereits Schichten mit interessanten Eigenschaften hergestellt werden konnten, bestehen diese zumeist aus mikrometergroßen Kristallen. Vorsichtige Kontrolle der Reaktionsbedingungen ist dabei notwendig um eine akzeptable Oberflächenhaftung und -rauigkeit zu erzielen. Weitere Probleme stellen sich damit speziell bei der Herstellung lateral nanostrukturierter Schichten.

Inspiziert durch die polymerkontrollierte Kristallisation von ZnO ist eine Strategie die Handhabung des Verfahrens der Chemischen Badabscheidung (CBD) zu verbessern, bei der organische Additive zu Wachstumskontrolle eingesetzt werden. Die hier vorgelegte Arbeit befasst sich mit der Synthese und Charakterisierung dünner ZnO Schichten auf mit Selbstorganisierten Monolagen (SAMs) funktionalisiertem Silicium mittels CBD. Weiter wurden Polymere der Reaktionslösung zugesetzt mit dem Ziel das Wachstum der sich bildenden ZnO Partikel zu kontrollieren. In dieser Arbeit wurde dabei die Eignung von zwei verschiedenen Polymeren untersucht.

### **Abscheidungen in der Gegenwart von PMAA-PEO Kammcopolymeren**

Für das erste Reaktionssystem wurden thiolmodifizierte Siliciumsubstrate eingesetzt. Zinkoxid-Schichten wurden aus wässrigen Lösungen von Zinksalzen mit einer Konzentration von 100mM/L und Hexamethylentetramin (HMTA) in einer Konzentration von 1-7 mM/L in der Gegenwart einer partiell mit Polyethylenoxid gepfropften Polymethacrylsäure  $P(\text{MAA}_{0.50}\text{-co}(\text{MAA-EO}_{20})_{0.50})_{70}$  abgeschieden. Die Herstellung der Schichten wurde bei 80°C durchgeführt. Ein Herstellungsdiagramm wurde erstellt, welches die Schichtmorphologie mit den Konzentrationen der Ausgangsverbindungen aufgrund von Rasterelektronen- (SEM) und Rasterkraftmikroskopischen (AFM) Aufnahmen beschreibt.

Nach der Einteilung in Filmmorphologien kann man drei verschiedene Kategorien einteilen: (a) inselartig gewachsene Schichten, (b) gleichförmige Schichten und (c) anschaulich "canyonartig" genannte Schichten. Nach Unterschreiten einer bestimmten Konzentration an HMTA oder oberhalb einer bestimmten Konzentration des Copolymers wurde das Schichtwachstum unterbunden, so dass keine signifikante Schichtbildung beobachtet werden konnte. Bei zu niedrig gewählter Konzentration des Copolymers tritt Fällung in der Reaktionslösung auf, wobei lediglich Sedimentation auf die Substrate erfolgt. Das Herstellungsdiagramm ermöglicht so die optimalen Schichtbildungsbedingungen zu bestimmen.

Der Einfluss der Substratoberfläche auf die Schichtherstellung wurde durch Variation der funktionellen Gruppe der eingesetzten SAMs untersucht. Keine Abscheidung erfolgte auf unmodifiziertem Silicium. Ungleichmäßige Schichtbildung oder nur partielle Substratbedeckung erfolgt auf sulfonat-funktionalisierten SAMs. Die Funktionalisierung von Silicium mit  $-\text{SCOCH}_3$ ,  $-\text{NH}_2$ , oder  $-\text{N}_3$ -terminierten SAMs führt, ähnlich wie der Verwendung von mercapto-terminierten SAMs, zur Abscheidung von Schichten mit canyonartiger Struktur, während beim Einsatz von  $-\text{Br}$ -terminierten SAMs nach einer Abscheiddauer von 7.5 h die Bildung gleichförmiger Schichte mit runden Partikeln beobachtet wurde.

Ausgehend von ZnO-Filmen mit canyonartigen Strukturen wurde der Prozess so modifiziert, dass schließlich gleichförmige Bedeckungen erzielt werden konnten. Die Dicke der ZnO-Schichten kann durch Variation der Abscheidezeit kontrolliert werden. Die chemische Zusammensetzung der Schichten wurde durch Röntgenphotoelektronenspektroskopie (XPS) untersucht. Die XPS-Spektren einer frisch abgeschiedenen und einer calcinierten Probe zeigten, dass der Zn 2p<sub>3/2</sub>-Peak nach Calciniierung bei 450°C bei 1022.5 eV liegt, was ein für ZnO zu erwartender Wert ist, wohingegen in der unbehandelten Probe das entsprechende Signal bei 1023.3 eV liegt, was auf das Vorhandensein des Copolymers in der Probe hinweist. Durchstrahlungselektronenmikroskopische (TEM) Untersuchungen ergaben, dass die frisch abgeschiedenen Schichten amorph waren. Nachfolgende Calciniierung wurde bei verschiedenen Temperaturen durchgeführt und der Einfluss auf Struktur und Photolumineszenz der Schichten untersucht. Proben, die bei 450°, 500°, 600° und 700°C calciniert worden waren, wurden durch Röntgenbeugung (XRD) an den Schichten untersucht. Calciniierung bei höheren Temperaturen führte zu Kornwachstum und verbesserte die Kristallinität. Die mittlere Korngröße für Schichten, die bei 600° bzw. 700°C calciniert wurden, lag bei 15 bzw. 25 nm aus Bestimmungen der Halbwertsbreite des (002) Peaks.

Polfiguren zeigten, dass die ZnO-Schichten eine bevorzugte Orientierung mit der c-Achse senkrecht zum Substrat nach Calciniierung bei 600°C aufwiesen, wobei die Textur bei den bei 700°C calcinierten Proben noch ausgeprägter war. Die bei 600 und 700°C calcinierten Proben wurden auch mittels TEM untersucht. Dabei war das Substrat nur noch von inselartigen Strukturen bedeckt, die aus nanometergroßen ZnO-Kristalliten bestanden. Nach Calciniierung bei 600° bzw. 700° hatten diese Inseln eine Höhe von 150 bzw. 110 nm. Weiter beobachtet man bei diesen erhöhten Temperaturen auch eine Festkörperreaktion zwischen ZnO und SiO<sub>2</sub> unter Bildung von Zn<sub>2</sub>SiO<sub>4</sub>. Diese erfolgt vermutlich durch Diffusion des ZnO, da sich das Zn<sub>2</sub>SiO<sub>4</sub> als gleichförmige Schicht auf dem Substrat bildet, welche nach 600° eine Dicke von 7 nm und nach 700° von 30 nm aufweist.

Photolumineszenzspektren wurden von frisch abgeschiedenen und nachträglich calcinierten Schichten, die bei Raumtemperatur mit einem He-Cd-Laser (266 nm) als Anregungsquelle aufgenommen wurden. Hier zeigten die bei 600° und 700°C calcinierten Proben ein intensives Emissionssignal im UV-Bereich. Dabei wies die Signal von 700° im Vergleich zu dem von 600°C eine Rotverschiebung auf, die mit dem Kornwachstum während der Calciniierung zu erklären ist.

### **Abscheidungen in Gegenwart von Polyvinylpyrrolidon (PVP)**

Ein System, das auf nicht-wässrigen Lösungen basiert, wurde ebenfalls untersucht. Dabei wurde 2-Propanol als Lösemittel, Zinkacetat und NaOH sowie PVP als Additiv verwendet. Die Wachstumsgeschwindigkeit der Schichten hängt stark von der Temperatur ab, wobei schließlich 55°C als geeignete Abscheidetemperatur gewählt wurde, so dass gleichförmige ZnO-Schichten erhalten werden konnten. Keine Abscheidung erfolgte auf unmodifiziertem Silicium, während gleichmäßige Schichtbildung beobachtet wurden auf sulfonat-funktionalisierten SAMs. Der Einfluss des Verhältnisses von [Zn] zu PVP auf die Schichtmorphologie wurde untersucht. XRD-Untersuchungen zeigten, dass der Film ZnO in der Wurtzit-Struktur enthält. Transmissionsspektren der Schichten im Bereich von 430-2000 nm wurden aufgenommen, die aufwiesen, dass der Film transparent (über 80%) im sichtbaren und infraroten Bereich war.

TEM-Untersuchungen an Querschnitten und Aufsichten der frisch abgeschiedenen Schichten zeigten, dass diese aus Domänen von 100-150 nm aufgebaut waren, die ihrerseits aus nanometergroßen ZnO-Kristalliten bestanden, die entlang einer bestimmten Richtung orientiert waren. Nachfolgende HRTEM-Untersuchungen bestätigten, dass orientierte

Anlagerung von ZnO-Nanopartikeln zur Ausbildung der Domänen führt. Obwohl die Filme keine Textur zeigten, existieren lokale Domänen mit bevorzugter Orientierung, die durch die Anordnung der zuerst auf dem Substrat abgeschiedenen ZnO-Partikel bestimmt wird.

Bei Raumtemperatur gemessene Photolumineszenzspektren der frisch abgeschiedenen ZnO-Schichten zeigten bei einer Anregungswellenlänge von 325 nm eine starke UV-Emission bei 388 nm und ein breites, grünes Emissionssignal mit einem Maximum bei etwa 535 nm.

### **Zum Schichtbildungsmechanismus auf SAM-modifizierten Substraten**

Basierend auf den oben zusammengefassten Ergebnissen für die beiden untersuchten Reaktionssysteme kann ein Schichtbildungsmechanismus vorgeschlagen werden. Das Wachstum der nanostrukturierten Schichten kann im Hinblick auf die beiden untersuchten Reaktionssystemen mittels der DLVO-Theorie gedeutet werden. Im Anfangsstadium der Schichtbildung dominieren zunächst elektrostatische Wechselwirkungen zwischen der Substratoberfläche und den ZnO/Polymer-Partikeln in der Lösung. Dabei liegt eine signifikante Potentialdifferenz zwischen den geladenen Partikeln und der Oberfläche vor. Die nachfolgende Anlagerung weiterer ZnO/Polymerpartikel wird durch Van der Waals-Wechselwirkungen gesteuert. Das elektrostatische Potential der keramischen Partikel wird durch die angelagerten Polymermoleküle beeinflusst, wie mittels Zeta-Potential-Messungen gezeigt werden kann. Die Polymermoleküle in der Lösung können außerdem durch Verminderungsflokkulierung zum Schichtwachstum beitragen.

Insgesamt wurde im Rahmen der vorliegenden Arbeit ein neues Verfahren zur Erzeugung von nanostrukturierten dünnen Schichten über einen CBD-Prozess gefunden. Hierbei kamen zwei Abscheidungssysteme zum Einsatz. Das erste System, bei dem ein Kammcopolymer verwendet wurde, führte zu amorphen Schichten. Mittels des zweiten Systems, das das Polymer PVP enthielt, wurden kristalline Schichten erhalten, woraus sich ein breites Spektrum für zukünftige Anwendungen ergibt.

## References

- [1965Par] G.A. Parks, "Isoelectric points of solid oxides solid hydroxides and aqueous hydroxide complex systems" *Chem. Rev.*, 65 (1965) 177-180.
- [1969Fos] N.F. Foster, "Crystallographic orientation of zinc oxide films deposited by triode sputtering" *J. Vac. Sci. Technol.*, 6 (1969) 111-114.
- [1976Bro] H.E. Brown, "Zinc oxide properties and applications" 1976.
- [1982Bor] F.G. Bordwell, D.L. Hughes, "Thiol acidities and thiolate ion reactivities toward butyl chloride in dimethyl sulfoxide solution. The question of curvature in Brønsted plots" *J. Org. Chem.*, 47 (1982) 3224-3232.
- [1983Cho] K.L. Chopra, S. Major, D.K. Pandya, "Transparent conductors—A status review" *Thin Solid Films*, 102 (1983) 1-46.
- [1983Nap] D.H. Napper, "Polymeric stabilization of colloidal dispersions" Academic Press, London, U.K., (1983) 4-13.
- [1985Koc] U. Koch, A. Fojtik, H. Weller, A. Henglein, "Photochemistry of semiconductor colloids. Preparation of extremely small ZnO particles, fluorescence phenomena and size quantization effects" *Chem. Phys. Lett.*, 122 (1985) 507-510.
- [1985Nic] Y.F. Nicolau, "Solution deposition of thin solid compound films by a successive ionic-layer adsorption and reaction process" *Appl. Surf. Sci.*, 22/23 (1985) 1061-1074.
- [1985Ris] M. Ristov, G.J. Sinadinovski, I. Grozdanov, *Thin Solid Films*, 123 (1985) 63-67.
- [1987Hun] R.J. Hunter, *Foundations of colloid science*, Oxford University Press, New York, 1 (1985).
- [1990And] M. Andrès-Vergès, A. Mifsud, C.J. Serna, "Formation of rod-like zinc oxide microcrystals in homogeneous solutions" *J. Chem. Soc. Faraday Trans.*, 86 (1990) 959-963.
- [1990Bal] N. Balachander, C.N. Sukenik, "Monolayer transformation by nucleophilic substitution: Applications to the creation of new monolayer assemblies" *Langmuir*, 6 (1990) 1621-1627.
- [1990Bri] C.J. Brinker, G.W. Scherer, *Sol-Gel Science*, Academic Press, San Diego, 1990.
- [1990Chi] A. Chittofrati, E. Matijevic, "Uniform particles of zinc oxide of different morphologies" *Colloid. Surface.*, 48 (1990) 65-78.
- [1991Spa] L.A. Spanhel, M.A. Anderson, "Semiconductor clusters in the sol-gel process: quantized aggregation, gelation, and crystal growth in concentrated ZnO colloids" *J. Am. Chem. Soc.*, 113 (1991) 2826-2833.
- [1991Ulm] A. Ulman, "Formation and Structure of Self-Assembled Monolayers" *Chem. Rev.*, 96 (1996) 1533-1554.
- [1992And] M. Andrès-Vergès, M. Martínez-Gallego, "Spherical and rod-like zinc oxide microcrystals: morphological characterization and microstructural evolution with temperature" *J. Mater. Sci.*, 27 (1992) 3756-3762.



- [1992Fuj] K. Fujita, K. Matsuda, "Formation of zinc oxide by homogeneous precipitation method" *Bull. Chem. Soc. Jpn.*, 65 (1992) 2270-2271
- [1992Pea] A.S. Pearl, "ZnO" *Ceram. Bull.*, 71 (1992) 821-822.
- [1993Mar] L.G. Mar, P.Y. Timbrell, R.N. Lamb, "An XPS study of zinc oxide thin film growth on copper using zinc acetate as a precursor" *Thin Solid Films*, 223 (1993) 341-347.
- [1993Olv] M. De la L. Olvera, A. Maldonado, R. Asomoza, M. Konagai, M. Asomoza, "Growth of textured ZnO:In thin films by chemical spray deposition" *Thin Solid Films*, 229 (1993) 196-200.
- [1994Tri] T. Trindade, J.D. Pedrosa de Jesus, P. O'Brien, "Preparation of zinc oxide and zinc sulfide powders by controlled precipitation from aqueous solution" *J. Mater. Chem.*, 4 (1994) 1611-1617.
- [1995Col] R.J. Collins, C.N. Sukenik, "Sulfonate-functionalized, siloxane-anchored, self-assembled monolayers" *Langmuir*, 6 (1995) 2322-2324.
- [1995Exa] G. Exarhos, S.K. Sharma, "Influence of processing variables on the structure and properties of ZnO films" *Thin Solid Films*, 270 (1995) 27-32.
- [1995Sae] T. Saeed, P. O'Brien, "Deposition and characterization of ZnO thin films grown by chemical bath deposition", *Thin Solid Films* 271 (1995) 35-38.
- [1996Ito] K. Ito, K. Nakamura, "Preparation of ZnO thin films using the flowing liquid film method" *Thin Solid Films*, 286 (1996) 35-36.
- [1996Jim] A. Jiménez-González, R. Suárez-Parra, "Effect of heat treatment on the properties of ZnO thin films prepared by successive ion layer adsorption and reaction (SILAR)" *J. Cryst. Growth*, 167 (1996) 649-655.
- [1996Liu] J. Liu, A.Y. Kim, L.Q. Wang, B.J. Palmer, Y.L. Chen, P. Bruinsma, B.C. Bunker, G.J. Exarhos, P.C. Rieke, G.E. Fryxell, J.W. Virden, B.J. Tarasevich, L.A. Chick, "Self-assembly in the synthesis of ceramic materials and composites" *Adv. Colloid Interface Sci.*, 69 (1996) 131-180.
- [1996O'B] P. O'Brien, T. Saeed, J. Knowles, "Speciation and the nature of ZnO thin films from chemical deposition" *J. Mater. Chem.*, 6 (1996) 1135-1139.
- [1996Ulm] A. Ulman, "Formation and structure of self-assembled monolayers" *Chem. Rev.*, 96 (1996) 1533-1554.
- [1996Van] K. Vanheusden, W.L. Warren, C.H. Seager, D.R. Tallant, J.A. Voigt, B.E. Gnade, "Mechanisms behind green photoluminescence in ZnO phosphor powders" *J. Appl. Phys.*, 79 (1996) 7983-7990.
- [1997Aga] M. Agarwal, M.R. De Guire, A.H. Heuer, "Synthesis of ZrO<sub>2</sub> and Y<sub>2</sub>O<sub>3</sub>-doped ZrO<sub>2</sub> thin films using self-assembled monolayers", *J. Am. Ceram. Soc.*, 80 (1997) 2967-2981.
- [1997Iza] M. Izaki, T. Omi, "Transparent zinc oxide films chemically prepared from aqueous solution" *J. Electrochem. Soc.*, 144 (1997) L3-L5.
- [1997Jim] A.E. Jiménez-González, "Modification of ZnO Thin Films by Ni, Cu, and Cd Doping<sup>\*1</sup>" *J. Solid State Chem.*, 128 (1997) 176-180.

- [1997Mar] J.M. Marentette, J. Norwig, E. Stöckelmann, W. H. Meyer, G. Wegner, "Crystallization of CaCO<sub>3</sub> in the presence of PEO-block-PMAA copolymers", *Adv. Mater.*, 9 (1997) 647-651.
- [1997Ohy] M. Ohyama, H. Kozuka, T. Yoko, "Sol-gel preparation of ZnO films with extremely preferred orientation along (002) plane from zinc acetate solution" *Thin Solid Films*, 306 (1997) 78-85.
- [1997Ros] A. Rose, G.J. Exarhos, "Ellipsometric studies of thermally induced transformation phenomena in oxide films" *Thin Solid Films*, 308 (1998) 42-49.
- [1997Shi] H. Shin, M. Agarwal, M.R. Guire, A. H. Heuer, "Deposition mechanism of oxide thin films on self-assembled organic monolayers", *Acta. Mater.*, 46 (1997) 801-815.
- [1997Shib] S. Shibata, T. Taniguchi, T. Yano, M. Yamane, "Formation of water-soluble dyedoped silica particles" *J. Sol-gel sci. Techn.*, 10 (1997) 263-268.
- [1998Bao] G.W. Bao, S. Li, "Characterization of atomic force microscopy (AFM) tip shapes by scanning hydrothermally deposited ZnO thin films" *Talanta*, 45 (1998) 751-757.
- [1998Bor] K. Borgohain, S. Mahamuni, "Luminescence behavior of chemically grown ZnO quantum dots" *Semicond. Sci. Technol.*, 13 (1998) 1154-1157.
- [1998Deg] M.R. De Guire, T.P. Niesen, S. Supothina, J. Wolff, J. Bill, C.N. Sukenik, F. Aldinger, A. Heuer, M. Rühle, "Synthesis of oxide and non-oxide inorganic materials at organic surfaces" *Z. Metallkd.*, 89 (1998) 758-766.
- [1998Meu] E.A. Meulenkamp, "Synthesis and growth of ZnO nanoparticles", *J. Phys. Chem. B*, 102 (1998) 5566-5572.
- [1998Nyf] R.M. Nyffenger, B. Craft, M. Shaaban, S. Gorer, G. Erley, R.M. Penner, "A hybrid electrochemical/chemical synthesis of zinc oxide nanoparticles and optically intrinsic thin films" *Chem. Mater.*, 10 (1998) 1120-1129.
- [1998O'B] P. O'Brien, J. McAleese, "Developing an understanding of the process controlling the chemical bath deposition of ZnS and CdS" *J. Mater. Chem.*, 8 (1998) 2309-2314.
- [1998Öne] M. Öner, J. Norwig, W.H. Meyer, G. Wegner, "Control of ZnO crystallization by a PEO-b-PMAA diblock copolymer", *Chem. Mater.*, 10 (1998) 460-463.
- [1998Sri] V. Srikant, D.R. Clarke, "On the optical band gap of zinc oxide" *J. Appl. Phys.*, 83 (1998) 5447-5451.
- [1998Wan] Y. Wang, S. Supothina, M.R. De Guire, A.H. Heuer, R. Collins, C.N. Sukenik, "Deposition of compact hydrous aluminum sulfate thin films on titania particles coated with organic self-assembled monolayers" *Chem. Mater.*, 10 (1998) 2135-2144.
- [1999Nun] P. Nunes, B. Femandes, E. Fortunato, R. Martins, "Performances presented by zinc oxide thin films deposited by spray pyrolysis" *Thin Solid Films*, 337(1999) 176-179.
- [1999Shi] H. Shin, Y. Wang, U. Sampathkuran, M.R. De Guire, A.H. Heuer, C.N. Sukenik, "Pyrolysis of self-assembled organic monolayers on oxide substrates" *J. Mater. Res.*, 14 (1999) 2116-2123.
- [1999Yel] K.E. Yelm, "A simple method for in situ generation of thiols from thioacetates" *Tetrahedron Lett.* 40 (1999) 1101-1102.

- [2000Ban] J.F. Banfield, S.A. Welch, H. Zhang, T.T. Ebert, R.L. Penn, "Aggregation-base crystal growth and microstructure development in nature iron development in natural iron oxyhydroxide biomineralization products" *Science*, 289 (2000) 751-754.
- [2000Deg] A. Degen, M. Kosec, "Effect of pH and impurities on the surface charge of zinc oxide in aqueous solution" *J. Europ. Ceram. Soc.*, 20 (2000) 431-440.
- [2000Guo] L. Guo, S. Yang, C. Yang, P. Yu, J. Wang, W. Ge, G.K.L. Wong, "Synthesis and characterization of poly(vinylpyrrolidone)-modified zinc oxide nanoparticles" *Chem. Mater.*, 12 (2000) 2268-2274.
- [2000GuoL-2] L. Guo, S. Yang, C. Yang, P. Yu, J. Wang, W. Ge, G.K.L. Wong, "Highly monodisperse polymer-capped ZnO nanoparticles : preparation and optical properties" *Appl. Phys. Lett.*, 76 (2000) 2901-2903.
- [2000Iza] M. Izaki, J. Katayama, "Characterization of boron-induced zinc oxide film chemically prepared from an aqueous solution" *J. Electrochem. Soc.*, 147 (2000) 210-213.
- [2000Jol] J.P. Jolivet, *Metal oxide chemistry and synthesis*, John Wiley, New York (2000)
- [2000Pat] M. Pattanaik, S.K. Bhaumik, "Adsorption behavior of polyvinyl pyrrolidone on oxide surfaces" *Mater. Lett.*, 44 (2000) 352-360.
- [2000Rie] J. Rieger, J. Thieme, C. Schmidt, "Study of precipitation Reactions by X-ray microscopy: CaCO<sub>3</sub> precipitation and the effect of polycarboxylates" *Langmuir*, 16 (2000) 8300-8305.
- [2000Sch] F. Schriber, "Structure and growth of self-assembling monolayers" *Prog. Surf. Sci.*, 65 (2000) 151-256.
- [2000Yos] M. Yoshimura, J. Livage, "Soft processing for advanced inorganic materials", *MRS Bullitin*, 9 (2000)12-13.
- [2001Aki] F.A. Akin, H. Zreiqat, S. Jordan, M.B.J. Wijesundara, L. Hanley, "Preparation and analysis of macroporous TiO<sub>2</sub> films on Ti surfaces for bone-tissue implants" *J. Biomed. Mater. Res.*, 57 (2001) 588-596.
- [2001Guo] L. Guo, J.X. Cheng, X. Li, Y.J. Yan, S.H. Yang, C.L. Yang, J.N. Wang, W.K. Ge, "Synthesis and optical properties of crystalline polymer-capped ZnO nanorods" *Mater. Sci. Eng. C*, 16 (2001) 123-127.
- [2001Hof] R.C. Hoffmann, J. Bill, F. Aldinger, " Influences of additives on the formation of thin ZnO films on self-assembled monolayers", in: M.R. DeGuire, M.Z. Hu, Y. Gogotsi, S.W. Lu (Eds.), *Ceramic Nanomaterials and Nanotechnology II*, Ceramic Transactions 148.
- [2001Hoz] A. Hozumi, H. Sugimura, Y. Yokogawa, T. Kameyama, O. Takai, "Zeta-potentials of planar silicon plates covered with alkyl- and fluoroalkylsilane self-assembled monolayers" *Colloid Surf. A: Physicochem. Eng. Asp.*, 182 (2001) 257-261.
- [2001Hu] M. Hu, S. Noda, T. Okubo, Y. Yamaguchi, H. Komiyama, "Stucture and morphology of self-assembled 3-mercaptopropyltrimethoxysilane layers on silicon oxide", *Appl. Surf. Sci.*, 81 (2001) 307-316.
- [2001Joh] P. John, "Toward diamond lasers", *Science*, 292 (2001) 1847-1848.

- [2001Kon] Y.C. Kong, D.P. Yu, B. Zhang, W. Fang, S.Q. Feng, "Ultraviolet-emitting ZnO nanowires synthesized by a physical vapor deposition approach", *Appl. Phys. Lett.*, 78 (2001) 407-409.
- [2001Kuz] I. Kuzmenko, H. Rapaport, K. Kjaer, J. Als-Nielsen, I. Weissbuch, M. Lahav, L. Leiserowitz, "Design and characterization at crystalline thin film architectures at the air-liquid interface: Simplicity to complexity", *Chem. Rev.*, 101 (2001) 1659-1696.
- [2001Nie] T.P. Niesen, M.R. De Guire, "Review: Deposition of ceramic thin films at low temperatures from aqueous solution", *J. Electroceram.*, 6 (2001) 169-207.
- [2001Ohy] Y. Ohya, T. Niwa, T. Ban, Y. Takahashi, "Thin film transistor of ZnO fabricated by chemical solution deposition" *Jpn. J. Appl. Phys.*, 40 (2001) 297-298.
- [2001Sai] N. Saito, H. Haneda, W.S. Seo, K. Koumoto, "Selective deposition of ZnF(OH) on self-assembled monolayers in Zn-NH<sub>4</sub>F aqueous solutions for micropatterning of zinc oxide" *Langmuir*, 17 (2001) 1461-1469.
- [2001Yan] C.L. Yang, J.N. Wang, W.K. Ge, L. Guo, S.H. Yang, D.Z. Shen, "Enhanced ultraviolet emission and optical properties in polyvinylpyrrolidone surface modified ZnO quantum dots" *J. Appl. Phys.*, 90 (2001) 4489-4493.
- [2001Yao] B. Yao, H. Shi, X. Zhang, L. Zhang, "Ultraviolet photoluminescence from nonbridging oxygen hole centers in porous silica" *Appl. Phys. Lett.*, 78 (2001) 174-178.
- [2002Ali] H.A. Ali, A.A. Iliadis, R.F. Mulligan, A.V.W. Crece, P. Kofinas, U. Lee, "Properties of self-assembled ZnO nanostructures" *Solid-State Electron.*, 46 (2002) 1639-1642.
- [2002Bil] J. Bill, R.C. Hoffmann, T.M. Fuchs, F. Aldinger, Z. "Deposition of ceramic materials from aqueous solution induced by organic templates", *Z. Metallkd.*, 93 (2002) 478-489.
- [2002Boy] D.S. Boyle, K. Govender, P. O'Brien, "Novel low temperature solution deposition of perpendicularly orientated rods of ZnO: substrate effects and evidence of the importance of counter-ions in the control of crystallite growth", *Chem. Commun.*, 15 (2002) 80-81.
- [2002Ful] B. Fultz, J. Howe, "Transmission electron microscopy and diffractometry of materials", 2002.
- [2002Gov] K. Govender, D.S. Boyle, P. O'Brien, "Room temperature lasing observed ZnO nanocolumns grown by aqueous solution deposition", *Adv. Mater.*, 14 (2002) 1221-1224.
- [2002Hof] R. Hoffmann, T. Fuchs, T.P. Niesen, J. Bill, F. Aldinger, "Influence of PMAA-graft-PEO copolymers on the formation of thin ZnO films from aqueous solutions", *Surf. Interface Anal.*, 34 (2002) 708-711.
- [2002Ish] H. Ishizaki, M. Imaizumi, S. Matsuda, M. Izaki, T. Ito, "Incorporation of boron in ZnO film from an aqueous solution containing zinc nitrate and dimethylamine-borane by electrochemical reaction" *Thin Solid Films*, 411 (2002) 65-68.
- [2002Isr] J. Israelachvili, *Intermolecular & surface forces*, 2nd Edition.
- [2002Liu] Y.X. Liu, Y.C. Liu, D.Z. Shen, G.Z. Zhong, X.W. Fan, X.G. Kong, R. Mu, D.O. Henderson, "Preferred orientation of ZnO nanoparticles formed by post-annealing zinc implanted silica" *Solid State Communications*, 121 (2002) 531-536.

- [2002Pac] C. Pacholski, A. Kornowski, H. Weller, "Self-assembly of ZnO: From nanodots to nanorods" *Angew. Chem. Int. Ed.*, 41 (2002) 1188-1191.
- [2002Sai-1] N. Saito, H. Haneda, T. Sekiguchi, N. Ohashi, I. Sakaguchi, K. Koumoto, "Low-temperature fabrication of light-emitting zinc oxide micropatterns using self-assembled monolayers" *Adv. Mat.*, 14 (2002) 418-421.
- [2002Sai-2] N. Saito, H. Haneda, D. Li, K. Koumoto, "Characterization of zinc oxide micropatterns deposited on self-assembled monolayer template" *J. Ceram. Soc. Jpn.*, 110 (2002) 386-390.
- [2002Tau-1] A. Taubert, G. Glasser, D. Palms, "Kinetics and particle formation mechanism of zinc oxide particles in polymer-controlled precipitation from aqueous solution", *Langmuir*, 18 (2002) 4488-4494
- [2002Tau-2] A. Taubert, D. Palms, Ö. Weiss, M. Piccini, D.N. Batchelder, "Polymer-assisted control of particle morphology and particle size of zinc oxide precipitated from aqueous solution", *Chem. Mater.*, 14 (2002) 2594-2601.
- [2002Wes] B. Wessler, F.F. Lange, W. Mader, "Textured ZnO thin films on (0001) sapphire produced by chemical solution deposition" *J. Mater. Res.*, 17 (2002) 1644-1649.
- [2002Xu] X. Xu, C. Guo, Z. Qi, H. Liu, J. Xu, C. Shi, C. Chong, W. Huang, Y. Zhou, C. Xu, "Annealing effect for surface morphology and luminescence of ZnO film on silicon", *Chem. Phys. Lett.*, 364 (2002) 57-63.
- [2002Yam] S. Yamabi, H. Imai, "Growth conditions for wurtzite zinc oxide films in aqueous solutions" *J. Mater. Chem.*, 12 (2002) 3773-3778.
- [2002Yan] P. Yang, M. Lv, C. Song, S. Liu, D. Yuan, D. Xu, F. Gu, D. Cao, D. Chen, "Preparation and characteristics of sol-gel derived Zn<sub>2</sub>SiO<sub>4</sub> doped with Ni<sup>2+</sup>" *Inor. Chem. Commun.*, 5 (2002) 482-486.
- [2002Zha] D.H. Zhang, Q.P. Wang, Z.Y. Xue, "Photoluminescence of ZnO films excited with light of different wavelength", *Appl. Sur. Sci.*, **9543** (2002)1-6.
- [2003Fuc] T. Fuchs, PhD thesis, University of Stuttgart (2003).
- [2003He] H. He, Y. Wang, Y. Zou, "Photoluminescence property of ZnO-SiO<sub>2</sub> composites synthesized by sol-gel method", *J. Phys. D: Appl. Phys.* **36** (2003) 2972-2975
- [2003Hof] R.C. Hoffmann, S. Jia, J.C. Bartolomé, T.M. Fuchs, J. Bill, P.C.J. Graat, F. Aldinger, "Growth behaviour of thin ZnO films from aqueous solution in the presence of PMAA-graft-PEO copolymers", *J. Eur. Ceram. Soc.*, **23** (2003) 2119-2123.
- [2003Iza] M. Izaki, Y. Saijo, "Transparent conducting and highly stable indium-incorporated zinc oxide film prepared by chemical reactions" *J. Electrochem. Soc.*, 150 (2003) C73-C76.
- [2003Ji] Z.G. Ji, L. Kun, Y.L. Song, Z.Z. Ye, "Fabrication and characterization of Mn-doped zinc silicate films on silicon wafer" *J. Cryst. Growth*, 255 (2003) 353-356.
- [2003Mun] O.L.S. Munoz, E.P. Hernandez, M. Lammerhofer, W. Lindner, E. Kenndler, "Estimation and comparison of zeta-potentials of silica-based anion-exchange type porous particles for capillary electrochromatography from electrophoretic and electroosmotic mobility" *Electrophor.*, 24 (2003) 390-398.

[2003Sch] C. Scheu, M. Gao, K. van Benthem, S. Tukimoto, S. Schmidt, W. Sigle, G. Richter, J. Thomas, "Advances in EELS spectroscopy by using new detector and new specimen preparation technologies" *J. Microscopy*, 210 (2003) 16-24.

[2003Str] A. Strecker, U. Bäder, M. Kelsch, U. Salzberger, M. Sycha, M. Gao, G. Richter, K. V. Benthem, „Progress in the preparation of cross-sectional TEM specimens by ion-beam thinning“, *Z. Metallkd.*, **94** (2003) 290-297.

[2003Xu] X. Xu, P. Wang, Z. Qi, H. Ming, J. Xu, H. Liu, C. Shi, G. Lu, W. Ge, "Formation mechanism of Zn<sub>2</sub>SiO<sub>4</sub> crystal and amorphous SiO<sub>2</sub> in ZnO/Si system", *J. Phys.: Condens. Matter.*, **15** (2003) L607-613.

[2003Zna] L. Zanidi, G.J.A.A. Soler Illia, S. Benyahia, C. Sanchez, A.V. Kanaev, "Oriented ZnO thin films synthesis by sol-gel process for laser application" *Thin Solid Films*, 428 (2003) 257-262.

[2004Bol] J. Bolze, D. Pontoni, M. Ballauff, T. Narayanan, H. Cölfen, "Time-resolved SAXS study of the effect of a double hydrophilic block-copolymer on the formation of CaCO<sub>3</sub> from a supersaturated salt solution" *J. Colloid Interface Sci.*, 277 (2004) 84-94.

[2004Cao] H. Cao, X. Qiu, B. Luo, Y. Liang, Y. Zhang, R. Tan, M. Zhao, Q. Zhu, "Synthesis and room-temperature ultraviolet photoluminescence properties of zirconia nanowires", *Adv. Funct. Mater.*, **14** (2004) 243-246.

[2004Hof] R.C. Hoffmann, S. Jia, J. Bill, F. Aldinger, "Influences of additives on the formation of ZnO films by forced hydrolysis", *J. Ceram. Soc. Jpn.*, **112** (2004) 1089-1092.

[2004Nor] D.P. Norton, Y.W. Heo, M.P. Ivill, K. Ip, S.J. Pearton, M.F. Chisholm, T. Steiner, "ZnO: growth, doping & processing" *Mater. Today* **6** (2004) 34-40.

[2004Sai] N. Saito, H. Haneda, T. Sekiguchi, T. Ishigaki, K. Koumoto, "Effect of postdeposition annealing on luminescence from zinc oxide patterns prepared by the electroless deposition process" *J. Electrochem. Soc.*, 151 (2004) H169-H173.

[2004Shy] J. Shyue, M.R. De Guire, T. Nakanishi, Y. Masuda, K. Koumoto, C.N. Sukenik, "Acid-based properties and zeta potentials of self-assembled monolayers obtained via in situ transformations" *Langmuir*, 20 (2004) 8693-8698.

[2004Tur] R. Turgeman, O. Gershevit, O. Palchik, M. Deutsch, B.M. Ocko, A. Gedanken, C.N. Sukenik, "Oriented growth of ZnO crystal on self-assembled monolayers of functionalized alkyl silans" *Crystal growth & design* 4 (2004) 169-175.

[2004Wan-1] Z.L. Wang, "Nanostructures of zinc oxide", *Mater. Today*, **6** (2004) 26-33.

[2004Wan-2] X. Wang, C.J. Summers, Z.L. Wang, "Mesoporous single-crystal ZnO nanowires epitaxially sheathed with Zn<sub>2</sub>SiO<sub>4</sub>", *Adv. Mater.*, 16 (2004) 1215-1218.

[2004Yu] S. Yu, H. Cölfen, "Bio-inspired crystal morphogenesis by hydrophilic polymers" *J. Mater. Chem.*, 14 (2004) 2124-2147.

## Curriculum Vitae (Lebenslauf)

Family name: **Jia**

First name: **Shijun**

Date of Birth: July 4, 1973.

Place of Birth: Shanxi province, P.R. CHINA

Nationality: Chinese

### ***Education:***

**10.2001-Now:** Max-Planck-Institute of Metals Research / University of Stuttgart, Stuttgart, Germany

Thesis advisor: Prof. Dr. Fritz Aldinger

The thesis is entitled “Polyelectrolyte-assisted preparation and characterization of nanostructured ZnO thin films”.

**09.1990-06.1994:** Major in Welding, Zhengzhou University of Technology, Zhengzhou, PR China

**09.1994-04.1997:** Major in Welding, Taiyuan University of Technology, Taiyuan, PR China

Thesis advisors: Prof. Pengsheng Zhao

The thesis was entitled “Arc-added glow discharge titanizing of ceramics and brazing of titanized ceramic to metal”.

**09.1997-06.2000:** Major in Welding, Institute of Metal research, Chinese Academy of Sciences (CAS), Shenyang, PR China

Thesis advisor: Prof. Xiaofeng Chen

The thesis was entitled “Mechanism of deep penetration and defects produced in electron beam welding”.